ΠΑΝΕΠΙΣΤΗΜΙΟ ΑΙΓΑΙΟΥ
Τμήμα Ναυτιλίας και Επιχειρηματικών Υπηρεσιών
&
ΠΑΝΕΠΙΣΤΗΜΙΟ ΔΥΤΙΚΗΣ ΑΤΤΙΚΗΣ
Τμήμα Μηχανικών Βιομηχανικής Σχεδίασης και Παραγωγής

ΔΙΙΔΡΥΜΑΤΙΚΟ

ΠΡΟΓΡΑΜΜΑ ΜΕΤΑΠΤΥΧΙΑΚΩΝ ΣΠΟΥΔΩΝ

«ΝΕΕΣ ΤΕΧΝΟΛΟΓΙΕΣ ΣΤΗ ΝΑΥΤΙΛΙΑ ΚΑΙ ΤΙΣ ΜΕΤΑΦΟΡΕΣ»

Σχεδιαστική επιλογή συστήματος μικροπροώθησης σε μικροδορυφόρους: 1.5U- 3U- 6U

Design Selection of micro-thruster system for cubesats: 1.5U-3U-6U

Ονοματεπώνυμο Σπουδαστή:

Petros Doukas

Ονοματεπώνυμο Υπεύθυνων Καθηγητών:

Dr. Nikitas Nikitakos	**Dr. Georgios Mantzouris**	**Dr. John Koukos**
Professor Dept. of Shipping Trade and Transport	Hellenic Space Agency	ex Nasa-JPL Member
University of the Aegean	CEO	Professor & Dean of the Hellenic Naval Academy

Φεβρουάριος 2019

“Σχεδιαστική επιλογή συστήματος μικροπροώθησης σε μικροδορυφόρους: 1.5U- 3U- 6U”

ΟΝΟΜΑ ΦΟΙΤΗΤΗ: Πέτρος Δούκας

Μεταπτυχιακή Διατριβή που υποβάλλεται στο καθηγητικό σώμα για την μερική εκπλήρωση των υποχρεώσεων απόκτησης του μεταπτυχιακού τίτλου του Διιδρυματικού Προγράμματος Μεταπτυχιακών Σπουδών «Νέες Τεχνολογίες στη Ναυτιλία και τις Μεταφορές» του Τμήματος Ναυτιλίας και Επιχειρηματικών Υπηρεσιών του Πανεπιστημίου Αιγαίου και του Τμήματος Μηχανικών Βιομηχανικής Σχεδίασης και Παραγωγής του Πανεπιστημίου Δυτικής Αττικής.

ΔΗΛΩΣΗ ΣΥΓΓΡΑΦΕΑ ΔΙΠΛΩΜΑΤΙΚΗΣ ΔΙΑΤΡΙΒΗΣ

Ο κάτωθι υπογεγραμμένος **Πέτρος Δούκας**, του **Δημητρίου**, με αριθμό μητρώου **104** φοιτητής του Διιδρυματικού Προγράμματος Μεταπτυχιακών Σπουδών Τμήματος «Νέες Τεχνολογίες στη Ναυτιλία και τις Μεταφορές» του Τμήματος Ναυτιλίας και Επιχειρηματικών Υπηρεσιών του Πανεπιστημίου Αιγαίου και του Τμήματος Μηχανικών Βιομηχανικής Σχεδίασης και Παραγωγής του Πανεπιστημίου Δυτικής Αττικής πριν αναλάβω την εκπόνηση της Διπλωματικής Διατριβής μου, δηλώνω ότι ενημερώθηκα για τα παρακάτω:

Η Διπλωματική Διατριβή (Δ.Δ.) αποτελεί προϊόν πνευματικής ιδιοκτησίας τόσο του συγγραφέα, όσο και των Ιδρυμάτων και θα πρέπει να έχει μοναδικό χαρακτήρα και πρωτότυπο περιεχόμενο.

Απαγορεύεται αυστηρά οποιοδήποτε κομμάτι κειμένου της να εμφανίζεται αυτούσιο ή μεταφρασμένο από κάποια άλλη δημοσιευμένη πηγή. Κάθε τέτοια πράξη αποτελεί προϊόν λογοκλοπής και εγείρει θέμα Ηθικής Τάξης για τα πνευματικά δικαιώματα του άλλου συγγραφέα. Αποκλειστικός υπεύθυνος είναι ο συγγραφέας της Δ.Δ.., ο οποίος φέρει και την ευθύνη των συνεπειών, ποινικών και άλλων, αυτής της πράξης.

Πέραν των όποιων ποινικών ευθυνών του συγγραφέα σε περίπτωση που του έχει απονείμει ο μεταπτυχιακός τίτλος , αυτός ανακαλείται με απόφαση της Ε.Δ.Ε. του ΠΜΣ. Η Ε.Δ.Ε. με νέα απόφασης της, μετά από αίτηση του ενδιαφερόμενου, του αναθέτει εκ νέου την εκπόνηση της Δ.Δ. με άλλο θέμα και διαφορετικό επιβλέποντα καθηγητή. Η εκπόνηση της εν λόγω Δ.Δ. πρέπει να ολοκληρωθεί εντός τουλάχιστον ενός ημερολογιακού 6μήνου από την ημερομηνία ανάθεσης της. Κατά τα λοιπά εφαρμόζονται τα προβλεπόμενα στον Κανονισμό Λειτουργίας του Π.Μ.Σ.

Ο Δηλών Ημερομηνία

Don't just aspire to make a living,

Aspire to make a difference…

~ Denzel Washington ~

Dedication…

To my family, who supported me and continues to support me in all my efforts.

ACKNOWLEDGMENTS

Upon completion of my dissertation, I would like to warmly thank the people who offered me considerable help at the various stages of this process.

This diploma thesis, entitled " Design Selection of micro-thruster system for cubesats:1.5U-3U-6U", was conducted within the framework of the Postgraduate Program "New Technologies in Shipping and Transport" of the University of the Aegean, Department of Shipping, Trade and Transport and the University of the West Attica. Automation Engineering Department.

At first I would like to thank my family for their help, understanding and patience throughout my postgraduate studies. My Professor **Koukos Ioannis** (Dean of Hellenic Naval Academy), because he has given me the opportunity to deal with such an interesting subject and provided me with basic principles that their full understanding proved necessary in the course of this work. I would also like to thank the Hellenic Space Agency CEO Dr **Georgios Mantzouris (**Commander Hellenic Navy) for the trust he has shown in my person and the understanding and support he provided me during this course. My friend and college, aeronautical engineer **Anastasios Papadopoulos** (2nd Lieutenant Hellenic Airforce) for his significant support in the implementation of the simulations. Finally, I would like to thank very much Mr. **Nikolaidis Dimitrios (**Colonel Hellenic Airforce Pilot) for his important advice and selfless help in the implementation of this work.

ABSTRACT

The following diploma thesis deals with the design selection of micro-thruster system for 1.5U-3U-6U cubesats. In this work, they were used three different free Matlab Orbital Decay calculation programs, so as to estimate the total satellite lifetime for a space mission. In the beginning there is an extensive survey of all space missions that are smaller than 10kg. In addition, simulations are made at various heights and dimensions. Moreover there is an extensive survey of all Cubase-compatible propulsion systems and all space missions with a propulsion system. After that, all the used propellers are presented and a comparison is made in order to find the optimum in each category. In conclusion are referred the findings of the research conducted in this thesis.

TABLE OF CONTENTS

List of figures

INTRODUCTION

In recent years, there has been a rapid increase in the manufacture and development of very small satellites weighing between 1 and 10 kilos, the so-called cubesats. These microsatellites are developed in the context of the creation of scientific experiments, measurements of natural variables and phenomena and their changes, communication needs, Earth observation, etc. A number of actors such as universities, public and private organizations, and construction companies participate in programs for the development of microsatellites with the main objective of acquiring know-how and experience in the design, construction and operational use of space programs. The result is the creation of companies involved in the construction of components and materials for the construction of such microsatellites.

The placement of micro-propulsion systems in these types of cubesats allows them to increase their time in trajectory, as well as their attitude control, thus optimizing their utilization. It also reduces overall costs by increasing the life-cycle of the microsatellite subsystem.

It is important the classification of the different types of cubesats for proposed different mission, which flight or not and equipped with micro thrusters or not. Moreover knowing that there are many different types of thrusters, it is essential to describe each type and to find how many of them have been used in flight. Furthermore exploring and comparing the performance characteristics of various micro-thrusters for cubesats 1.5U, 3U and 6U consists a significant research goal.

CHAPTER 1 – SATELLITE CUBESATS

1.1 Theory of Cubesats

Cubesats (Kyriakos G. Gouskos-Katsaros, 2018) are low weight and cost satellites that are placed in Low Earth Orbits via orbital platforms like the International Space Station, Rockets Launched to Near Earth Space, Aircraft or even Balloons. This chapter presents an overview of the orbital characteristics of typical cubesats having initial velocity vector that of the launch vehicle without further assistance, and analyzes the orbital parameters degradation due to perturbations from gravitational anomalies and atmospheric drag which eventually draw the satellite into denser atmospheric layers that eventually will burn the vehicle, thus ending its life. A lifetime extension is realized by firing small rockets (microthrusters) whose propulsion characteristics are referred to in the chapter 2 that follows. The cubesats are launched from the ISS via the NANORACKS ISS Microsatellite Deployment System (NANONRACKS, 2018), so that its trajectory will be perpendicular to that of the ISS (LEO). The elements for its trajectory are:

Closest Trajectory height: 422 km

Rperigee (SAT) = rearth + rperigee (ISS) = 6378.1370 + 422 = 6800.1370 km

The International Space Station (ISS) is a space research laboratory, orbiting at Low Earth orbit (LEO). The ISS mission is to carry out unique scientific experiments in low gravity environment. The ISS[1], orbital characteristics are shown below:

Eccentricity: 0.0003390

Inclination: 501.6393°

Perigee height: 402 km

Apogee height: 407 km

Right ascension of ascending node: 96.8675°

Argument of perigee: 141.7330°

Revolutions per day: 15.54105838

Orbital velocity: 7.66 km/s

[1] http://www.n2yo.com/

The ISS is orbiting the Earth in a nearly identical cyclical orbit, as its eccentricity is close to zero, at an inclination of 51.63°, from the Earth's equatorial plane and at an altitude between 402km to 407km. Among many tasks that must be fulfilled, the ISS astronauts have to prepare and launch the Cube Satellites that are delivered from the Earth. The deployer currently in use, for launching Cube Satellites from ISS, is the NanoRack CubeSat Deployer[2].

The NanoRack CubeSat Deployer[3] is a stackable, modular case which is preloaded with the above-mentioned satellites on earth, which also follows the "CubeSat Design Specifications (CDS)"[4]. Each case can accommodate up to 6.5U. Eight such cases are installed on the Multi-Purpose Experiment Platform, which is then deployed by the JEM (Japanese Experiment Module) Small Satellite Orbital Deployer (J-SSOD), passing through the JEM Airlock opening, to prepare and launch the Cube Satellites[5] .

1.2 Orbital Mechanics Equations

The dominant force except gravity is the drag force that the satellite experiences due to the continuous impact of atmosphere molecules on its orbiting body. The direction of this force is opposite to the direction of its motion and the magnitude is given by the expression:

$$D = \frac{1}{2}\rho v^2 ACd \quad (1)$$

Where D is the drag force, ρ is the atmospheric density at the height of the trajectory, υ is the satellite's speed, A is the cross-sectional area perpendicular to the direction of the motion and Cd is the drag coefficient. Considering that the satellite will orbit having set attitude control in a way that one of the flat surfaces of cubesats, faces the earth at all times, then the cross-sectional area is a rectangle with dimensions the diameter and the height of the cylinder. At the moment of the launch, the velocity of the satellite is the sum of the vector addition of the velocity of the ISS and the initial

[2] https://www.nasa.gov/mission_pages/station/research/experiments/1350.html
[3] http://nanoracks.com/products/iss-cubesat-deployment/
[4] CubeSat Design Specification Rev. 12, set by California Polytechnic State University.
[5] https://www.nasa.gov/mission_pages/station/research/experiments/908.html

velocity that the satellite gains from the push of the deployer. When the satellite orbits in space, molecules of the atmosphere hit its surface. As Keesee stated (Keesee, 2003) the drag coefficient can be expressed as a relation of the velocities of the molecules that hit the surface of the satellite and those that they are re-emitted from the surface:

$$Cd = -2\frac{v_{re-emitted} - v_{hit}}{v_{hit}} \quad (2)$$

Having accepted that the molecules after hitting the surface they are diffusely re-emitted in random directions (according to one of Sentman's cases) we come to $\upsilon_{\text{re-emitted}} = 0$, so that finally Cd=2. The last parameter of eqn.1 to be determined is the air density at the height of the trajectory which simplified is expressed as follows:

$$\rho = 1.3e^{\frac{-h}{7000}} \quad (3)$$

where h is the trajectory height.

One of the most significant law in physics which is applied at cubesatsis the law of conservation of energy. From the law of conservation of energy:

$$E = \frac{v^2}{2} - \frac{\mu}{r} = -\frac{\mu}{2\alpha} = -\frac{GM}{2\alpha} \quad (4)$$

implies that the orbital speed equals to:

$$v = \sqrt{GM(\frac{2}{r} - \frac{1}{a})} \quad (5)$$

Where G is the standard gravitational parameter, M the mass of the earth, r the radius of the orbit and α the semi-major axis of the elliptical orbit. If we consider the work of F_D as:

$$W_D = F_D \cdot s$$

Then:

$$\frac{dW_D}{dt} = F_D \cdot \frac{ds}{dt} = F_d \cdot v \quad (6)$$

The above rate of change of work is the rate of change of total energy due to drag (as we considered, in this paper, drag as the dominant force exerted on the satellite for deorbiting). The eqn. 4 can be written as

$$E = -\frac{GM}{2\alpha^2}\, a \Longrightarrow \frac{dE}{dt} = -\frac{GM}{2\alpha^2}\frac{d\alpha}{dt} \qquad (7)$$

which is the change of energy in relation to the change of semi-major axis during time dt.

The calculation of orbital velocity is the assumption that drag is the dominant force exerting on our satellite, which leads to acceleration due to drag the only acting one and that it is constant throughout the orbit guides us to the expression of velocity:

$$\upsilon = \upsilon_0 + \alpha t \qquad (8)$$

Where υ is the velocity after time t, υ_0 is the initial velocity, α the acceleration and t the time that the acceleration takes place. We use eqn.5 because we consider the magnitude of the acceleration constant. As mentioned earlier υ_0 is the vectoral addition of the velocity of ISS and the initial push given to the satellite from the deployer. From eqn.1 and Newton's law, the acceleration is:

$$a = -\frac{\frac{1}{2}\rho v^2 ACd}{m} \qquad (9)$$

Now, if we multiply the acceleration from eqn.9 with the initial period (for the first revolution):

$$T = 2\pi\sqrt{\frac{\alpha^3}{\mu}} \qquad (10)$$

we take as a result the change in velocity for our satellite after completing the first orbit. For eqn.10 we consider as initial semi-major axis that of the orbit of the ISS and μ of course is the standard gravitational parameter. So, using eqn.8 we calculate the velocity after the completion of 1 revolution.

Combining equations (1), (6) and (7) we take (concerning the magnitudes):

$$\frac{GM}{2\alpha^2}\frac{d\alpha}{dt} = \frac{1}{2}\rho v^3 ACd \;\Rightarrow\; \frac{d\alpha}{dt} = \frac{a^2 \cdot A \cdot Cd \cdot \rho}{GM} v^3 \qquad (11)$$

From the equqtion eqn.10:

$$T = 2\pi\sqrt{\frac{\alpha^3}{\mu}} \Longrightarrow T^2 = 4\pi^2\frac{a^3}{\mu} \Longrightarrow (T^2)' = \left(4\pi^2\frac{a^3}{\mu}\right)' \Longrightarrow 2T\frac{dT}{dt} = \frac{4\pi^2}{\mu}3\alpha^2\frac{da}{dt} \Longrightarrow$$

$$\frac{4\pi\sqrt{\alpha^3}}{\sqrt{\mu}}\frac{dT}{dt} = \frac{4\pi^2 3\alpha^2}{\mu}\frac{da}{dt} \Longrightarrow \frac{dT}{dt} = \frac{\sqrt{\mu}\cdot 4\pi^2\cdot 3\alpha^2}{4\pi\mu\sqrt{\alpha^3}}\frac{da}{dt}$$

$$= \frac{3\pi\sqrt{\alpha}}{\sqrt{\mu}}\frac{da}{dt} \qquad (12)$$

Substituting eqn.11 to eqn.12:

$$\frac{dT}{dt} = \frac{3\pi\sqrt{\alpha}}{\sqrt{\mu}}\cdot\frac{a^2\cdot A\cdot Cd\cdot\rho}{GM}v^3 \Longrightarrow \frac{dT}{dt} = \frac{3\cdot 2\pi\cdot\alpha^{\frac{5}{2}}\cdot\rho v^3\cdot A\cdot Cd}{2\cdot\mu\cdot\sqrt{\mu}}$$

$$= \frac{3}{2}\cdot\left(2\pi\frac{\alpha^{\frac{3}{2}}}{\mu^{\frac{1}{2}}}\right)\cdot\frac{\alpha\cdot A\cdot Cd\cdot\rho}{\mu}v^3$$

So the rate of change of period becomes:

$$\frac{dT}{dt} = \frac{3}{2}T\frac{a\cdot Cd\cdot A\cdot\rho}{\mu}v^3$$

Finally, the change in orbital period after 1 revolution is:

$$\frac{\Delta T}{T} = \frac{3\cdot\alpha\cdot Cd\cdot A\cdot\rho}{2\cdot G\cdot M}\int v^3 dt \qquad (13)$$

From eqn13 combined with eqn.10 it is calculated the value for the new semi-major axis (a) . From semi-major axis eqn.5 it is calculated the new value for r (for instance r_{apogee} because $r_{perigee}$).

1.3 Cubesats with Propulsion

There is variety of satellites that have been launched in orbit from October 4, 1957 when the Soviet Union rocketed Sputnik into space. This thesis is referred to cubesats which are types of miniaturized satellites for space research that are made up of multiples of 10×10×10 cm cubic units and “small” satellites which weight less than 10 kg. The first of these satellites is the TUBSAT-N from the Technische Universitätin Berlin which weighted 8.5 kg and was launched on July 7, 1998. It was placed at 404 x

770 km, 78.9 deg (orbital characteristics). From that day till April 2, 2018 when the DebrisSat-1 (DS-1, Net, RemoveDEBRIS) Satellite of Surrey Space Centre (United Kingdom) which was placed at ISS Orbit, the total number of satellites that weight less than 10kg and have been launched into orbit are 925.

This thesis concentrates mainly on the potential of cubesats to have a propulsion system installation so as to increase their lifetime in space. The number of cubesats that have been launched with propulsion system is 40, which is the 4.30% of 925 cubesats[6].

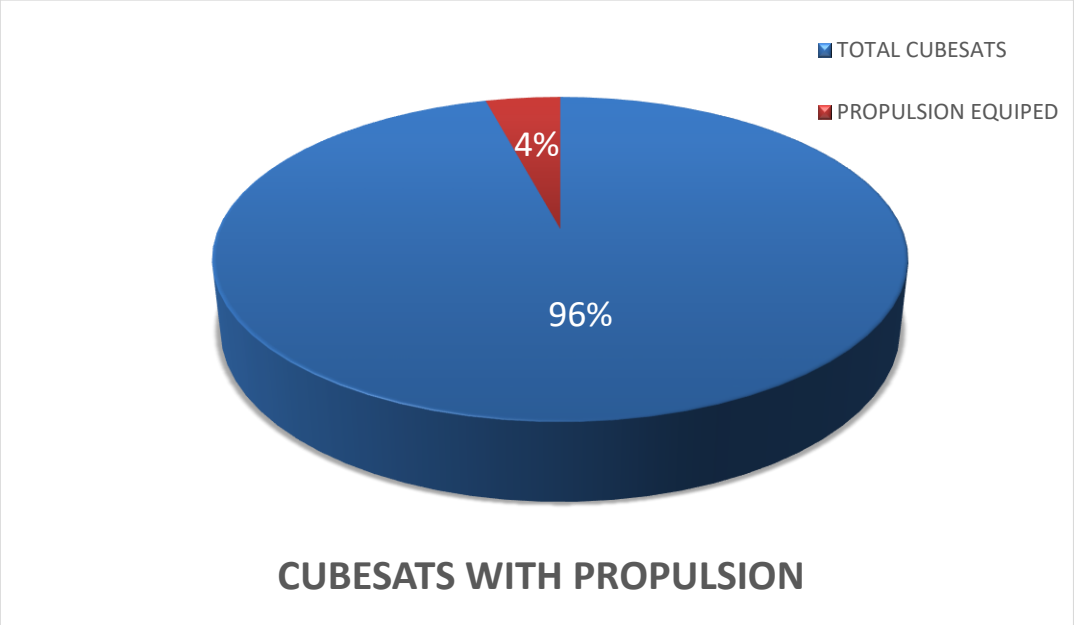

Furthermore there is a variety of propulsion systems. The systems that have been used in cubesats are:

1. Cold Gas
2. Electrospray
3. Pulsed Plasma
4. Ion
5. Solid
6. Laser
7. Liquid

[6] https://www.nanosats.eu/

The following diagram presents a percentage analysis of the propulsion systems that have been used in the 40 satellites since April 2, 2018[7].

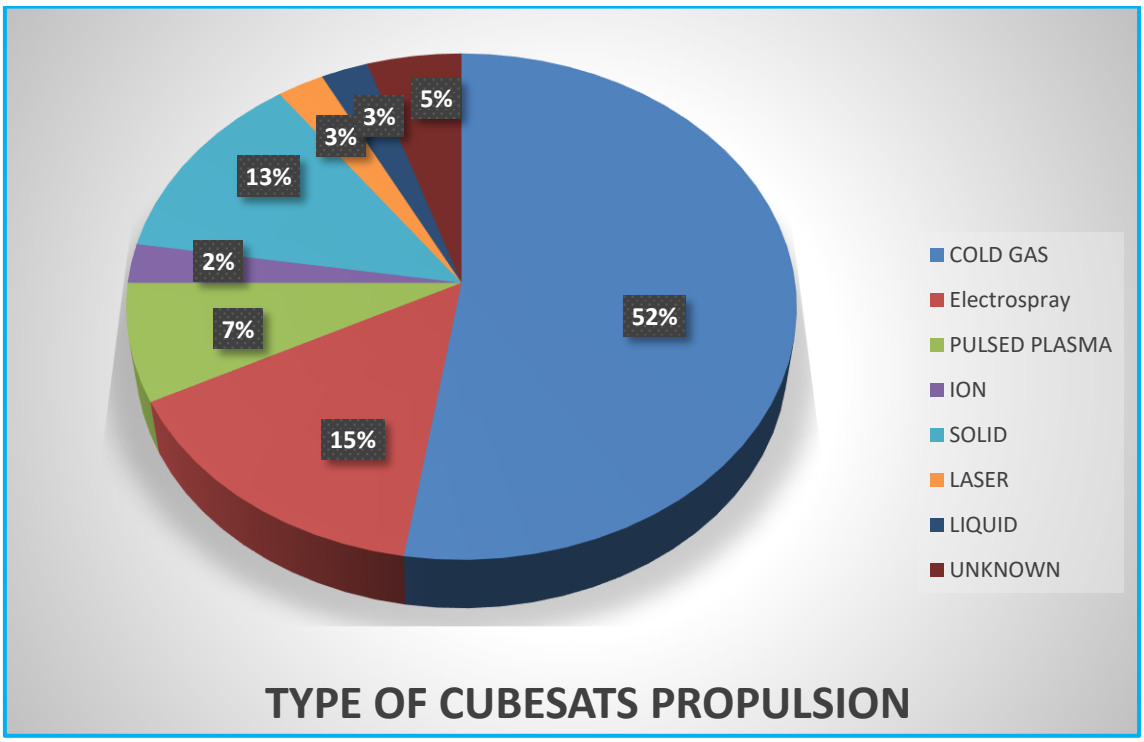

Half of propulsion equipped satellites are with Cold gas (52%).The Electrospray cubesats are 6 (15%).The Solid ones are 5 (13%).The Pulsed Plasma ones are 3 (7.5%). There is one ION, Laser and Liquid (2.5% respectively). There are also 2 "Unknown" cubesats with propulsion (5%). So one observes that most of cubesats are cold gas (21 cubesats) and there is tendency in the use of electric and plasma propulsion (22.5% in total).

1.3.1 Organization

The cubesats with propulsion system are produced by a variety of organizations. The Military cubesats are 10 and they constitute 25% of the total. Companies and universities have produced 8 cubesats, each of which constitutes 20%. Institutes with 7 cubesats have played an important role by having produced 17.5% of the total. The Aerospace Corporation has produced 7 cubesats with a variety of propellants (Solid rockets motors, ION-Electrospray and Cold gas), which also constitute 17.5% of the

[7] https://www.nanosats.eu/

total. The Aerospace Corporation has launched cubesats from 2008. Most of them are 1.5U (1U is the main cubesat with its payload and at the other 0.5U is installed in the propulsion system). So the installation of propellant in a cubesat, analyzing the Aerospace Corporations missions, demands at least 0.5U space[8].

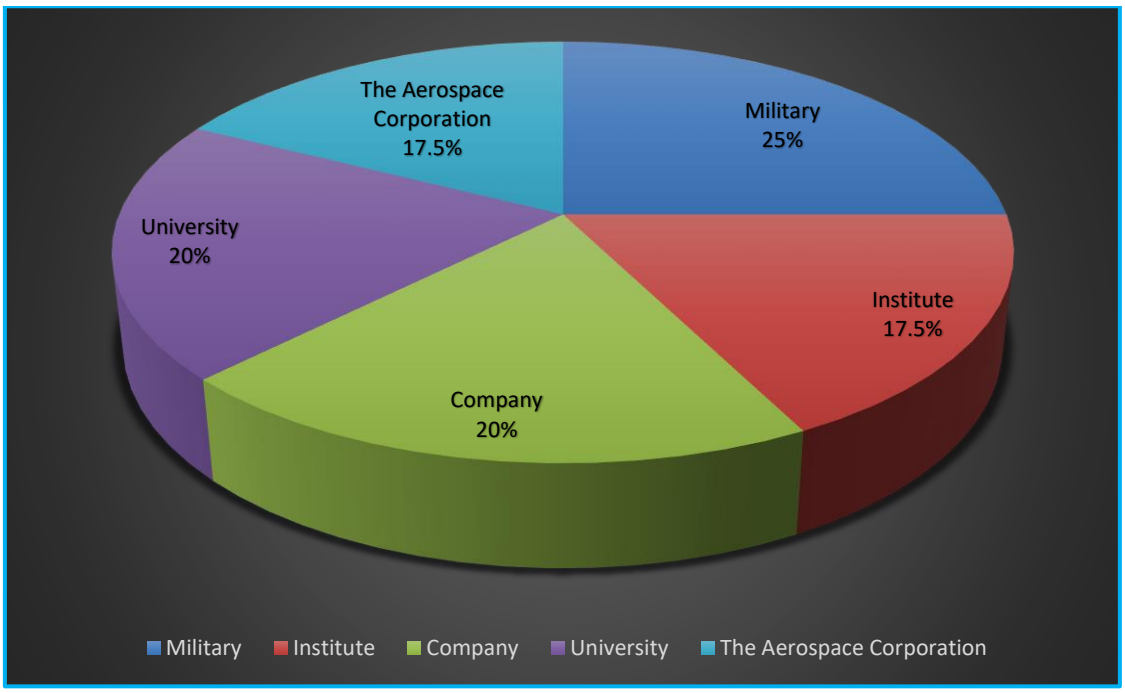

[8] https://www.nanosats.eu/

1.3.2 Cubesats by Nations

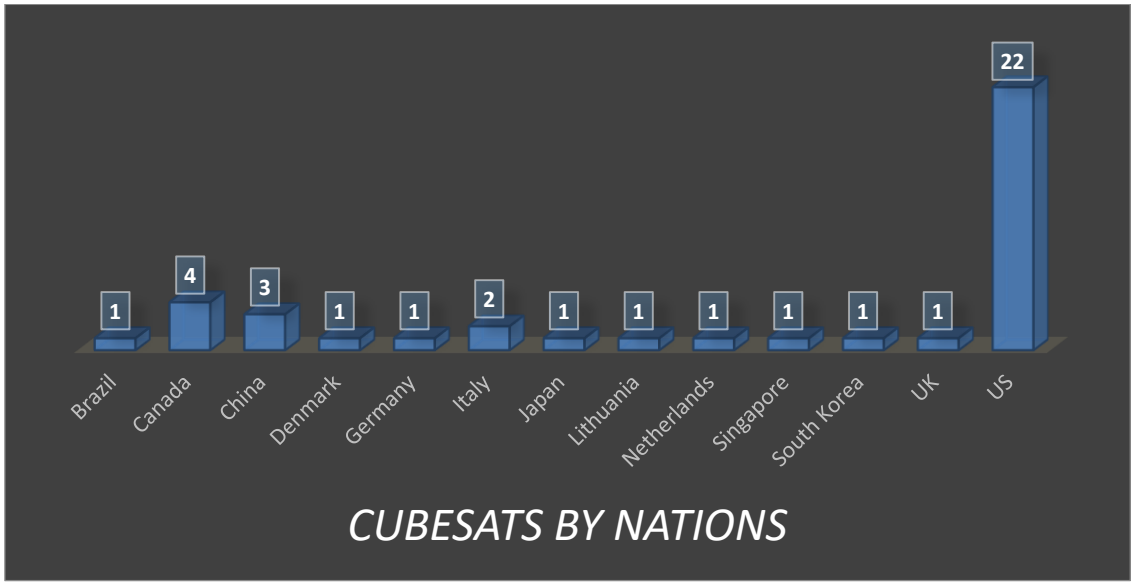

Most of cubesats with propulsion system that have been launched till April, 4, 2008 were from the **United States of America**[9]. More than half of these cubesats (22 in number) are from United States, **Canada** follows with 4 cubesats. Third country is **China** with 3 satellites and **fourth** is Italy with 2. There are also other nations that have executed one mission with propulsion system. These are:

1. Brazil
2. Denmark
3. Germany
4. Japan
5. Lithuania
6. Netherlands
7. Singapore
8. South Korea
9. United Kingdom

[9] https://www.nanosats.eu/

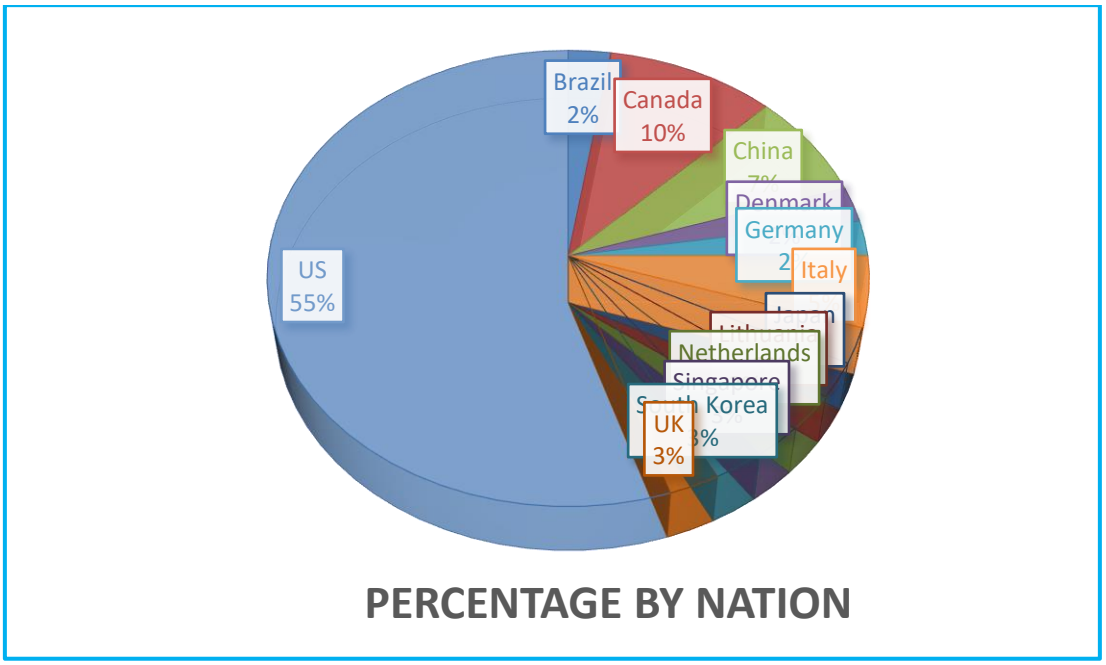

So it is obvious that U.S. plays significant role in propulsion systems of cubesats. From the 22 U.S. cubesats 10 have Cold Gas propellants, 5 Solid Motors, 6 were Electric and 1 Unknown. Therefore approximately half of U.S. cubesats propellants are installed wih Cold Gas propulsion system. All four (4) cubesats from Canada have also Cold Gas propellants. So it is noticed that the most ‘‘preferred’’ propulsion system is the Cold Gas[10].

[10] https://www.nanosats.eu/

1.3.3 Dimensions of Cubesats

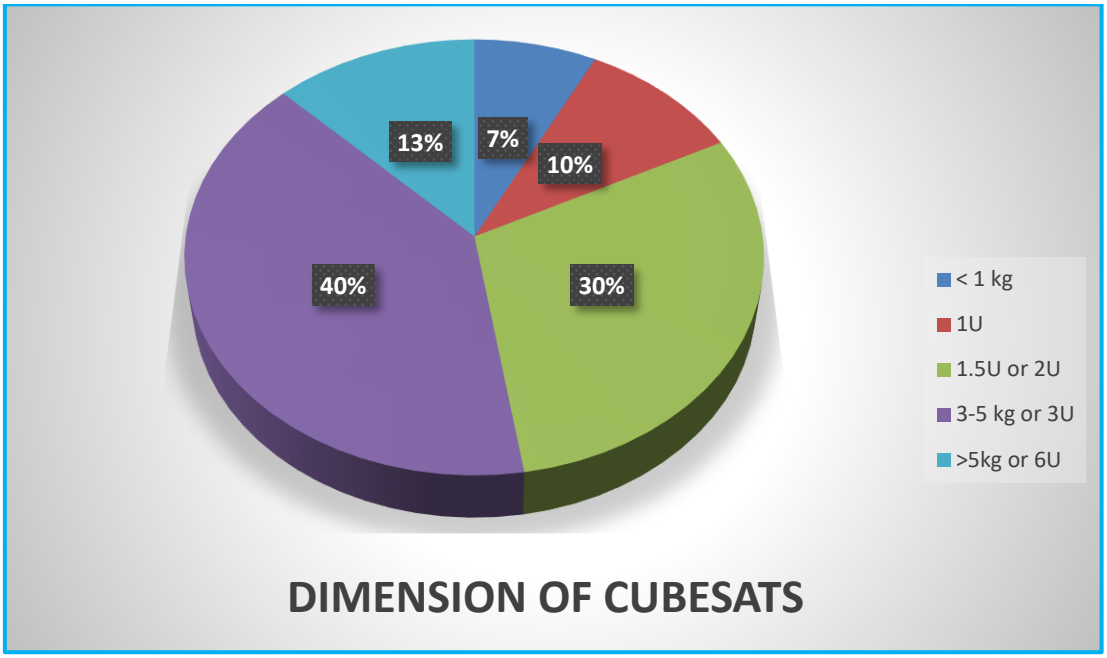

It was mentioned previously that most of cubesats constructed by Aerospace Corporation were at least 1.5U. This observation is confirmed by the upper diagram where the 1U or below 1 kg cubesats where only 17%. The cubesats with dimensions 1.5 and 2U are 12 in number, which is 30% overall. The majority of cubesats with propellants (40%) are 3-5kg or 3U. Cubesats above 5kg or 6U are 5 (13%). The summary of satellites above 1.5U to 6U is the 83% out of all 40. The installation of a propulsion system at a satellite demands at least 0.5U space and is used more in 3U cubesats. So 1U volume is the most ‘‘preferred’’ space for propellants’ installation. Even a 6U cubesat provides more space than a 1.5U or a 3U, it is observed higher concentration at 3U satellites[11].

[11] https://www.nanosats.eu/

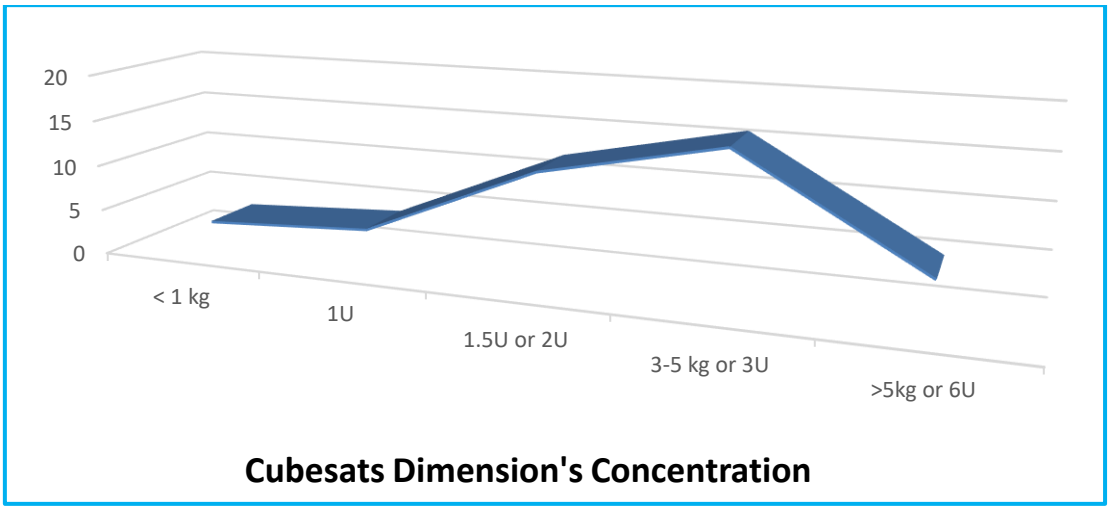

1.3.4 Year of Launch

The first cubesats with propulsion system were launched at January, 27, 2000. They were MEMS 1A (Pico 21, PICOSAT-1) and MEMS 1B (Pico 23, PICOSAT-1) from DARPA. Their mission objective was the demonstration of the basic functional elements of a low-power LEO "swarm" or formation PICOSAT array. To communicate from space they use node-type radios and to report the results of MEMS-switched tests. These 2 satellites built by Aerospace Corporation, sponsored by DARPA. At 2002another 2 satellites were set in orbit by DARPA. They were MEPSI 1A (MEMS-based PicoSat Inspector) and MEPSI 1B (MEMS-based PicoSat Inspector). Their mission objective was the demonstration of deploying an onboard miniature autonomous inspector, tasked to conduct visual inspection of the host satellite. Their propulsion system was cold gas with 5 thrusters (with 0.1N thrust each of them). From 2006 till 2013 the cubesats launch is constant. Until 2013 they had launched 14 cubesats. At the beginning of 2014 a high increasing in launches was observed. From 2014 until 2016 the cubesats which were launched were 14 (the same number until 2013). From 2017 till February 2, 2018 (only 14 months) the launches were 10[12].

[12] https://www.nanosats.eu/

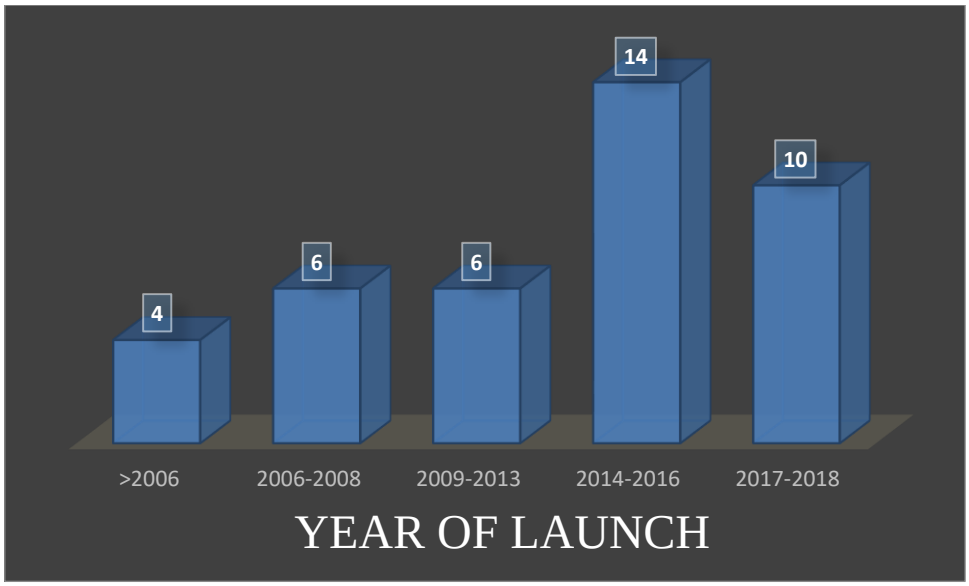

So in the beginning the use of propulsion systems was not so common. The necessity of increasing the lifetime of a cubesat has led to the development of thrusters.[13]

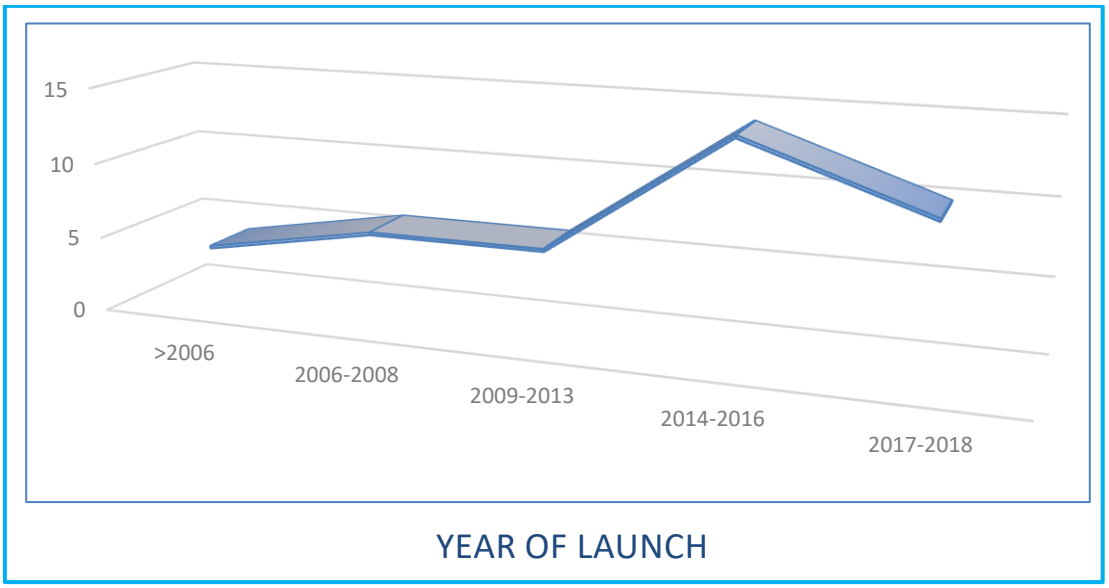

[13] https://www.nanosats.eu/

Even it is noticed a reduction at 2017-2018 the research stops at February, 2, 2018. So in only 14 months the launches were 10 which a high number relative with the previous years. So in the year of launches change the diagram will become:

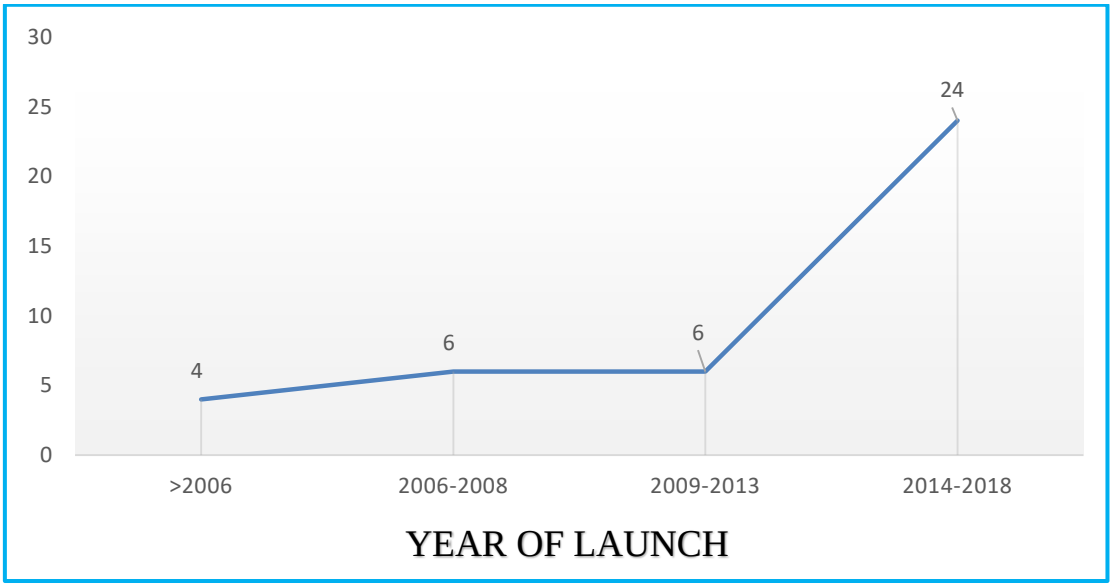

From this analysis it is noticed that **60%** out of 40 cubesats have been placed into orbit the last 4 years. In conclusion more and more have installed a propulsion system.

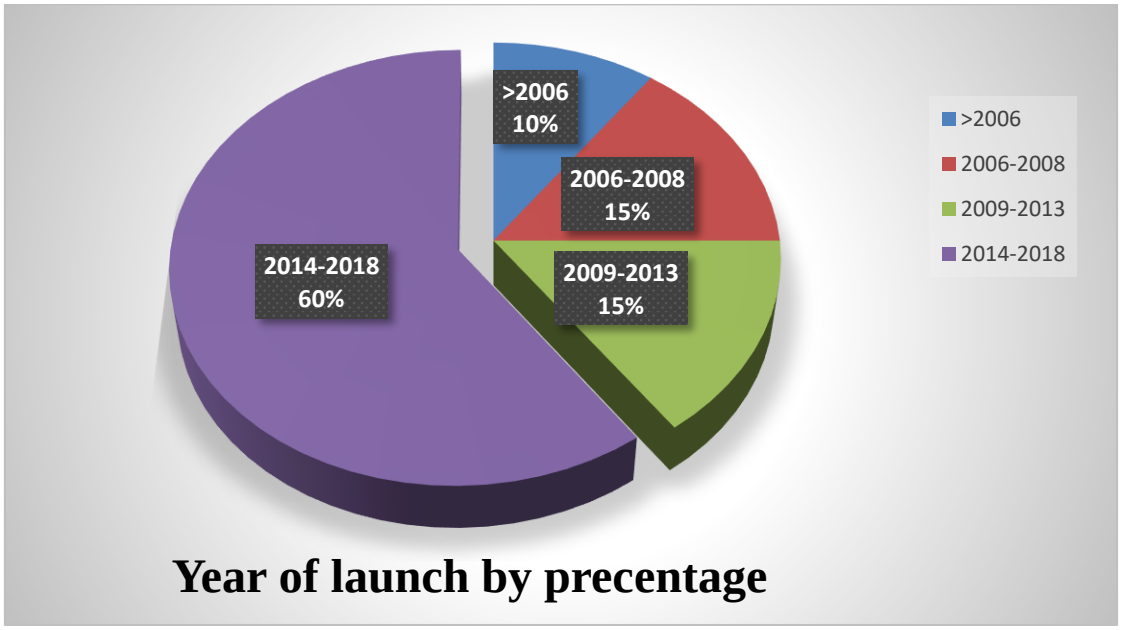

1.3.5 Orbit Height

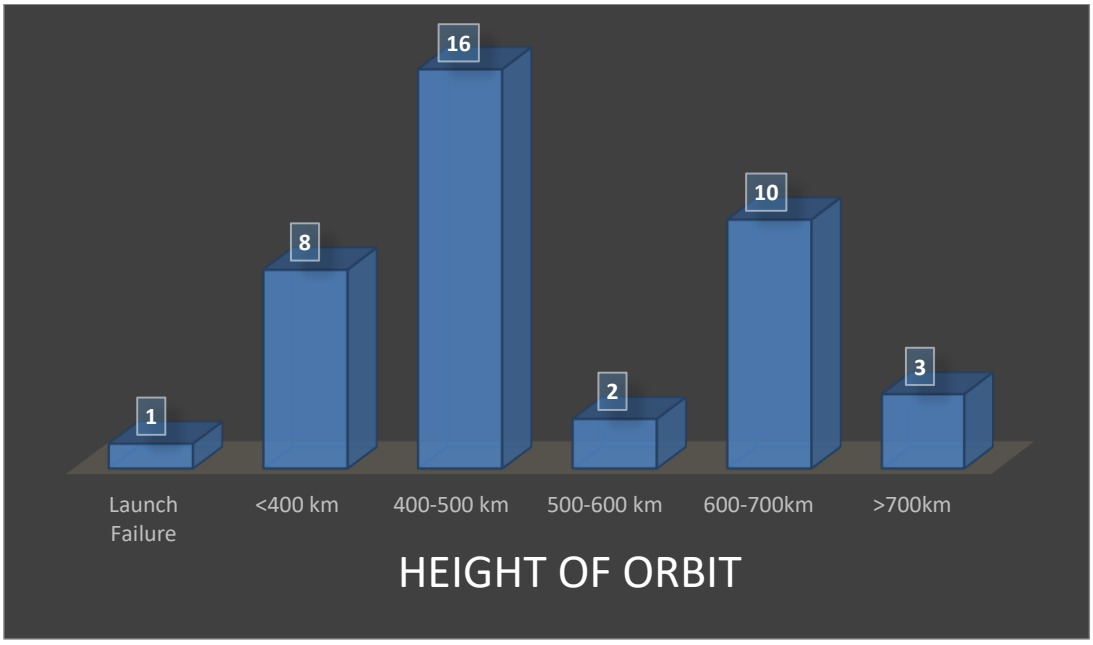

From the 40 cubesats which had thrusters only 1 had a launch failure. It was a 2U cubesat called ION. This satellite had a new MicroVacuum Arc Thruster (μVAT) with high dynamic range. Furthermore some other mission objectives were the Oxygen measuring air glow emissions from the Earth's mesosphere, a new SID processor board testing and small CMOS camera for Earth imaging[14].

[14] https://www.nanosats.eu/

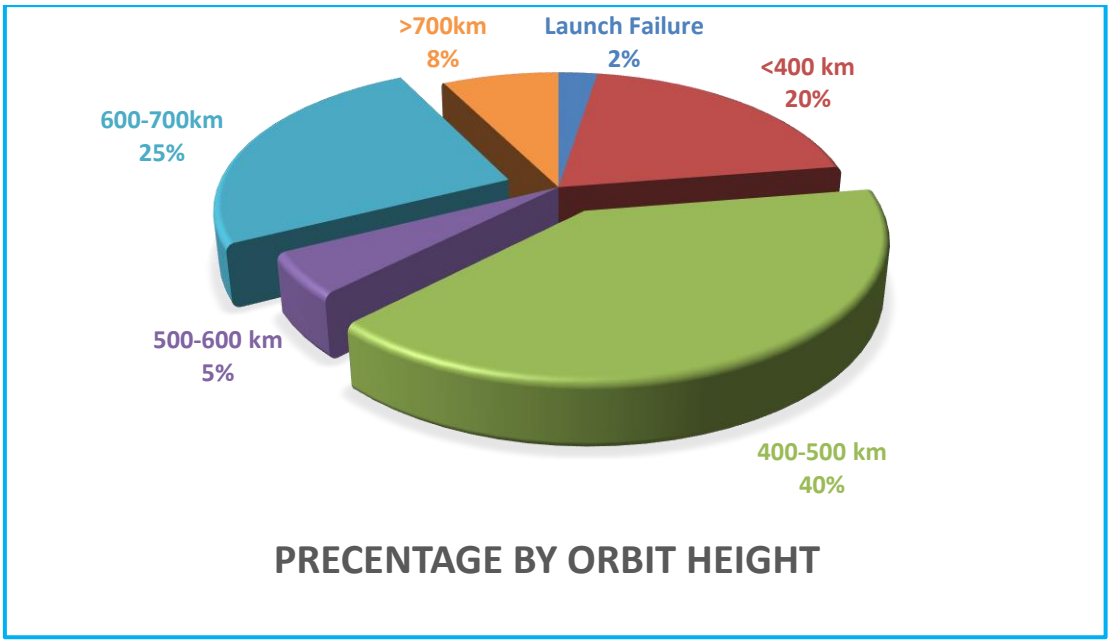

From the diagram above one notes that **20%** of cubesats' height is below 400km. The highest concentration is at 400-500km which is **40%.** At 600-700km one notices an increase (**25%** of cubesats). There is a reduction above 700km **8%** (only 3 satellites). There are only 2 cubesats at 500-600km (**5%**). The first was NanoACE a 3U cubesat which launched on July 14, 2017 and had8 cold gas thrusters. Its objectives were to validate the endeavor suite technologies that will be used for future missions and is solely for the purpose of internal Tyvak development as an attitude control experiment. The second was CANYVAL-X 2U Tom 2U satellite (which was divided to 2 cubesats) from Yonsei University launch on January 12, 2018 and was a Corporation between Korean Aerospace Research Institute and NASA. Its objective was the use of virtual telescope alignment. The two cubesats maintain Inertial-hold in about 10 min using vision alignment system. This could pave the way for a new class of instrument that can peer through the sun's glare or at distant alien planets, without requiring a massive single scope[15].

[15] https://www.nanosats.eu/

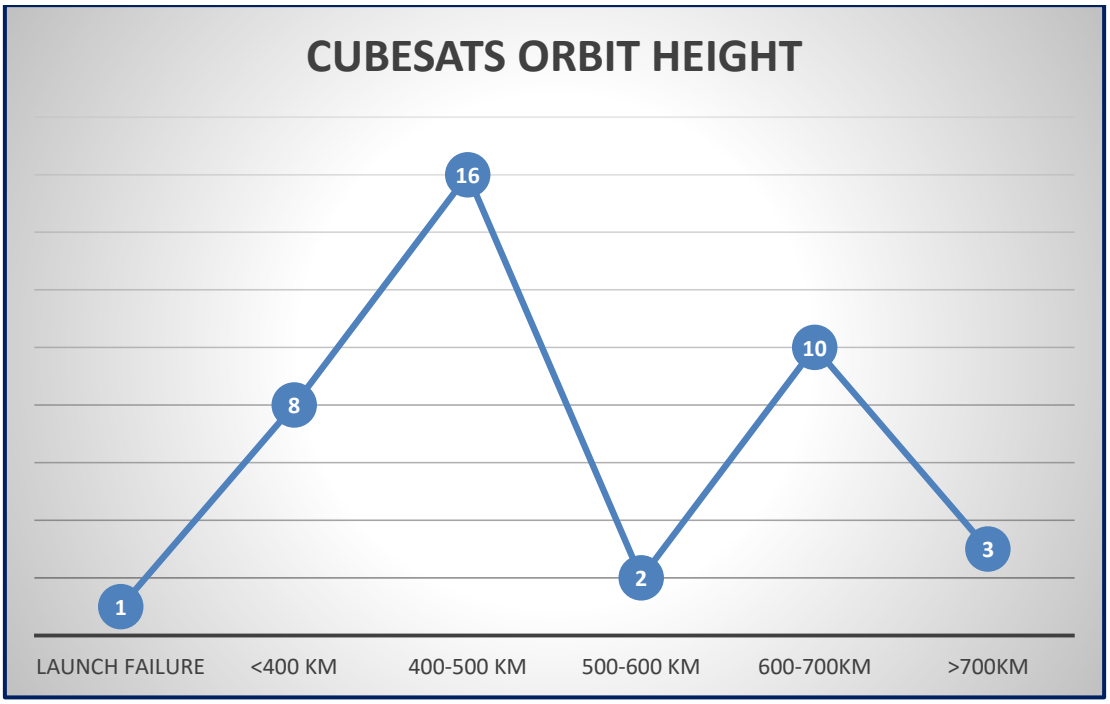

From the upper diagram the highest concentration is at 400-500km which is near ISS orbit. This occurs because most cubesats are launched from NanoRack CubeSat Deployer

One also notices a concentration of 600-700km (**25%**). Most of the thrusters at this orbit are cold gas. At this height took place the first mission of laser ignition thruster. It was KKS-1 (KoukuKosen Satellite-1, KISEKI) a 3.17 kg satellite from Tokyo Metropolitan College of Industrial Technology. Its objective were the attitude controls by small reaction wheel and photographs by a CMOS camera（320×240 pixel color). KKS-1 carries messages from supporters to space[16].

In conclusion, it is noticed that the most ‘‘preferred’’ orbit height for a cubesat with thruster is at 400-500km (which is ISS orbit).

[16] https://www.nanosats.eu/

1.4 Satellite Lifetime

1.4.1. Duration of a satellite mission

The duration of a satellite mission is a very significant factor. The prediction of satellite's entry into the atmosphere constitutes the operational time of the satellite. The basic factors that lead to altitude loss are the atmospheric drag, the solar radiation flux and disturbed magnetosphere conditions. This section of the write-up simulates the lifetime of a 1.5U, 3U and 6U cubesat. Supposing that cubesat is launched from ISS, the initial altitude of simulations will be approximately from 450 km to 385 km. The atmospheric drag is calculated from the following equation:

$$D = \frac{1}{2}\rho v^2 ACd$$

Where D is the drag force, ρ is the atmospheric density at the height of the trajectory, υ is the satellite's speed, A is the cross-sectional area perpendicular to the direction of the motion and Cd is the drag coefficient. The drag coefficient (Cd) is approximately for the cubesat 2.2. The cross-sectional area (A) is 0.015 m^2, 0.03m^2 and 0.06 $m^2$for 1.5U, 3U and 6U cubesat.

The solar radiation flux measures mean solar electromagnetic radiation (solar irradiance) per unit area. At the simulations the F10.7cm values will be used. The value of F10.7cm = 68.88888889 which is the average value of November 5, 2018 to December 19, 2018 (45 days) according to USAF table. The table is at Appendix B1.

The disturbed magnetosphere conditions are relative with the cubesat lifetime. At the simulations it will be used the Ap* values. The value of Ap*= 7.822222 which is the average value of November 5, 2018 to December 19, 2018 (45 days) according to USAF table. The table is presented in the Appendix.

1.4.2 1st Simulation: Satellite Orbital Decay Calculations (circular orbit 450km)

The Australian Government Bureau of Meteorology has published the Satellite Orbital Decay Calculations article[17] which is a simple simulation on how to calculate orbital lifetimes of satellites for low earth orbits (below 500km). This article has used a model written in QBASIC program language. In the current simulation there is a translation from QBASIC to Matlab program language. The program's function ends below 200 km which constitutes practically the atmosphere. The code written is presented in the Appendix. In this code there is reaction only in five variables. First at satellite's mass and satellite's area, the initial altitude, the solar radiation flux and the geomagnetic index.

The simulation in this program has 3 scenarios. In the first, the satellite **1.5U** begins its mission at 450 and its characteristics are:

```
M = 1.5; %satellite mass (kg)
A = 0.015; %satellite area (m^2)
H = 450; %starting height (km)
F10 = 68.88889; %solar radio flux
Ap = 7.822; %geomagnetic index
```

So with these values the cubesat orbital decay prediction is **2158 days.**

In the second, the satellite **3U** begins its mission at 450 and its characteristics are:

```
M = 3; %satellite mass (kg)
A = 0.03; %satellite area (m^2)
H = 450; %starting height (km)
F10  = 68.88889; %solar radio flux
Ap = 7.822; %geomagnetic index
```

So with these values the cubesat orbital decay prediction is again **2158 days.**

[17]http://www.sws.bom.gov.au/Category/Educational/Space%20Weather/Space%20Weather%20Effects/SatelliteOrbitalDecayCalculations.pdf

In the third scenario the satellite **6U** begins its mission at 450 and its characteristics are:

```
M = 6; %satellite mass (kg)
A = 0.06; %satellite area (m^2)
H = 450; %starting height (km)
F10 = 68.88889; %solar radio flux
Ap = 7.822; %geomagnetic index
```

So with these values the cubesat orbital decay prediction is again **2158 days.**

This similarity in the 3 scenarios occurs because more mass increases the lifetime of cubesat because it increases the momentum so the Rate of Change of momentum (which is Force) and the cross-sectional area (A) increases the Drag force which is one basic factor of Height reduction.

1.4.3 2nd Simulation: Matlab Tool for Orbital Decay (elliptical orbit 450 km)

The Matlab Tool for Orbital Decay: **compute Orbital Decay [18](a,e,A,Cd,m0,F107,Ap)** uses more variables such us the eccentricity and coefficient drag. As eccentricity one inserts the value of ISS (e=0.0003390) and for coefficient drag Cd=2.2. The program prints a diagram with the cubesat begins its mission at 450km, 425km, 400km and 375km and stops at 180km. The program is written in Matlab and the code is written in the Appendix.

The analysis simulate this code again with the same 3 scenarios. In the first, the satellite **1.5U** weights 1.5kg and the characteristics of simulation are:

```
a = Re+(375:25:450);Semi-Major Axis (km)
m0 = 1.5; %Satellite Mass (kg)
A = 0.015; %Effective Area (m^2)
e = 0.0003390; %Eccentricity
Cd = 2.2; %Coefficient of Drag
F107 = 68.8889; %F10.7 Solar Radio Flux
Ap = 7.822222222; %Geomagnetic Index
```

[18]https://www.mathworks.com/matlabcentral/fileexchange/55371-vectorized-orbital-decay-routine-for-space-objects-between-180-and-500-km-altitude

The program presents the following results:

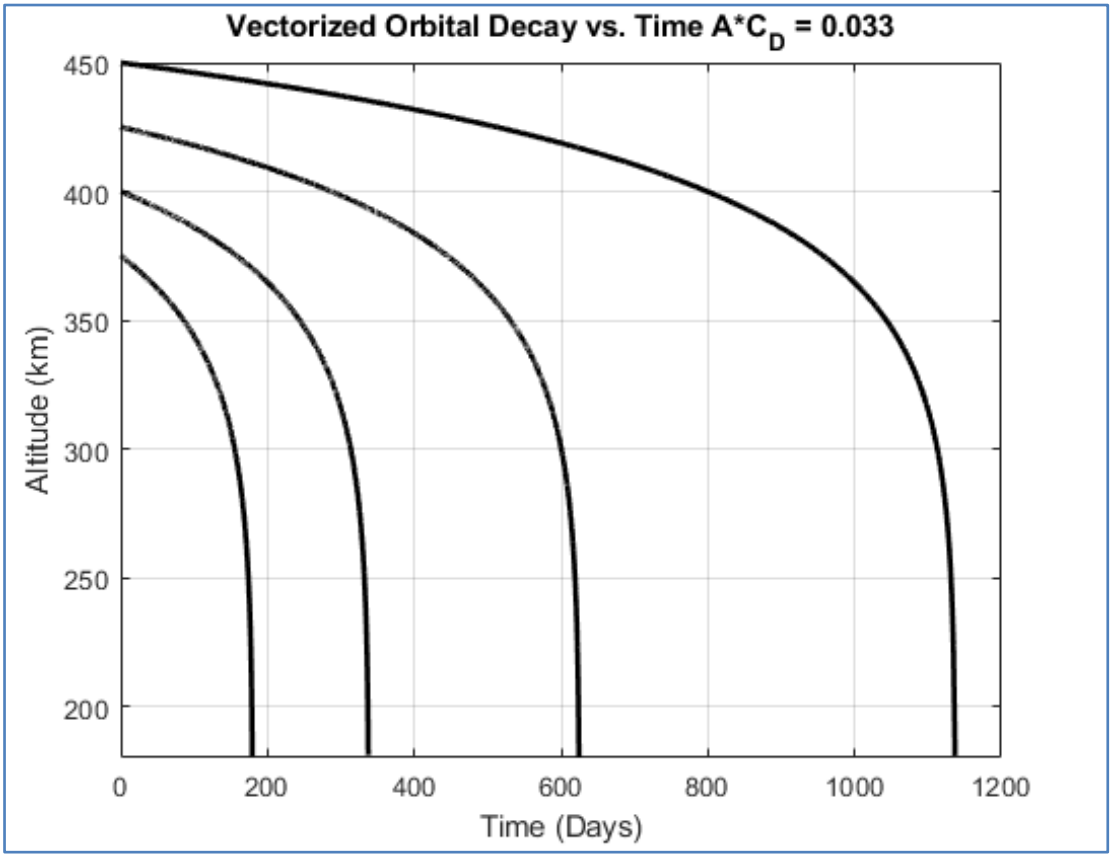

In the second, the **3U** satellite weights 3kg and the characteristics of simulation are:

```
a = Re+(375:25:450); %Semi-Major Axis (km)
m0 = 3; %Satellite Mass (kg)
A = 0.03; %Effective Area (m^2)
e = 0.0003390; %Eccentricity
Cd = 2.2; %Coefficient of Drag
F107 = 68.8889; %F10.7 Solar Radio Flux
Ap = 7.822222222; %Geomagnetic Index
```

The program presents the following results:

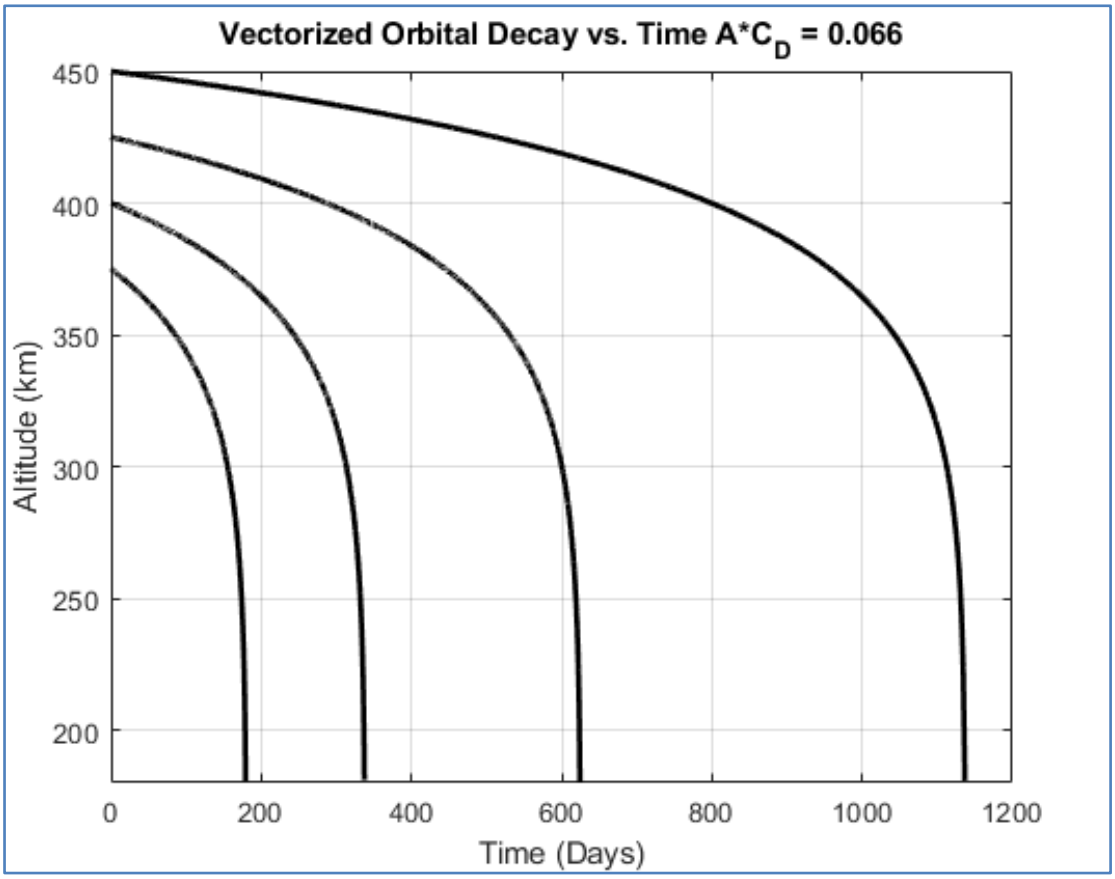

In the third, the **6U** satellite weights 6kg and the characteristics of simulation are:

```
a =  Re+(375:25:450);%Semi-Major Axis (km)
m0 =6; %Satellite Mass (kg)
A = 0.06; %Effective Area (m^2)
e = 0.0003390; %Eccentricity
Cd = 2.2; %Coefficient of Drag
F107 = 68.8889; %F10.7 Solar Radio Flux
Ap = 7.822222222; %Geomagnetic Index
```

The program presents the following results:

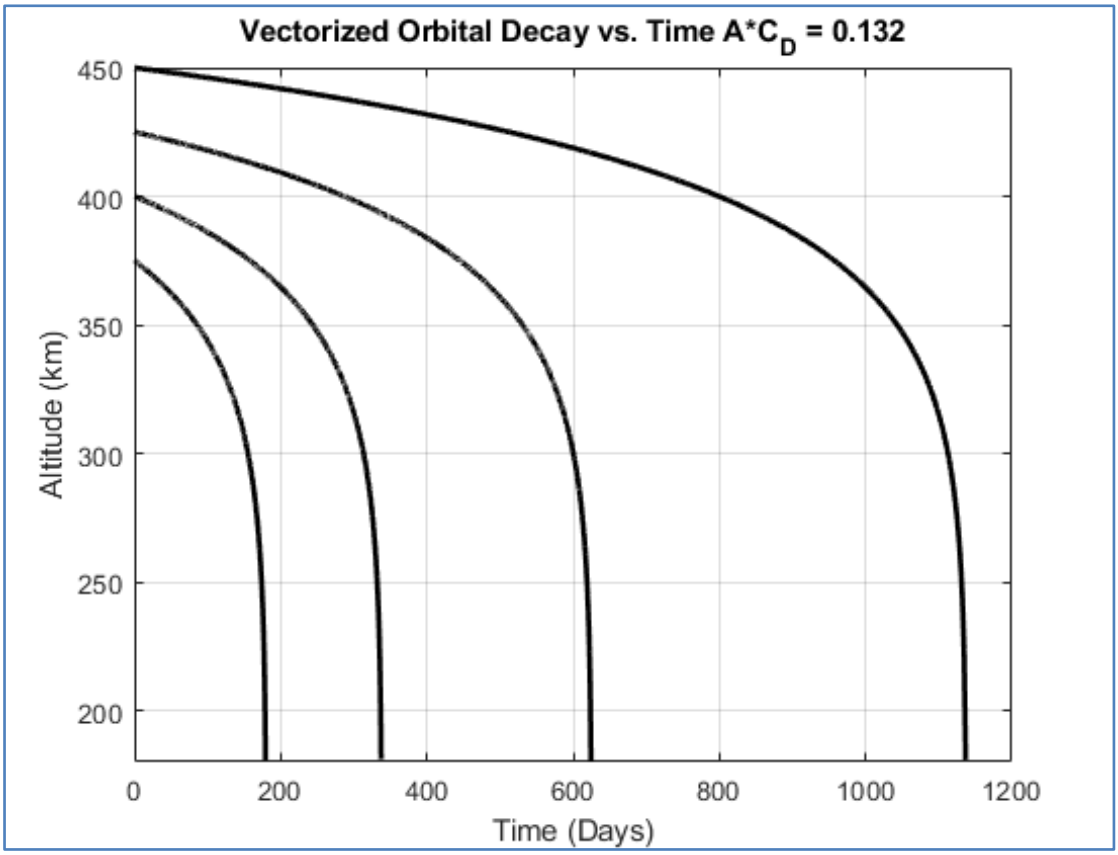

This similarity in the 3 scenarios diagrams occurs again because more mass increases the lifetime of cubesat because it increases the momentum so the Rate of Change of momentum (which is Force) and the cross-sectional area (A) increases the Drag force which is one basic factor of Height reduction. In this simulation the elliptical orbit predicts approximately **1175** days lifetime in all 3 scenarios.

1.4.4 3rd Simulation: Comparison between 2 programs at 450 km circular orbit

If the eccentricity becomes e=0 (circular orbit) as in the first code the program for a satellite **1.5 U,** which weights 1.5kg and the characteristics of simulation are:

```
a = Re+450; %Semi-Major Axis (km)
m0 = 1.5; %Satellite Mass (kg)
A = 0.015; %Effective Area (m^2)
e = 0.0003390; %Eccentricity
Cd = 2.2; %Coefficient of Drag
```

```
F107 = 68.8889; %F10.7 Solar Radio Flux
Ap = 7.822222222; %Geomagnetic Index
```

The program presents the following results:

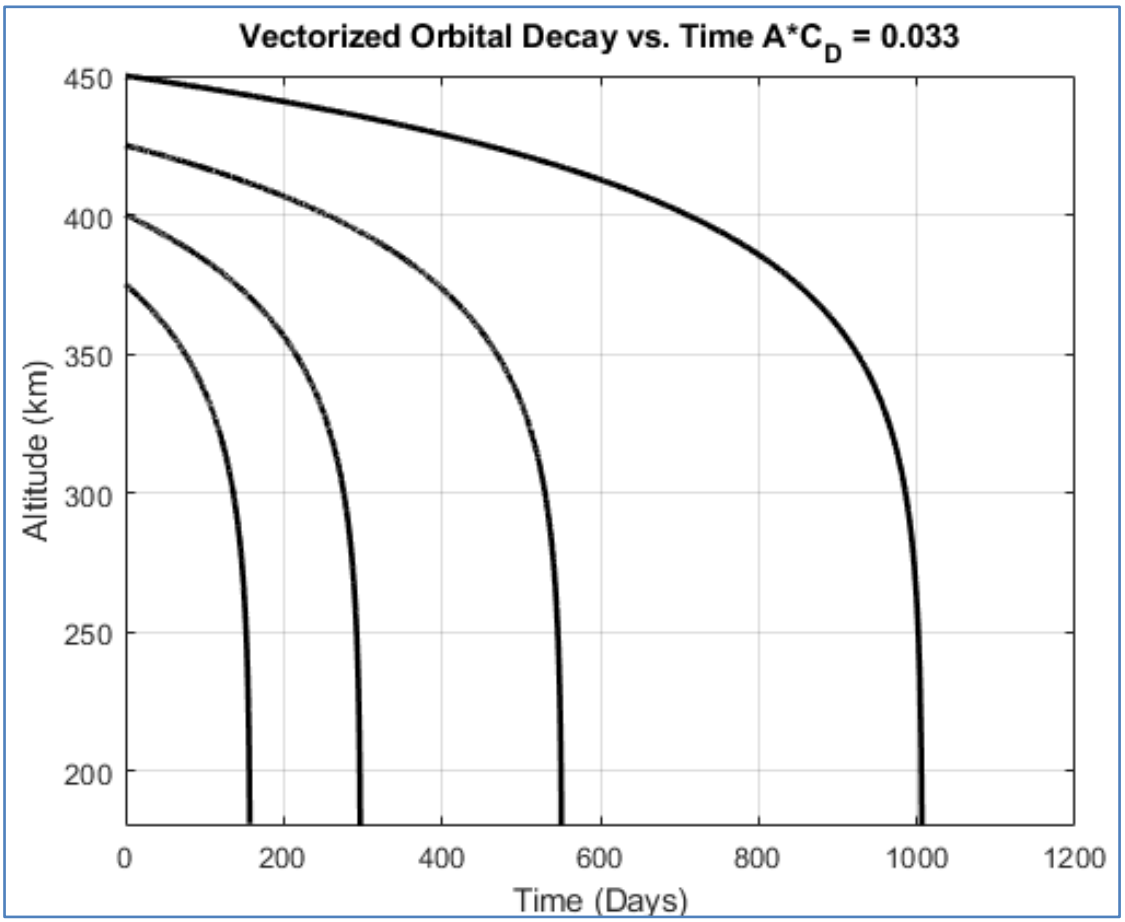

So in comparison with the first code from the Australian Government Bureau of Meteorology the lifetime of the same cubesat at same orbit (circular orbit at 450 km) is approximately the half. The first gave **2158** days lifetime and the second (the diagram) calculates approximately **1050** days

.

1.4.5 4th Simulation: Comparison between 2 programs at 500 km circular orbit

In the Australian Government Bureau of Meteorology prediction of lifetime with the following values:

```
M = 1.5; %satellite mass (kg)
A = 0.015; %satellite area (m^2)
H = 450; %starting height (km)
F10 = 68.88889; %solar radio flux
Ap = 7.822; %geomagnetic index
```

The cubesat orbital decay prediction is **6871.6 days.**

At the Matlab Tool for Orbital Decay prediction with following values:

```
A = Re+500; %Semi-Major Axis (km)
m0 = 1.5; %Satellite Mass (kg)
A = 0.015; %Effective Area (m^2)
e = 0; %Eccentricity
Cd = 2.2; %Coefficient of Drag
F107 = 68.8889; %F10.7 Solar Radio Flux
Ap = 7.822222222; %Geomagnetic Index
```

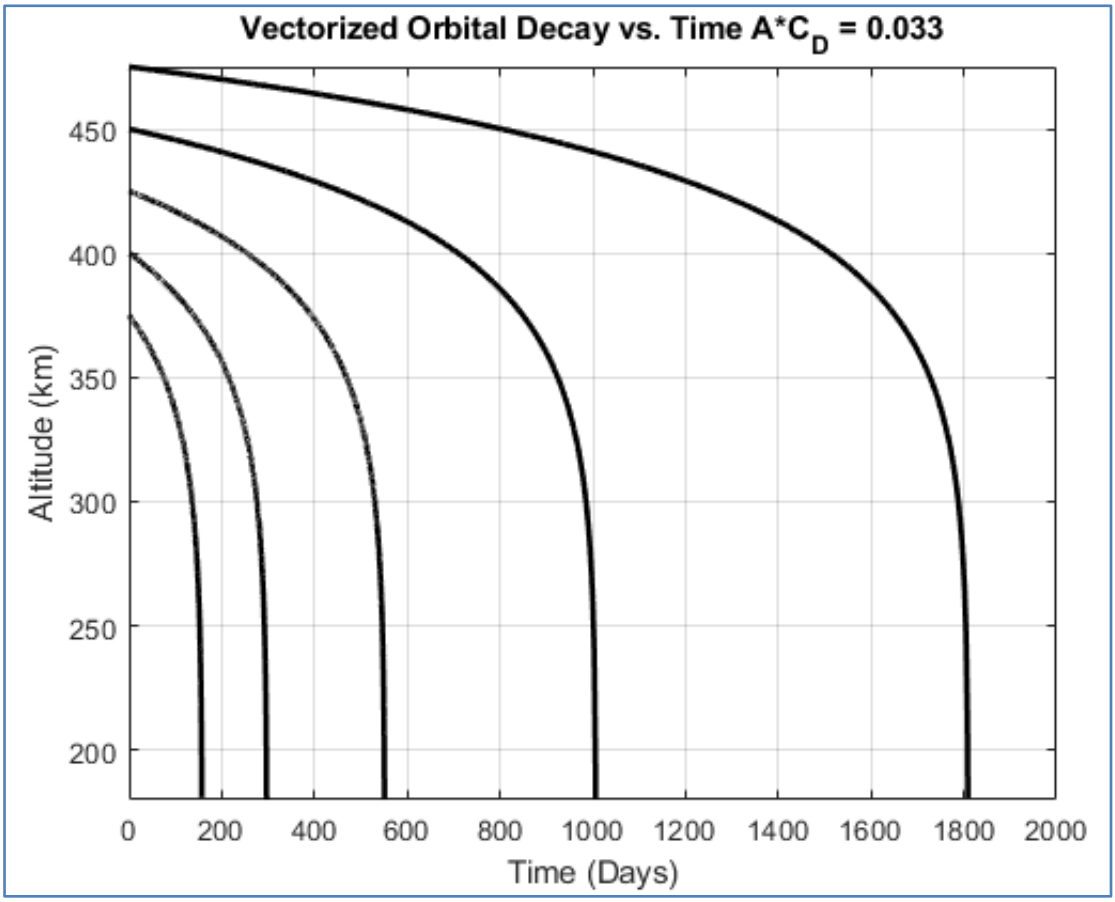

So in comparison with the first code from the Australian Government Bureau of Meteorology the lifetime of the same cubesat at same orbit (circular orbit at 500 km) is approximately one fourth. The first gives **6871.6**days lifetime and the second (the diagram) calculates approximately **1850** days.

1.4.6 5th Simulation: Matlab Tool for Orbital Decay (elliptical orbit 500 km)

In the Matlab Tool for Orbital Decay prediction with following values:

```
a = Re+500; %Semi-Major Axis (km)
m0 = 1.5; %Satellite Mass (kg)
A = 0.015; %Effective Area (m^2)
e = 0.000339; %Eccentricity
Cd = 2.2; %Coefficient of Drag
```

```
F107 = 68.8889; %F10.7 Solar Radio Flux
Ap = 7.822222222;%Geomagnetic Index
```

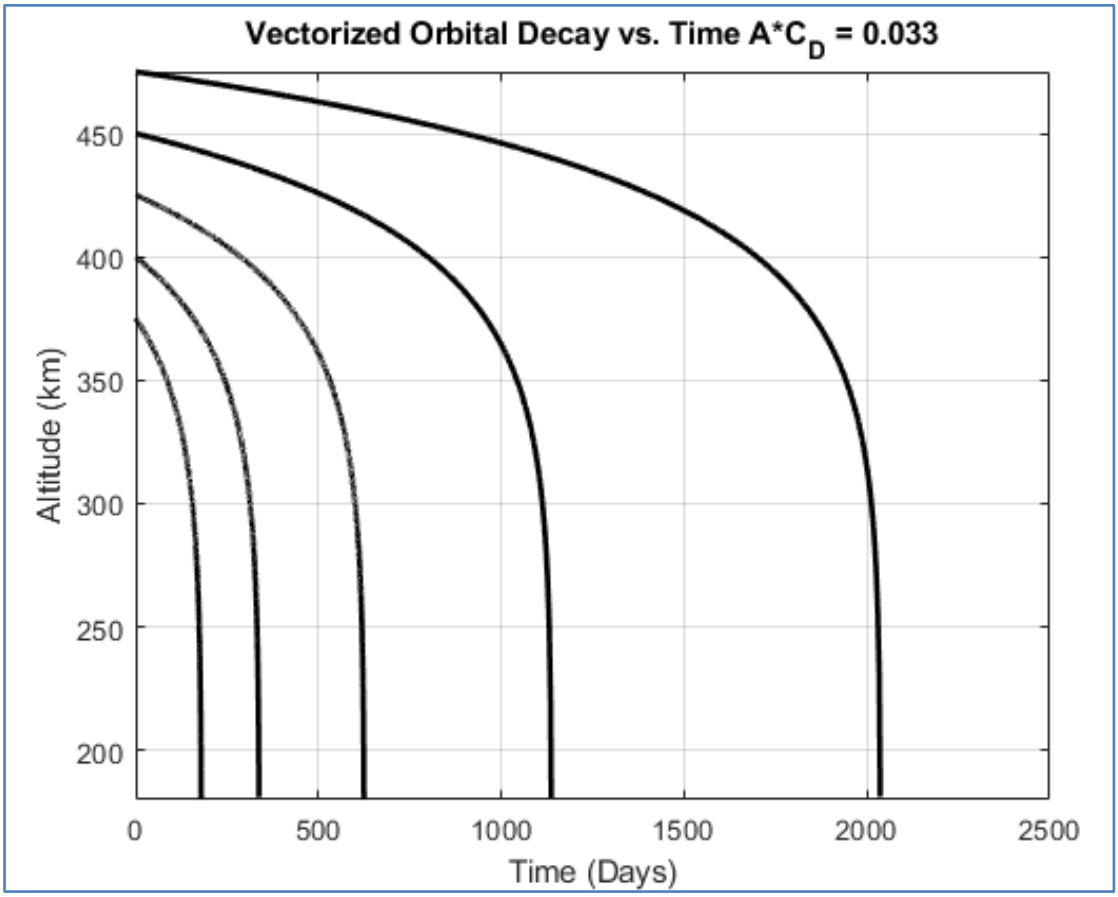

So the lifetime at 500 km with elliptical orbit is approximate **2050 days** which increases the lifetime for **200 days** in comparison with the circular orbit (**1850 days**).

1.4.7 ORBITAL MECHANICS for Engineering Students MATLAB lifetime calculation

This is a program written in MATLAB from the book Orbital Mechanics for Engineering Students (Curtis, H.D. Orbital Mechanics for Engineering Students. 3rd Edition). It calculates the lifetime of satellite taking under consideration a number of parameters. The program is functioning simultaneously with other programs so as to

provide the total lifetime of satellite. It is more accurate because the user is able to insert a variety of orbital characteristics. The variables of A (satellite area (m^2)) and M (satellite mass) are proportional. So in these programs simulations the changing variable will be **only** the orbital height. For the other orbital characteristics it is assumed that the satellite has the same with the ISS (1.20.2019)[19].

```
hours = 3600;                %Hours to seconds
days = 24*hours;             %Days to seconds
deg = pi/180;                %Degrees to radians%...Constants;
mu = 398600;                 %Gravitational parameter (km^3/s^2)
RE = 6378;                   %Earth's radius (km)
wE = [ 0 0 7.2921159e-5]';   %Earth's angular velocity (rad/s)

            %...Satellite data:

CD = 2.2;                    %Drag coefficient
m = 3;                       %Mass (kg)
A = 0.03*(1^2) ;             %Frontal area (m^2)

        %...Initial orbital parameters (given):
rp = RE + ***;               %perigee radius (km)
ra = RE + ***;               %apogee radius (km)
RA = 12.8462*deg;            %Right ascension of the node (radians)
i =51.6398*deg;              %Inclination (radians)
w = 288.3162*deg;            %Argument of perigee (radians)
TA = 330.1464*deg;           %True anomaly (radians)
```

1.4.7.1 6th Simulation: Orbital height 380km

Inserting the orbital parameters below.

```
%...Initial orbital parameters (given):
rp = RE + 380; %perigee radius (km)
ra = RE + 400; %apogee radius (km)
```

[19] https://heavens-above.com/orbit.aspx?satid=25544

The program presents the following results:

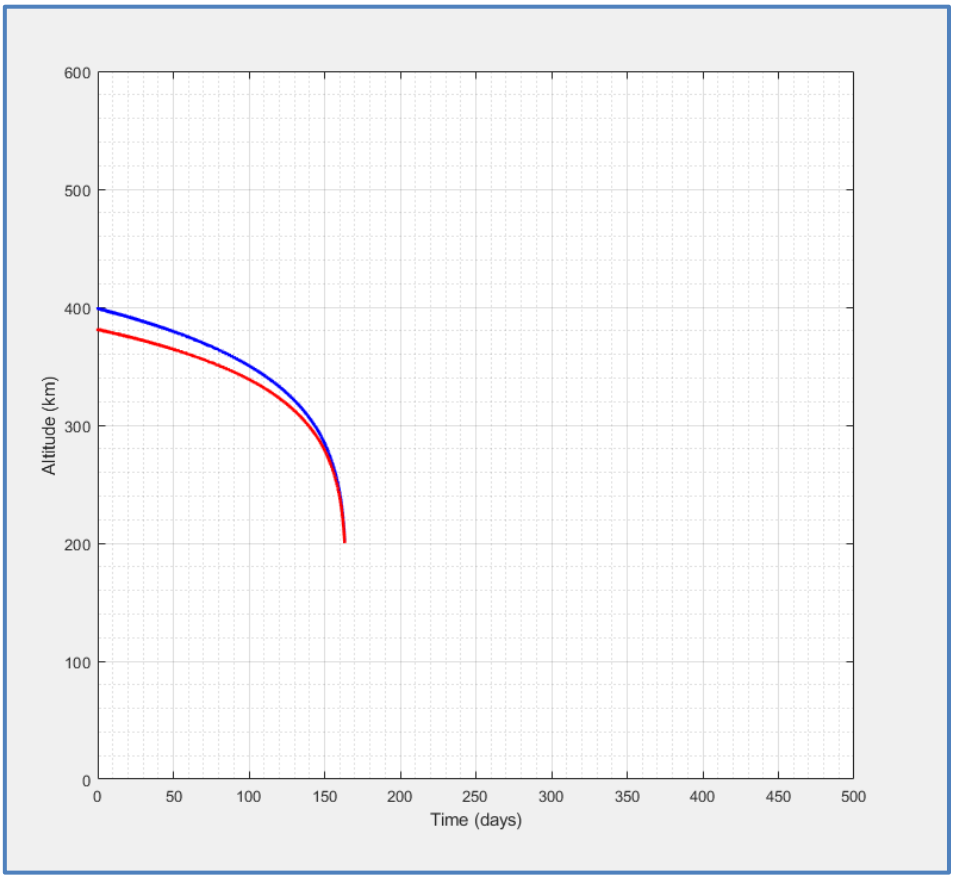

So with these values the cubesat's orbital decay prediction is **165 days.**

1.4.7.2 7th Simulation: Orbital height of ISS

Inserting the orbital parameters below.

```
%...Initial orbital parameters (given):
```

```
rp = RE + 404; %perigee radius (km)
ra = RE + 410; %apogee radius (km)
```

The program presents the following results:

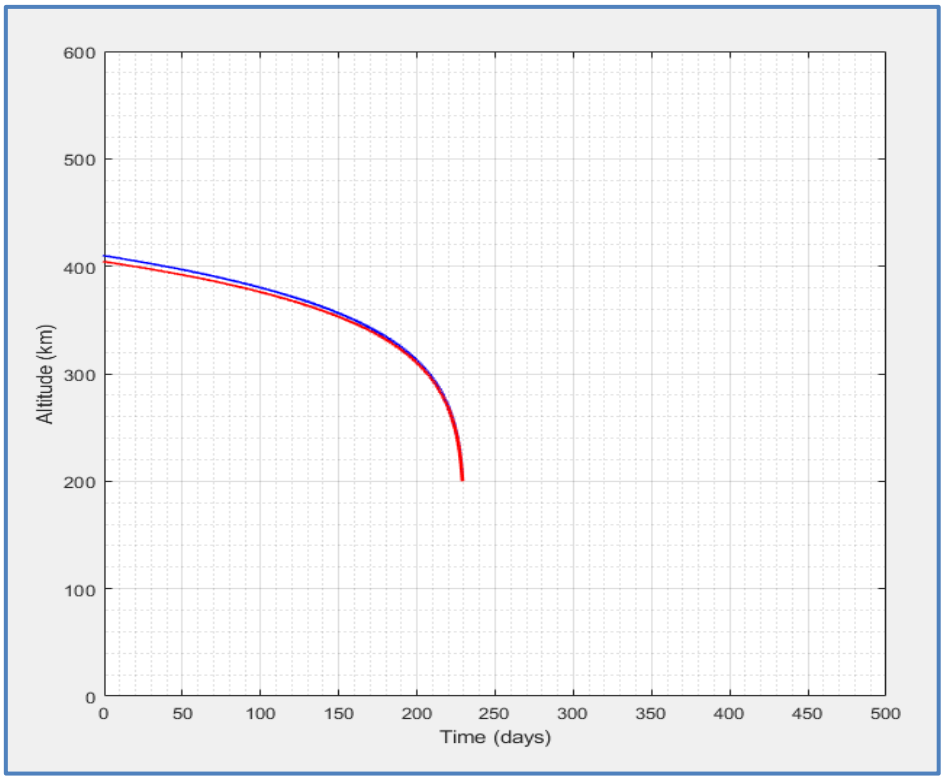

So with these values the cubesat's orbital decay prediction is **230 days.**

1.4.7.3 8th Simulation: Orbital height 450km

Inserting the orbital parameters below.

```
%...Initial orbital parameters (given):
rp = RE + 430; %perigee radius (km)
```

```
ra = RE + 450; %apogee radius (km)
```

The program presents the following results:

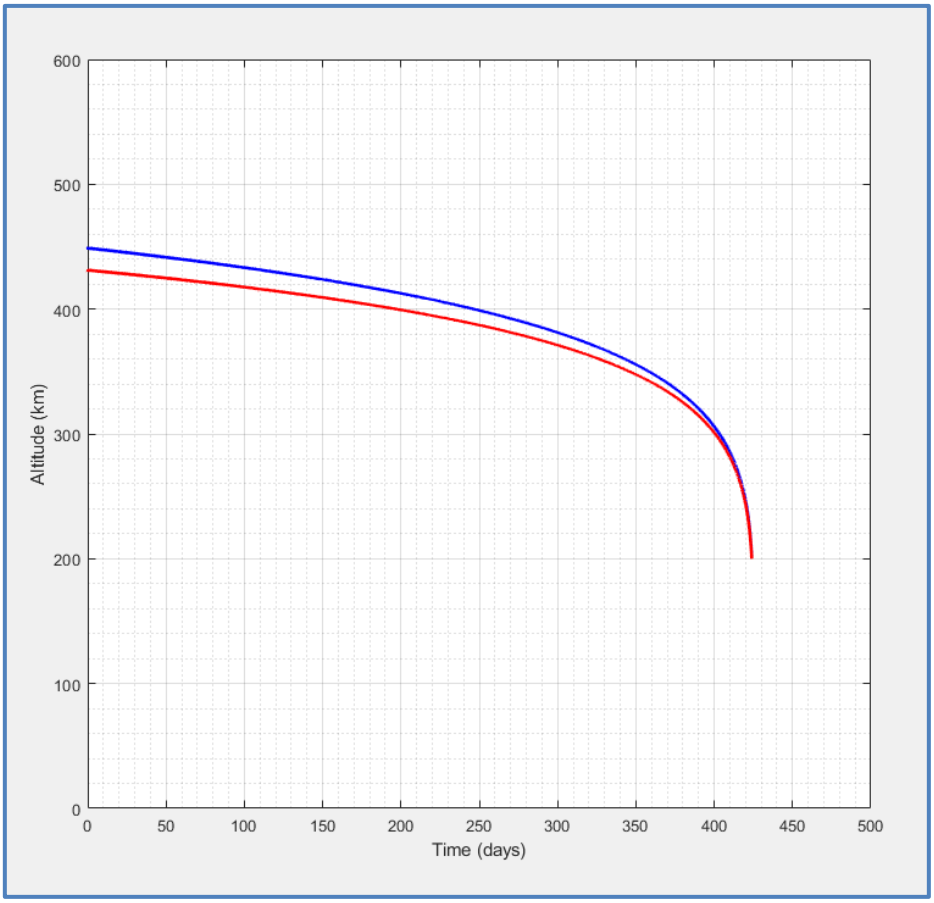

So with these values the cubesat's orbital decay prediction is **435 days.**

1.4.7.4 9th Simulation: Orbital height 500km

Inserting the orbital parameters below.

```
%...Initial orbital parameters (given):
rp = RE + 480; %perigee radius (km)
ra = RE + 520; %apogee radius (km)
```

The program presents the following results:

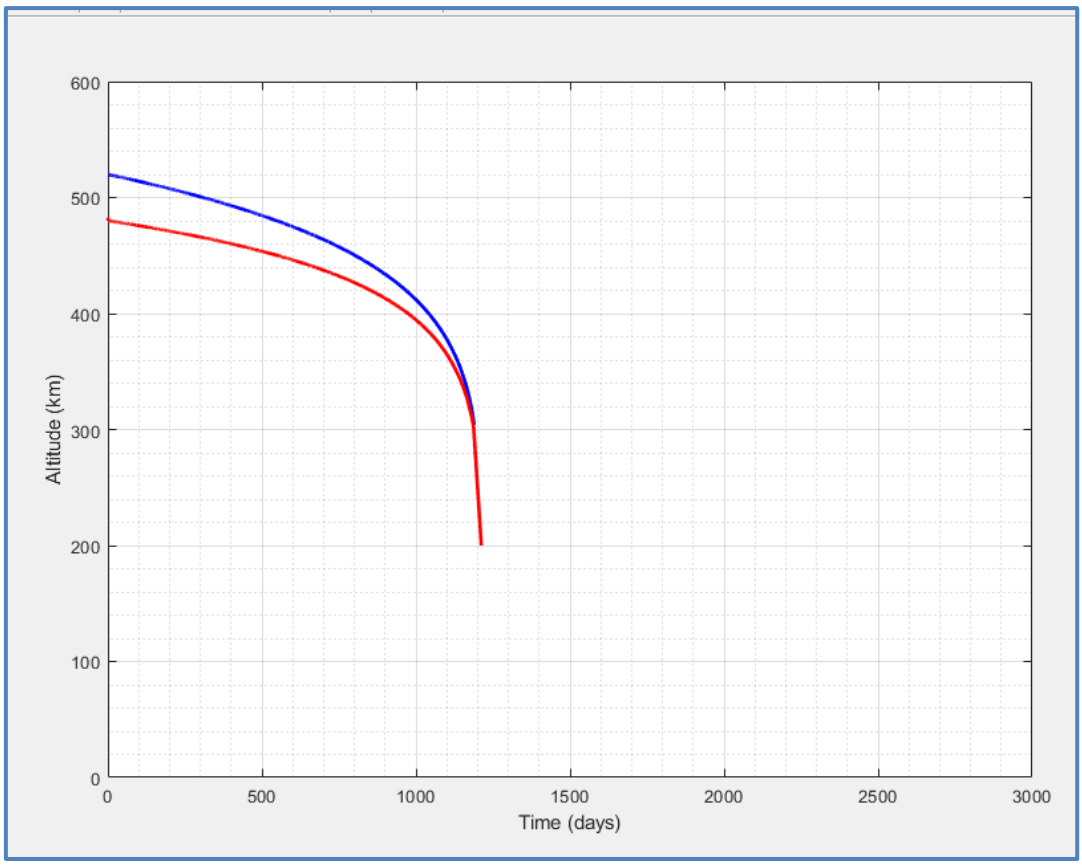

So with these values the cubesat's orbital decay prediction is **1200 days.**

1.4.7.4 10th Simulation: Orbital height 600km

Inserting the orbital parameters below.

```
%...Initial orbital parameters (given):
```

```
rp = RE + 570; %perigee radius (km)
ra = RE + 630; %apogee radius (km)
```

The program presents the following results:

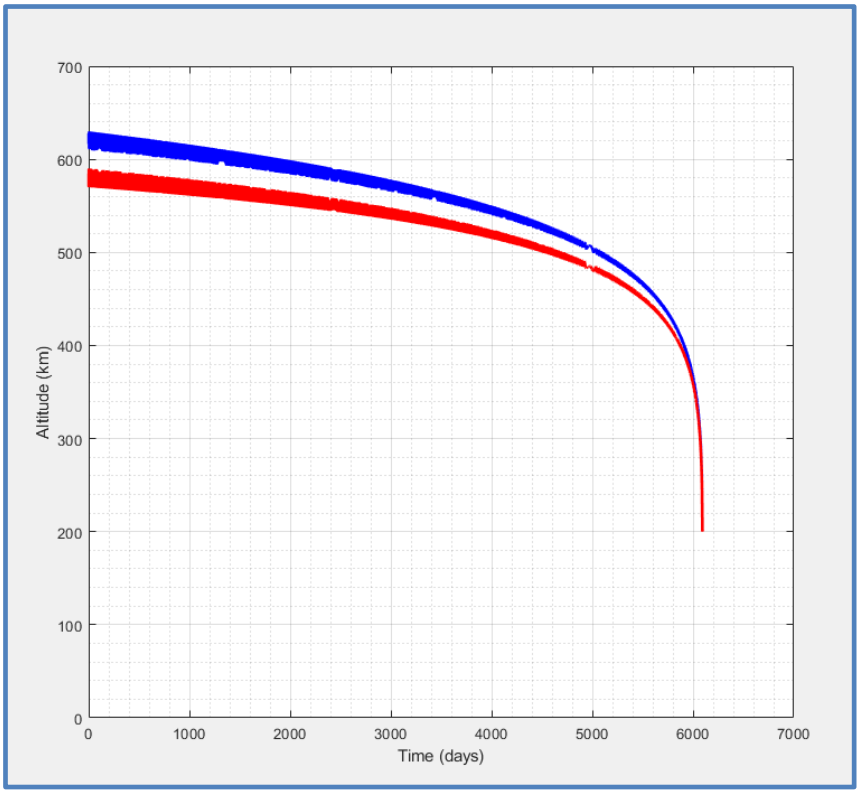

So with these values the cubesat's orbital decay prediction is **6100 days.**

CHAPTER 2 – MICROTHRUSTERS

2.1 Rockets and thrust equations

Spacecrafts, like CubeSats, require a propulsion system that will allow them to undertake delta-v maneuvers. These systems employ devices that vehicle mass to be thrown overboard. According to Newton's balance of momentum principle, when mass is ejected from a system in one direction, the mass left behind must acquires a velocity in the opposite direction.

Rocket motors employ chemical energy that is produced from the steady and rapid burning of solid or liquid propellants, which is converted to a large quantity of hot high-pressure gas and is subsequently expanded and accelerated through a nozzle. This large mass of combustion products flowing out of the nozzle at supersonic speed possesses a lot of momentum and, leaving the vehicle behind, causes the vehicle itself to acquire a momentum in the opposite direction. This is represented as the action of the force, which is defined as thrust (Curtis, 2010).

In order to better comprehend the operation of a propulsion system, four important performance factors for any propulsion system must be outlined (Sutton & Biblarz, 2001):

1. **Thrust (τ) –** The thrust is generated from a combination of
    a. **momentum thrust**, which depends on the mass flow rate (m) of propellant and the exit (exhaust) velocity (v_e); and
    b. **pressure thrust**, which depends on the exit area (A_e), exit pressure (P_e) and ambient pressure (P_a).

    The exterior of the rocket is surrounded by the static pressure p_a of the atmosphere everywhere except at the rocket nozzle exit where the pressure is p_e. This p_e acts over the nozzle exit area A_e. The value of p_e depends on the design of the nozzle. For simplicity, it is assumed that no other forces act on the system. At time t the mass of the system is m and the absolute velocity in its axial direction is v. The propellants combine chemically in the rocket's combustion chamber, and during the small time interval Dt a small mass Dm of combustion products is forced

out of the nozzle, to the left. Because of this expulsion, the velocity of the rocket changes by the small amount *Dv*, to the right. The absolute velocity of *Dm* is *v*e, assumed to be to the left. According to Newton's second law of motion,

(momentum of the system at t + Δt) – (momentum of the system at *t*) = net external impulse

Or

$$\left[(m-\Delta m)(v+\Delta v)\hat{\mathbf{i}}+\Delta m\left(-v_e\hat{\mathbf{i}}\right)\right]-mv\hat{\mathbf{i}}=(p_e-p_a)A_e\Delta t\hat{\mathbf{i}} \quad (14)$$

The final equation for thrust is:

$$\tau = \dot{m}v_e + (P_e - P_a)A_e \quad (15)$$

2. **Specific impulse (I_{sp}) –** This refers to the impulse (integral of thrust over time) generated per unit weight (at sea level) of propellant and is dependent on the thrust generated and mass flow rate of the propellant (*m*).

$$I_{sp} = \frac{\tau}{\dot{m}g_o} \quad (16)$$

3. **Effective exit velocity (or exit velocity) (v_e) –** This refers to the velocity of the propellant at the exit region of the nozzle and can be calculated from the product of the specific impulse and acceleration due to gravity at sea level (g_o).

$$v_e = g_o I_{sp} \quad (17)$$

4. **Delta-v (Δv) –** It can be calculated from the widely known Tsiolkovsky Rocket Equation, which relates exit velocity of a spacecraft to its initial (m_i) and final (m_f) masses.

$$\Delta v = v_e ln\left(\frac{m_i}{m_f}\right) \quad (18)$$

The sections that follow analyze: (1) the operating principles; (2) key design considerations; and, (3) performance factors of micro-propulsion systems based on a comparison of thrust and specific impulse for all propulsion systems, and, a comparison

of power and specific impulse, as also thrust-to-power ratio and specific impulse for electric propulsion systems.

2.2 Classification categories

This section provides an overview of the propulsion systems that are considered suitable for CubeSats. The propulsion system primarily provides a mobility system, which helps the spacecraft with various maneuvering operations (e.g., orbit changing and station keeping). A differentiating factor that propulsion systems have is their dependence on the on-board power. Based on this, propulsion systems can be classified into two major types (Tummala & Dutta, 2017):

1. **Non-electric systems**, which require on-board power only to regulate (initiate and terminate) the propulsion process, and include propulsion systems based on:
    a. Cold Gas
    b. Liquid
    c. Solid Rocket
2. **Electric propulsion systems**, which actively require on-board power for their operation and include:
    a. Resistojets
    b. Radio-Frequency Ion Thruster (RIT)
    c. Hall Effect Propulsion/ Hall Thrusters
    d. Electrospray Propulsion System/ Electrospray Thrusters
    e. Pulse Plasma Thruster (PPT)
3. **Solar Sails**, which are a form of propellant-less spacecraft propulsion systems that generate thrust by means of momentum exchange with the incoming solar radiation.

2.2.1 Non-electric systems: Cold Gas Propulsion (CGP) Systems

The CPG system uses controlled ejection of compressed liquid or gaseous propellants in order to generate thrust. As no combustion process is undertaken, this type of system requires only one propellant (without an oxidizer), and its design is relatively simple. The main components of typical CGP system are a propellant storage

tank and a nozzle. The simplicity keeps the mass of the system to the minimum and lowers its power requirements for regulation purposes. But this has a disadvantage, as it monotonically decreases the thrust profile over a period of time. The thrust produced is directly proportional to the pressure of the propellant inside the tank (propellant storage). However, over the course of the mission, tank pressure decreases because the propellant is being used, which results in a decrease of the maximum thrust that is generated by the system (Tummala & Dutta, 2017).

Specific impulse (Eq19) of a CGP system mainly depends on the exit-to-chamber-pressure (P_e/P_c) and characteristic velocity (C*) (Anis, 2012). The exit-to-chamber-pressure is related to the expansion of the propellant, while Poisson constant (g) is the ratio of specific heats at constant pressure and constant volume. Characteristic velocity of a CGP system at any instant is a function of the velocity of propellant in Mach number (Anis, 2012). Exit velocity (Eq20) is another important performance factor that not only depends on the exit-to-chamber-pressure, but also on the chamber temperature (T_c) (Anis, 2012). This is represented mathematically by the following equations:

$$I_{sp} = \frac{\gamma C^*}{g_o}\sqrt{\frac{2}{\gamma-1}\left(\frac{2}{\gamma+1}\right)^{\frac{\gamma+1}{\gamma-1}}\left(1-\frac{P_e}{P_c}\right)^{\frac{\gamma-1}{\gamma}}} \tag{19}$$

$$v_e = \sqrt{\frac{2\gamma T_c}{\gamma-1}\left(1-\frac{P_e}{P_c}\right)^{\frac{\gamma-1}{2}}} \tag{20}$$

CGP systems can utilize either liquid or gaseous propellants. An advantage of using of liquid propellants is that they allow a reduction in the storage volume. Moreover, the selected propellants must have high-density - I_{sp} (Specific impulse/unit volume) in order to increase the longevity of the on-board propellant. Using lower storage pressure allows the design of storage tanks that have higher safety margins. Finally, ease of availability and environmental friendliness and toxicity of the propellant

need to be also taken into consideration manufacturing and assembly operations of the spacecraft are undertaken. Thus, environment friendly propellants allow a decrease in costs as less needs to be spent on safety measures, storage and transportation (Gibbon, 2010). A disadvantage of liquid propellants is the de-stabilizing effect that can be initiated due to sloshing of propellant inside the tank (Bauer, 1963).

Recently, solar thermal propulsion based on solar energy has been employed in improving the performance of CGP systems. Solar energy directly heats the propellant, and this enters the nozzle at an elevated temperature, the thrust is significantly enhanced. However, a disadvantage of this technology relates to its dependence on direct solar illumination at the time of propulsive maneuvers (Reid et al., 2013).

ENGINE	THRUST	Isp
SNAP 1	50	43
CNAPS	10–40	<35
POPSAT-	1	43
MEMS Cold Gas	1	50–75
CPOD	25	40

Table 1 – Summary of Cold Gas Propulsion Systems (Tummala & Dutta, 2017).

2.2.2 Non-electric systems: Liquid Propulsion (LP) Systems

Contrary to the previous system, LP systems generate thrust by ejecting gases that are produced from the combustion of the liquid propellants. The mission requirements define whether one (mono) or two (bi) propellants are employed. The mono-propellant (e.g., hydrazine or nitrous oxide) (Ley, Wittmann & Hallmann, 2009).

LP systems generate thrust by decomposing the propellant in the presence of a catalyst (e.g., liquid permanganates, solid manganese dioxide, platinum, or iron oxide) (Sutton & Biblarz, 2001), at the same time the propellant is injected into the combustion chamber through the catalyst bed (Sutton & Biblarz, 2001). The bi-propellant LP systems use a combination of oxidizers and fuels (e.g., liquid oxygen with kerosene or liquid oxygen and RPI) (Ley, Wittmann & Hallmann, 2009). A bi-propellant LP system typically consists of a combustion chamber, nozzle and propellant storage for both oxidizer and fuel.

The thrust and specific impulse of an LP system can be obtained from the Eq1 and Eq2 respectively. Exit velocity (Eq21) of an LP system, like a CGP system is dependent on the exit-to-chamber-pressure-ratio (P_e/P_c) and combustion chamber temperature (T_c) (Sutton & Biblarz, 2001). Also, g is the Poisson constant and R is the universal gas constant (Tummala & Dutta, 2017).

$$v_e = \sqrt{\frac{2\gamma}{\gamma - 1}\Re T_c \left[1 - \left(\frac{P_e}{P_c}\right)^{\frac{\gamma-1}{\gamma}}\right]}, \quad (21)$$

In designing LP systems one needs to deal with issues related to storage and operational pressures of the propellant. The highest possible pressure at which the propellant is expected to operate, referred to Maximum Expected Operating Pressure (MEOP), should be desirably high so that thruster performance (thrust, specific impulse) can be maximized (Stratton, 2004). As hydrazine and other propellants previously used were highly toxic, emphasis is now being given to more environmentally safe compounds, to reduce risks incurred due to contamination during laboratory testing and mission phases while in space. Green propellants (e.g., Sulfur Hexaflouride, AF-M315E, Ammonium Dinitramide) have less benign toxicology even for probable levels of unintentional ingestion, and less risk of being inhaled due to their lower vapor pressure. Moreover, some of these propellants have additional advantages compared to hydrazine, which include better physical characteristics (e.g., higher

density), better performance for the propulsion system (e.g., higher thrust and specific impulse), and reduced thermal conditioning requirements for storage. They, unfortunately also have a disadvantage, which relates to them requiring higher preheat temperatures, higher than the typical 120–150^{o}C of hydrazine thrusters (Sackheim & Masse, 2014).

Form-factor customization, which relates to the amount of on-board propellant that can be carried, is factor that has been employed in order to cater to the needs of different CubeSat missions. CubeSats of 0.5 U to 2 U have been fitted with MPS-120 CHAMPS, HPGP, BGT-X5 or VACCO/ECAPS micro-propulsion systems designed in multiple configurations, with the only difference in configurations being mostly in the amount of propellant they carry (Tummala & Dutta, 2017).

ENGINE	**THRUST**	**Isp**
GPIM Propulsion System	400–1100	235
MPS-120 CHAMPS	260	215
MPS-130 CHAMPS	1.5	240
HPGP	1000	231–232
BGT-X1	100	214
BGT-X5	500	220–225
HYDROS	250–600	256

Table 2 – Summary of Liquid Propulsion Systems (Tummala & Dutta, 2017).

2.2.3 Non-electric systems: Solid Rocket Propulsion (SRP) Systems

A SRP system generates thrust by burning solid propellants and ejecting the gases that are produced from their combustion. They also employ oxidizers like the LP systems, but differ from them in two ways: (1) the solid propellants are stored within the combustion chamber itself; and, (2) no sloshing effects are observed as both fuel and oxidizer are solids. Thrust regulation is, however, compromised as there is lack of control over propellant burn rate. A typical SRP system is made of a combustion chamber that holds the solid propellant, an igniter that initiates the combustion process and a nozzle (Tummala & Dutta, 2017).

Taking into account that thrust regulation is difficult in SRP systems, in system design one can employ the burn rate to understand the combustion process, as this governs the mass flow rate of hot gases generated during combustion. The burn rate (r) (Eq22) is dependent on the chamber pressure (P*c*), temperature coefficient (α) and combustion index (*n*). Temperature coefficient is a non-dimensional empirical constant, while the combustion index describes the influence of chamber pressure on the burn rate. For a propulsion system equipped with a de Laval (CD) nozzle, the characteristic velocity (C*) (Eq23) relates to the efficiency of the combustion process and is independent of nozzle characteristics (Sutton & Biblarz, 2001). The thrust, specific impulse and exit velocity of an SRP system can be calculated the same way as it is done for LP systems from Eq15, Eq16 and Eq21 respectively. The mathematical relations summarizing burn rate and characteristic velocity are described below (Tummala & Dutta, 2017):

$$r = aP_c^n \quad (22)$$

$$C^* = \frac{P_c A_t}{\dot{m}} \quad (23)$$

As it was mentioned previously, trust regulation is an important parameter of the whole operation of the system. In order to address this issue, the Aerospace Corporation, El Segundo, CA, USA proposed and designed ad additional device for the I_{sp} 30 s Motor SRP system. The device consists of an external movable mass (pitch/yaw

system) with 8 jet paddles. The jet paddles are located just after the nozzle, and constitute rectangular moving arms (plates or slabs) with one of their faces exposed to the exhaust flow. The regulation of thrust is accomplished through the control of the orientation of the paddles and imparting desired directionality to the flow (Zondervan, Fuller, & Rowen, 2014).

Another disadvantage of SRP systems is their one-shot use owing to a lack of control over propellant burn rate. To address this disadvantage, a system of hundreds of Solid Propellant Micro-thrusters (SPMs) has been proposed. The micro-thrusters can be placed together to form a tightly spaced matrix (within the constraints of available external surface area). During the combustion process the solid energetic propellant in each successive microthruster is burnt and the resultant gases are accelerated through micro-nozzles. Programmable thrust delivery through simultaneous or sequential firing of multiple thrusters can be achieved by varying the size of thrusters to suit the thrust requirements (Sathiyanathan Miller et al., 2011).

A typical SRP micro-thruster makes use of MEMS technology and comprises of several laminated layers containing a combustion chamber, an igniter, a nozzle, and a seal (Rossi Miller et al., 2006). Combustion chamber stores the solid energetic-propellant and igniter section heats the propellant by means of a resistive heating element. Silicon or nichrome are generally used as materials for the heating element (Rossi Miller et al., 2006). Nozzles are designed to meet mission-specific thrust requirements and de-Laval (CD) nozzles are commonly chosen for their higher performance. The seal comprises of an epoxy or similar material or mechanisms. Also, silicon wafer is used in these micro-thrusters because it improves the ignition efficiency by minimizing the current leakage (Zhang, Chou & Ang, 2004).

Burn rate regulation can also be achieved by the was proposed by the use of a new Electric Solid Propellant (ESP), which was developed by Digital Solid State Propulsion (DSSP), Reno, NV, USA. The new compound used is Hydroxyl Ammonium Nitrate (HAN), which theoretically offers a higher theoretical performance and is inherently more safe because ignition is possible only through continuous supply of electrical power, thereby reducing the chances of flames generated due to accidents

and it has the potential to be used as propellant in both chemical and electrical propulsion systems (Thrasher Miller et al., 2016).

Recently other inexpensive propellants have been researched. One of them is aluminum wool used as a propellant, accompanied by a mixture of sodium hydroxide and water as he oxidizer. After tests it was found to produce a thrust of 32 mN and specific impulse of 45 s. A major advantage of these propellants is that they are low cost, easy to handle, and can be stored over a long duration without any decomposition (David & Knoll, 2017).

ENGINE	**THRUST**(N)	**Isp**
Isp 30 s	37	187
STAR 4G	13	269.4
CAPS-3	-	245–260
CDM-1	76	226

Table 3 – Summary of Solid Propulsion Systems (Tummala & Dutta, 2017).

2.2.4 Electric systems: Resistojets

Resistojet is an electric system in which the propellant is passed through a heat exchanger (or heating element), where it is super-heated and ejected through an expansion nozzle (Frisbee, 2003). Temperatures of 600–1050 ^{o}C have been observed for methanol and 300–1175 ^{o}C for ammonia propellants (Robin, Brogan & Cardiff, 2008). Heating helps in the reduction of the gas propellant's flow rate, which raises its upstream pressure by passing it through a given nozzle area, a factor that leads to an increase in specific impulse, which is proportional to the square root of temperature (Eq11) (Martinez-Sanchez & Pollard, 1998). Although Resistojets are in working principle similar to a CGP system, they differ in that the propellant is heated before the expansion process. The heating increases the propellant's energy, which means that they

can achieve an exhaust velocity much greater than that of a CGP system (Frisbee, 2003). Exit velocities of micro CGP systems range between approximately 300–700 m/s (Matticari Miller et al., 2006; Skuhersky Miller et al., 2017), while those of micro resistojets are about approximately 2.2 km/s (Slough Miller et al., 2005).

Resistojets have a major drawback, as their performance (thrust, Isp) is limited by the melting temperature of the heating element used. Moreover, power and thermal losses during heating of the element contribute to the inefficiency of Resistojets (Chianese & Micci, 2006). The main components of Resistojets are the following: propellant storage, heating element and nozzle .

The thrust (Eq24) produced by the propellant at stagnation pressure also depends on stagnation number density of propellant (n_o) in m^{-3}, stagnation temperature (To) and the probability (c) of a molecule exiting the expansion slot area (A_o). Specific impulse (Eq25) is a function of the stagnation temperature, and the mass of the propellant (m) (Ketsdever, Wadsworth & Muntz, 2001). While k is the Boltzmann constant and go is the acceleration due to gravity at sea level (Tummala & Dutta, 2017).

$$\tau = A_o\left(\frac{n_o k T_o}{2}\right)\chi \quad (24)$$

$$I_{sp} = \sqrt{\frac{\pi k T_o}{2m}}\frac{1}{g_o}, \quad (25)$$

Resistojets also experience issues related to sloshing within the tanks (Lee Miller et al., 2008). A system that was developed to deal with sloshing is the Free Molecule Micro Resistojet (FMMR), where water has been used as the propellant (Lee Miller et al., 2008). This type of Resistojet operates by heating a propellant gas as it expands through a series of slots (Ahmed, Gimelshein & Ketsdever, 2006). Its advantages also include its low cost, low power consumption and low mass. There are three major advantages that are related to the use of water as the propellant: (1) it is

stored as a liquid and can save the volume occupied by the propellant due to its high storage density; (2) it has lower molecular mass, which can improve the specific impulse; and, 3) it has sufficiently high vapor pressure at typical smallsat (<10 kg) on-orbit temperature because of which it can be directly used to produce thrust without pre-vaporization (Lee Miller et al., 2008).

ENGINE	THRUST	Isp	POWER
LPR	18	48	30
PUC	5.4	65	15
CHIPS	30	82	30
AMR	10	150	15
FMMR	0.129	79.2	-

Table 4 – Summary of Resistojet Propulsion Systems (Tummala & Dutta, 2017).

2.2.5 Electric systems: Radio-Frequency Ion Thruster (RIT)

Radio frequency ion thrusters are gridded ion thrusters. Thrust is generated through the acceleration of the ionized propellant (plasma) through an electrostatic grid. The propellant stored in the thrusters is allowed to enter into a discharge chamber, where it is ionized and becomes plasma by means of Radio Frequency (RF) power that is generated from RF coils. Subsequently, the ionized propellant is then extracted from the discharge chamber and is accelerated by a series of grids (ion optics) called screen and accelerator grids. The screen grid extracts propellant cations (for instance, Xe^+, Kr^+ ions) from the ionized plasma and directs them downstream towards the accelerating grid (Goebel & Katz, 2008). A neutralizer cathode, present on the exterior of the thruster in all ion engines, provides electrons to neutralize the ionized propellant that is

emitted from the thruster [63]. By changing the voltage that is applied to the accelerating grids one can vary the specific impulse of a gridded thruster (Fearn, Solutions & Crookham, 2003). An advantage of ion thrusters is their high thruster efficiency (60% to >80%) resulting in high specific impulse (from 2,000 s to over 10,000 s) (Goebel & Katz, 2008); but they have operational issues relating to the issues that are caused by cathode wear (Goebel, Polk & Mikellides, 2011) and contamination over prolonged usage (Brinza Miller et al., 2001). An RF Ion propulsion system typically includes a propellant storage area, an RF coil, discharge chamber, grids (screen and accelerator) and a neutralizing (external) cathode.

The ion exhaust velocity (Eq26) and thrust (Eq27) are both functions of the charge of propellant ion (q), mass of propellant ion (m_{ion}) and ion accelerating voltage (Vi). Ion engines use heavier elements (elements with higher atomic mass) as propellants because the thrust generated is proportional to mass of the ion (propellant). Thrust, however, also depends on the ion beam current (Ii) (Goebel & Katz, 2008). Specific impulse (Eq28) is a function of ion accelerating voltage and mass of ion (Goebel & Katz, 2008). While η_m is the thruster mass utilization efficiency and gc is the total thrust correction factor. The performance factors of ion engines are explained below with their mathematical equations:

$$v_{e_i} = \sqrt{\frac{2qV_i}{m_{ion}}} \quad (26)$$

$$\tau = \sqrt{\frac{2m_{ion}V_i}{q}} I_i \quad (27)$$

$$I_{sp} = 1.417 \times 10^3 \gamma_c \eta_m \sqrt{\frac{V_i}{m_{ion}}}, \quad (28)$$

Unfortunately, the operation of the ion thruster can interfere with spacecraft instruments (e.g., ionized propellant), can lead to contamination and can cause field interactions. The use of inert propellants (e.g., xenon and krypton) can mitigate

contamination effects but does not deal with the issues that emanate from plasma interactions (Brinza Miller et al., 2001).

ENGINE	THRUST	Isp	POWER
BIT-1	0.1–0.18	2150–3200	28
BIT-3	1.15	2500	75
RIT-mX	0.05–0.5	300–3000	<50
RIT 10 EVO	5, 15, 25	>1900, >3000, >3200	145

Table 5 – Summary of RF Ion Propulsion Systems (Tummala & Dutta, 2017).

2.2.6 Electric systems: Hall Effect Propulsion/ Hall Thrusters

Hall Effect Propulsion Thrusters are electrostatic devices (Goebel & Katz, 2008) that have been employed to generate thrust through the ionization and subsequently the acceleration of the propellant in mutually perpendicular electric and magnetic fields. According to the Hall Effect: "when electric current is applied to a conductive material (propellant) placed in mutually perpendicular electric and magnetic fields, a potential difference is developed that is perpendicular to the applied electric and magnetic fields" (Hall, 1879).

Hall thrusters typically consist of a propellant storage chamber, a discharge channel, an external cathode, anodes and the magnetic field generator. The applied magnetic field is radial, while the accelerating electric field (acting from anode towards cathode) is axial [63]. Contrary to gridded ion thrusters, Hall thrusters do not have a grid system (series of grids), which is replaced with a strong magnetic field perpendicular to the flow of ions. This magnetic field reduces the mobility of electrons coming from the external cathode, thereby restraining their flow towards anode in the accelerating electric field (Goebel & Katz, 2008; Lary, Meyerand & Salz, 1962; Seikel, & Reshotko, 1962). They have many advantages that emanate from their high

specific impulse (higher than most systems except ion engines), their higher thrust density (Tamida Miller et al., 2015) and their simplicity in design (when compared to gridded ion engines due to lack of accelerator grids) (Dankanich, 2005). They also have some disadvantages that relate to the erosion of magnetic circuitry due to discharge plasma and lower efficiency (6–30% at 0.1–0.2 kW and 50% at 1 kW) (Pigeon, Nathan & Orr, 2015).

The performance factors for Hall thrusters like ion exit velocity (Eq12), thrust (Eq13) and specific impulse (Eq14) are the same as the ones for RITs (Goebel & Katz, 2008).A typical Hall thruster, applies a magnetic field (*B*) across an accelerating electrical discharge (*E*) allowing the entrapment of the electrons in the Hall effect (*ExB*) direction. The anode acts as the source of the neutral propellant, while an external cathode provides electrons that move towards the anode across the radial magnetic field (Ito Miller et al., 2007). When the electrons enter the magnetic field, they spiral around the thruster axis in the (*ExB*) direction and their interaction with the incoming propellant leads to the ionization of the propellant (Goebel & Katz, 2008).

There are two types of Hall thrusters: (1) magnetic layer thrusters, which have continuous and extended acceleration zones (for sufficient ionization and stability), and a ceramic wall, and their acceleration channel length is longer than the channel width; and (2) anode layer thruster, which have a narrow acceleration zone (length of the discharge channel is shorter compared to the channel width) (Yamamoto, Komurasaki & Arakawa, 2005; Zhurin, Kaufman & Robinson, 1999). The electron temperature of anode layer thrusters is higher than that of magnetic layer thrusters due to the lower electron energy losses (Yamamoto, Komurasaki & Arakawa, 2005).

Similar to ion engines, the Hall thrusters make use of heavy elements as propellants, for instance, xenon (Xe), krypton (Kr), iodine (I), bismuth (Bi) and argon (Ar). Of these, xenon has been favored for its lower ionization energy, higher atomic mass and easy storage. However, it is expensive to purchase and to perform ground tests with xenon (Kieckhafer & King 2007). Many cheaper alternatives to xenon exist, but further experiments have to be conducted to prove their usefulness (Hillier et al., 2011).

Hall thrusters have limited lifetime due to the erosion of the components protecting its magnetic circuitry from discharged plasma (ionized propellant). The exposure of the magnetic poles erodes them over time, while further degradation or overheating may occur, affecting the nominal magnetic field and thereby the thruster's performance (Cheng & Martinez-Sanchez, 2008).

Contrary to gridded ion thrusters, where ion beam can be properly controlled, one cannot easily control it in Hall thrusters, a disadvantage that leads to erosions in their walls. This is attributed mainly to the ions that are driven towards the wall material because of elevated parallel component of electric field and the high electron temperature (Mikellides Miller et al., 2014).

Scaling/ sizing relations have been employed in order to assess the performance of newly designed Hall thrusters, as it is often a tedious and expensive process (Biagioni, Saverdi & Andrenucci 2003). These studies showed that the propellant mass flowrate and the applied power were proportional to the channel length, while the magnetic field strength was inversely proportional to the channel length. This means that oen has the value of the power of a larger Hall thruster, the mass flow rate of propellant, strength of applied magnetic field and channel length can be determined (Dannenmayer & Mazouffre, 2011).

ENGINE	THRUST	Isp	POWER
BHT-200	12.8	1390	200
BHT-600	39.1	1530	600
HT 100	10	1100	100
HT 400	50	1750	100
MHT-9	20–50	300–1500	30–200
CHT	1–10	1139	<200

Table 6 – Summary of Hall Thrusters (Tummala & Dutta, 2017).

2.2.7 Electric systems: Electrospray Propulsion System/ Electrospray Thrusters

Electrospray thruster is an electric propulsion system that does not employ plasma technology (Grustan-Gutierrez & Gamero-Castaño, 2017), and functions based on the principle of electrostatic extraction and acceleration of charged particles (ions) from a liquid (propellant) surface to produce thrust. In essence they are based on a process in which the conductive liquid surface of the propellant is deformed into a sharp cone-shaped meniscus called Taylor Cone. As soon as a certain threshold of the electric potential is surpassed, ions are extracted from the cone's apex (Krejci Miller et al., 2015; Legge & Lozano, 2011). Positive or negative ions are accelerated, respectively generating either a positive or negative ion beams thereby eliminating the need for an external cathode to neutralize the ejected ions unlike in plasma propulsion devices (ion and Hall thrusters) where an external cathode is essential (Mier-Hicks & Lozano, 2016). The propellants used for electrospray thrusters are usually ionic liquids, and their negligible vapor pressure serves as an advantage by resolving the need for propellant pressurization and helps with system miniaturization (Krejci Miller et al., 2017). A typical electrospray propulsion system is comprised of a propellant storage chamber,

emitter and extractor electrode. By changing the voltage passed through the emitter and the extractor electrodes one can vary the performance of this system (Grustan-Gutierrez & Gamero-Castaño, 2017).

One must note that the mass-to-charge ratio plays an important role, as it determines the exit velocity and thrust. The average mass-to-charge-ratio (q/m_{ion}) (Eq29) is inversely proportional to the density (r) of the propellant ion/droplet and the volume flow rate (Q) of ion/droplet. The exit velocity (Eq30) is a function of the square root of ion accelerating voltage (V_i), ion beam current (Ii) and average mass-to-charge-ratio. The thrust (Eq31) is a function of ion accelerating voltage, ion beam current and mass flow rate of ions (m_{ion}) (Song & Shumlak, 2010). The following equations summarize these relationships:

$$\left\langle \frac{q}{m_{ion}} \right\rangle = \frac{1}{\rho Q} \quad (29)$$

$$v_{e_i} = \sqrt{2V_i I_i \left\langle \frac{q}{m_{ion}} \right\rangle} = \sqrt{\frac{2V_i I_i}{\rho Q}} \quad (30)$$

$$\tau = \dot{m}_{ion} v_{e_i} = \sqrt{2V_i I_i \dot{m}_{ion}} \quad (31)$$

These types of devices employ the extraction of charged particles through two methods: (1) the cone-jet regime, in which the meniscus (of the propellant) breaks up into droplets; and, (2) the ionic regime where pure ions are extracted. The specific impulse observed in ionic regime is greater than in cone-jet regime (Krejci Miller et al., 2017). Thrusters are specific in which method they employ. As they use ionic liquids as propellants, they do not require heating, which in turn allows them to operate with low voltage, to have high conductivity in the pure state and to have negligible vapor pressure (Alexander Miller et al., 2006; Courtney, Dandavino & Shea, 2015). Formamide, propylene carbonate, water, Tri-Ethylene Glycol (TEG) solutions doped with Sodium Iodide (NaI), 1-Ethyl-3-Methyl Imidazolium bis(tri-fluoro-methyl-sulfonyl) imide ([Emim][Im]), formamide, tri-butyl phosphate, 1-Butyl-3-Methyl

Imidazolium Di-Cyanamide ([Bmim][DCA]) and 1-Ethyl-3-Methyl Imidazolium Tetra-fluoro-borate (EMIBF4) are some of the propellants used in electrospray systems (Gamero-Castano & Hruby, 2001; Miller et al., 2007; Miller et al., 2014). Liquid metals like cesium, gallium and indium have also been used as propellants due to their high atomic mass and a low ionization potential (Kim & Micci, 2013). In order to yield the thrust required several emitters are required (Alexander Miller et al., 2006).

ENGINE	THRUST	Isp	POWER
S-iEPS	0.1	1200	1.5
TILE 5000	1.5	1800	30
BET-1mN	0.7	800	<9
BET-100	0.005–0.1	1800	5.5

Table 7 – Summary of Electrospray Propulsion Systems (Tummala & Dutta, 2017).

2.2.8 Electric systems: Pulse Plasma Thruster (PPT)

Pulsed Plasma Thrusters (PPTs) are devices that function through the application of pulsed, high-current discharge across the exposed surface of a solid insulator (r.g. Teflon), which acts as a propellant. The arc discharge facilitates the ablation (sublimation/vaporization) of the propellant material from their surface, which in turn ionizes and accelerates the propellant to high speeds. A current pulse lasting few micro-seconds is generally driven by a capacitor that is charged and discharged approximately once every second (Burton & Turchi, 1998).

A typical PPT is made of a spring loaded mechanism, propellant, capacitor, anode, cathode, acceleration chamber and a spark plug (Figure 8). The propellant, which is usually solid, is fed by the spring between the anode and the cathode), while the spark

plug is simultaneously fired to raise the electrical conductivity of the acceleration chamber. Subsequently, the electric current from Power Processing Unit (PPU) flows to the electrodes through the capacitor and then into the arc, thereby completing a current loop and simultaneously generating a magnetic field. The electric arc formed ablates the propellant and ionized plasma is formed. The plasma is then accelerated due to Lorentz Force generated by electric arc and the induced magnetic field (Brito et al., 2004).

The PPTs have many advantages, which are the following: (1) ability to provide small impulse bits for precision maneuvering; (2) robustness, as their impulse bits can be programmed to cater for the needs of different mission needs; (3) simple design, as they can employ a wide variety of propellants (solid/liquid); and, (4) ability to maintain constant specific impulse and efficiency over a wide range of input power levels. However, they also have disadvantages that emanate from electrode erosion, presence of macro-particles in the plume due to non-uniform ablation and very low thruster efficiency (Brito et al., 2004; Keidar, et al., 2004; Keidar, Boyd & Beilis 2001; Mikellindes, & Turchi, 1996; Polzin, 2011).

The law of conservation of momentum is employed to calculate thrust (Eq32). In all electric thrusters, Lorentz Force describes the relationship between the forces (thrust) produced due to charged particles moving through a self induced magnetic field. Thrust produced also depends on the charge of ions (q), sum of all collision forces per particle (propellant) over all particles ($(P\mathrm{i})_k$) and particle velocity (vi). The effective exit velocity (Eq33) of the ionized propellant is a function of the thrust generated and the mass flow rate of propellant (m) and efficiency (h). Effective exit velocity can also be calculated in terms of the radius of anode (R_a) and radius of cathode (R_c). The specific impulse of a PPT can be obtained from the Eq2. Also m_0 is the permeability of free space (Lee, Richard & Branam, 2011).

$$\tau = m_{ion}\frac{d\tilde{\mathbf{v}}_i}{dt} = q\left(\tilde{\mathbf{E}} + \tilde{\mathbf{u}}_i \times \tilde{\mathbf{B}}\right) + \Sigma(P_i)_k \tag{32}$$

$$v_e = \frac{\tau}{\dot{m}\eta} = \frac{1}{\eta}\frac{\mu_0}{4\pi} ln\left(\frac{R_a}{R_c}\right), \tag{33}$$

ENGINE	THRUST	Isp	POWER
mPPT	-	578–727	2–10
EO-1 PPT	0.14	1150	12.5
MPACS	0.144	830	<10
BmP-220	0.14	536	7.5
mCAT	0.001–0.02	3000	<10
mBLT	0.054	-	4
UWE4 Arc Thruster	0.002–0.01	900–1100	0.5–2

Table 8 – Summary of Electrospray Propulsion Systems (Tummala & Dutta, 2017).

The very low efficiency (10–20%) of PPTs is attributed to delayed ablation and particulate emissions (Keidar, Boyd & Beilis 2001). During the emission of a pulse the PPTs may also emit particulates that have the potential to react with the surrounding plasma or consume about 40% of the total propellant mass (Keidar, Boyd & Beilis 2001). The efficiency of the thrusters and their specific impulse can be raised when late ablation is diminished or totally prevented (Mikellindes, & Turchi, 1996).

The solid propellant that usually employed in PPTs is Teflon, as it is inert and non-toxic (Rayburn, Campbell & Mattick, 2005). In order to provide a large supply of free electrons to initiate an electric discharge between the electrodes across the exposed surface of the propellant, the PPTs employ spark (igniter) plugs (Dubey, Ravi & Kushari, 2005).

Another technology that is based on an adaption of the PPT system is Vacuum Arc Thrusters (VATs). This system employs a mechanism in which the cathode material (solid propellant) is ablated and consumed in a vacuum, and in doing so produce fully

ionized plasma jets having high velocity [120]. These devices provide several potential advantages: (1) simplified thruster design and lower mass (due to the absence of gas feed system); (2) higher efficiency (due to the highly-ionized plasma generation); and, (3) discrete pulse operation without sacrificing plasma production efficiency (this control allows for fine-tuning of spacecraft maneuvers) (Gibbs, 2014; Keidar, 2015). However they come with two major limitations: (1) the force generated per pulse is non-adjustable for each specified cathode material, and the thrust level can be adjusted only by varying the pulse duty cycle; and, (2) the plasma is generated from cathode and transported out of thruster channel by plasma pressure gradient alone, the directional efficiency of the thrust generated is strongly dependent on the geometry of the thruster electrodes (Keidar, 2015).

2.2.9 Solar Sails

Solar sails are spacecraft propulsion systems that do not employ propellants for generating thrust. In order to generate thrust they employ momentum exchange with the incoming solar radiation (Gibbs, 2014). Solar sails have a flat surface and are usually made of thin reflective material supported by a lightweight deployable structure. By definition they do not infinite specific impulse, because they do not use a propellant (Frisbee, 2003). They have, however, a major limitation related to the very low thrust levels that result from the long time that needs to pass before they gain appreciable momentum change. The generated force vector (f_{srp}) on a solar sail is a function of the solar radiation pressure (P), surface area of the sail (A) and angle of attack (a) (Michael & Souder, 2008). Accordingly, the acceleration is obtained from Newton's Second Law as described below:

$$\tilde{\mathbf{a}}_{\mathbf{srp}} = \frac{\tilde{\mathbf{f}}_{\mathbf{srp}}}{m_s} = \frac{2PA\cos^2(\alpha)\tilde{\mathbf{n}}}{m_s}, \quad (34)$$

A typical solar sail has four components: (1) a central bay; (2) an offset boom; (3) masts; and, (4) sail (Murphy, Murphey, & Gierow, 2002). The devices have a central bay, which houses the control boom and the sail, while the masts (stowed) are

placed symmetrically around the central bay. In essence the masts constitute the supportive structure on which the sail is attached. As soon as the solar arrays are deployed to space they unfold their solar arrays. They first deploy their offset boom, followed by the deployment of masts and the sail. The offset boom is rotated by means of a motor (after the sail is deployed) to provide altitude control (Murphy, Murphey & Gierow, 2002).

Performance (acceleration) of solar sails is proportional to the ratio of its area and mass. This means that as sails get larger and consequently heavier, one needs to find ways to lower their launch mass. This is achieved by designing sails that are as thin and light as possible. This gives rise to flexibility issues (Eldad, Lightsey & Claudel, 2017). Designers face a major challenge, which relates to their inability to accurately measure flexibility of a sail in a land based laboratory setting, as solar sails cannot be deployed and tested in vacuum and zero gravity conditions (Eldad, Lightsey & Claudel, 2017).

A sail-craft (spacecraft bearing solar sail) usually requires a desired attitude to obtain the maximum momentum transfer from solar radiation (Rizvi, 2014). To achieve this, torque from on-board attitude control mechanism (such as reaction wheels) is required, enforcing limitations on the design (mass, power, volume) of the sail-craft. However, studies have shown that the spacecraft can take advantage of environmental torques due to solar radiation, gravity gradient or atmospheric drag in order to reduce the involvement of the attitude control mechanism (Rizvi, 2014).

The large surface area of solar sails increases the importance of controlling their thrust vector. Stabilization of solar sails can be done in two ways: (1) spin stabilization, in which sails are stiffened by spinning about a central hub resulting in high propulsive efficiencies without strong compressive mast loads; and, (2) three-axis stabilization, in which sails are supported using long booms similar to a kite (Botter, Coverstone, & Burton, 2008).

2.3 Comparison of microthruster propulsion systems

At paragraph 2.2 were analyzed all the possible microthrusters. The next step is the comparison between them relative with their performance. Firstly the comparison will take place at the basic characteristics :

1. Thrust
2. Spesific Impulse (Isp)
3. Power

Subsequently there will take place a combined comparison:

1. Thrust - Specific Impulse
2. Power - Specific Impulse
3. Thrust to Power Ratio - Specific Impulse

2.3.1 Thrust

From the tables at paragraph 2.2 is calculated the average thrust at every thruster. So in the following there is a concentrated table with all microthrusters average thrust.

Engine	**Average THRUST(Nm)**
Cold Gas	20,4
Liquid	505,8333333
Solid	42000
Resistrojets	14175,41111
ION	15
Hall	31,66666667
Electrospray	0,588
Plasma	1144

So the propulsion system with the highest produced thrust is the Solid. In the 2nd place comes the Resistrojets. In 3rd place is the liquid. The other thrusters have very low thrust in comparison with the first 3.

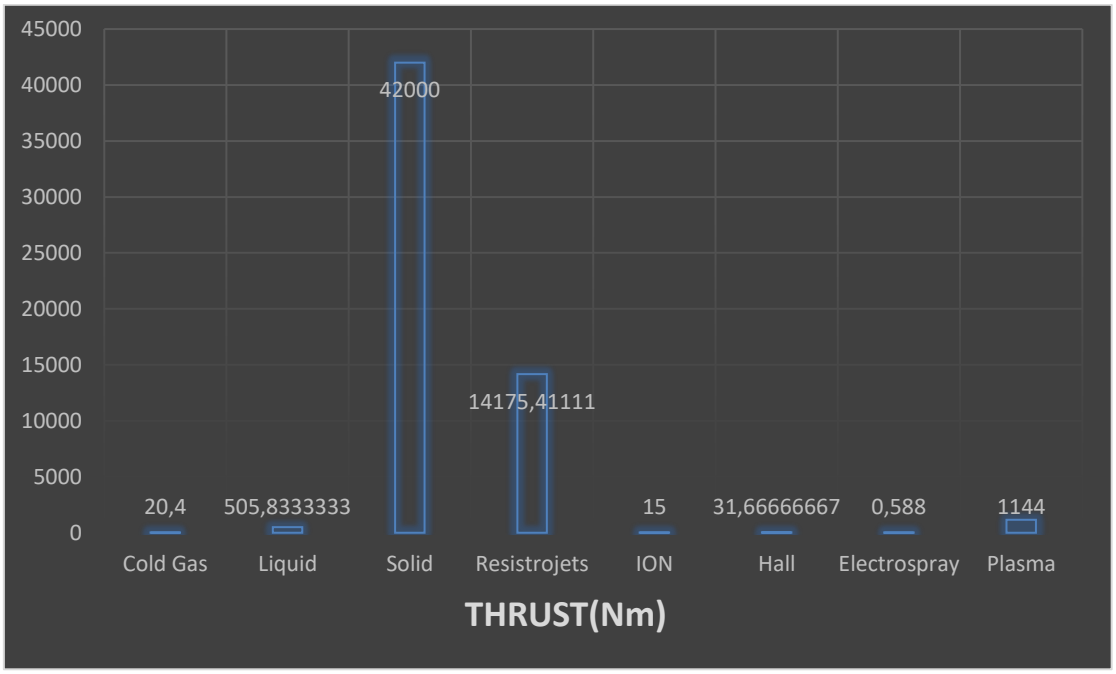

2.3.2 Specific Impulse (Isp)

From the tables at paragraph 2.2 is calculated the average Isp at every thruster. So in the following there is a concentrated table with all microthrusters average Isp.

Engine	Average Isp
Cold Gas	40
Liquid	232
Solid	206,5
Resistrojets	86,25
ION	2487,5
Hall	1301,5
Electrospray	1400
Plasma	1303,2

At this category the electric propellants are ahead in comparison with the non-electric engines. First is the ION thruster, second the electrospray and at the 3rd place with small difference are Hall and Plasma thrusters.

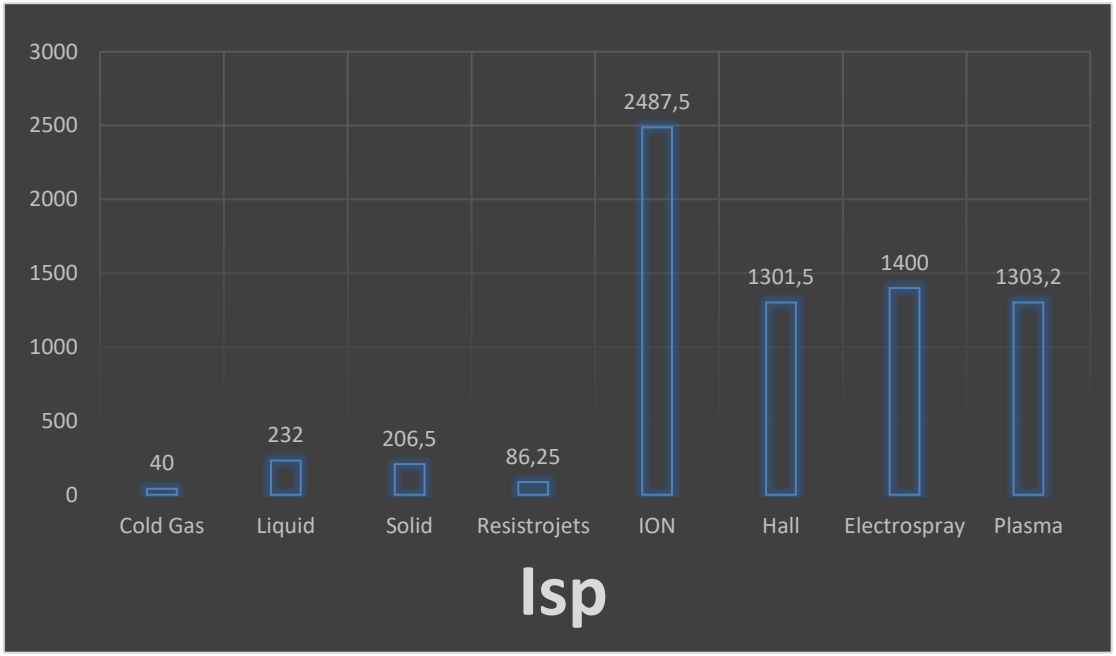

2.3.3 Power

From the tables at paragraph 2.2 is calculated the average power at every thruster. So in the following there is a concentrated table with all microthrusters average power.

Engine	Average Power
Resistrojets	22,5
ION	74,5
Hall	219,1666667
Electrospray	19,5
Plasma	7,5

At this category the ‘‘best’’ thruster is Plasma and 2nd is the Electrospray (they demand the least power to operate). Resistrojets thrusters are approximately the same with Electrosprays.

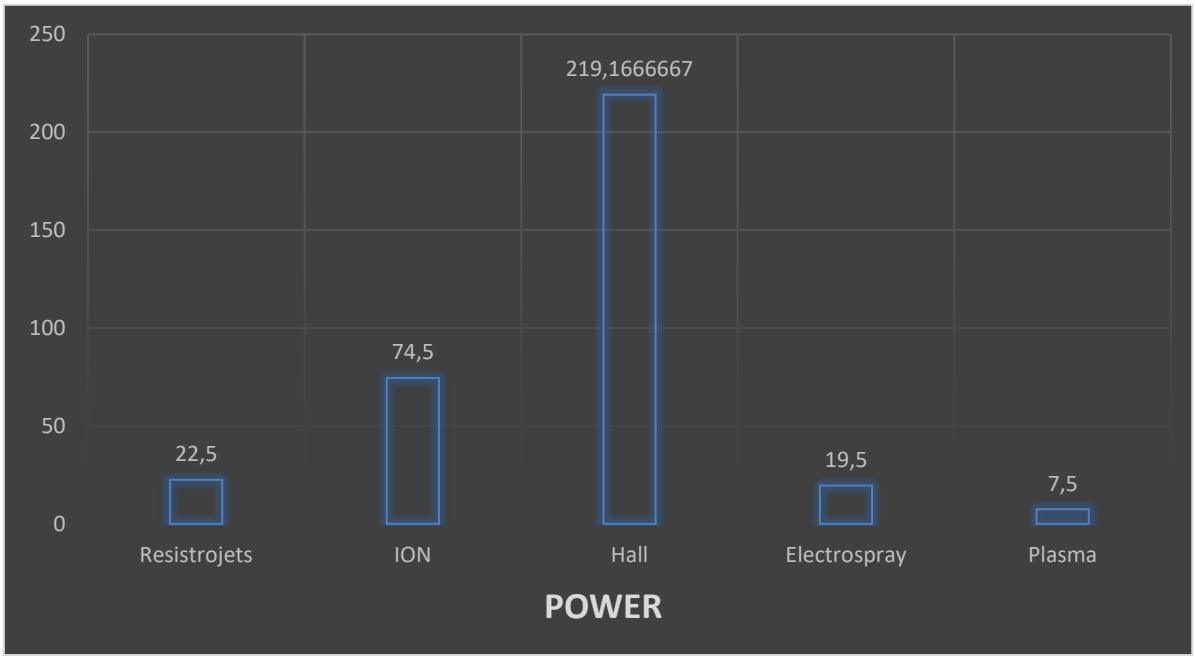

2.3.4 Thrust - Specific Impulse

From the paragraphs 2.3.1 and 2.3.2 paragraphs are calculated the average Isp and the average thrust at every thruster.

Engine	AVG Isp	AVG Thrust
ION	2487,5	15
Electrospray	1400	0,588
Plasma	1303,2	1144
Hall	1301,5	31,66667
Liquid	232	505,8333
Solid	206,5	42000
Resistrojets	86,25	14175,41
Cold Gas	40	20,4

The propulsion systems that generate the highest thrust are solid rocket devices. This is accomplished through the expansion of the burnt propellants in the nozzle. However, these non-electric systems come with a disadvantage, as the specific impulse generated by them is low, compared to electric propulsion systems, as the exit velocity of the propellants is lower. .The lowest specific impulse is observed in cold gas propulsion systems. This is attributed to their simple operational physics, as chemical transformations are involved, and the only thing that needs to be taken into account is the expansion of propellants. On the other hand, resistojets compared to cold gas propulsion systems, have higher specific impulse and thrust, because they have the ability to super-heat the propellant prior to the expansion in the nozzle. This provides the propellant with additional kinetic energy giving more favorable results is imparted to the propellant resulting in (Tummala & Dutta, 2017).

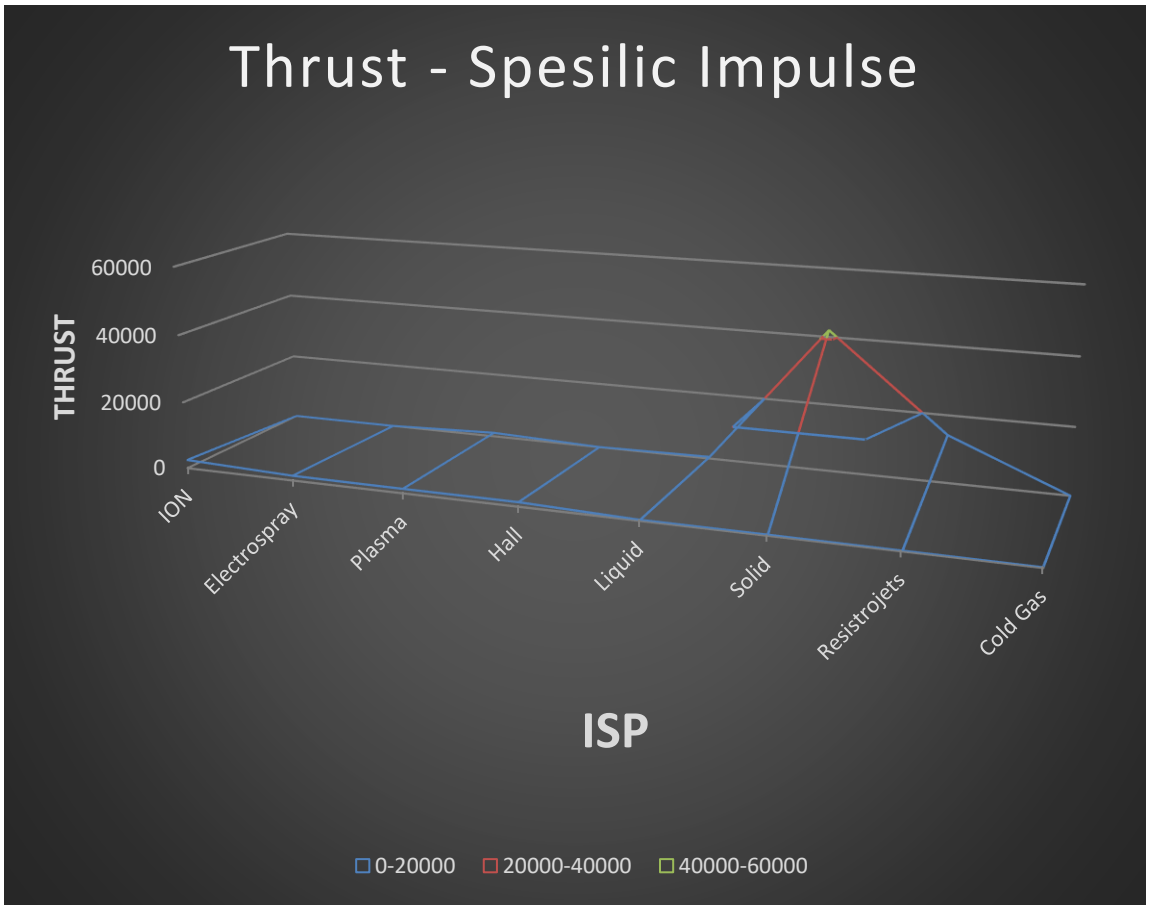

2.3.5 Power - Specific Impulse

From the paragraphs 2.3.1 and 2.3.2 paragraphs are calculated the average Power and the average Specific Impulse at every thruster.

Engine	AVG Power	AVG Isp
Plasma	7,5	1303,2
Electrospray	19,5	1400
Resistrojets	22,5	86,25
ION	74,5	2487,5
Hall	219,1667	1301,5

So at this table it is observed that the electric thrusters provide approximately (except ION) similar performance.

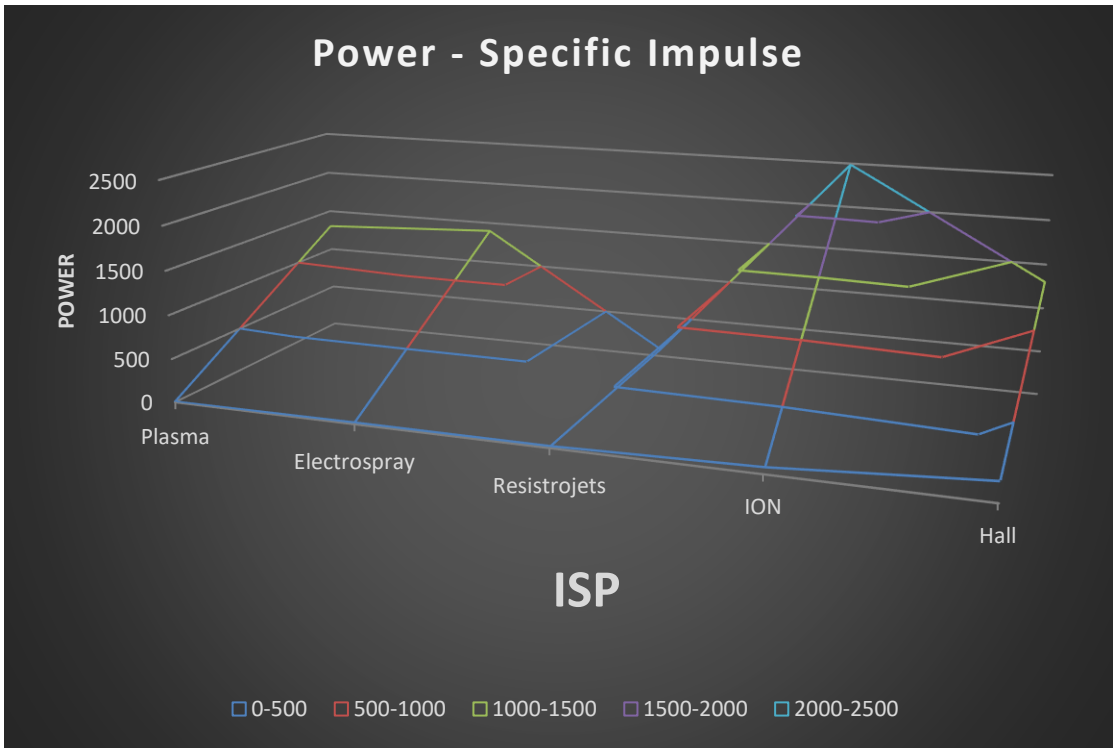

2.3.6 Thrust to Power Ratio - Specific Impulse

From the paragraphs 2.3.1 and 2.3.3 paragraphs are calculated the average Thrust to Power Ratio at every thruster. From the tables at paragraph 2.2 is calculated the average Isp at every thruster.

Engine	Thrust	Power	Thrust- to - Power	Isp
Resistrojets	14175,41111	19,5	726,9441595	86,25
Hall	31,66666667	219,1666667	0,144486692	1301,5
Plasma	1144	7,5	152,5333333	1303,2
Electrospray	0,588	19,5	0,030153846	1400
ION	15	74,5	0,201342282	2487,5

So at this table it is observed that the electric thrusters provide approximately similar Thrust to Power ratio with Isp except resistrojets (which is the lowest) and ION (which is the highest). From Hall, Plasma and Electrospray, which are similar, the highest price is the Electrospray Engine.

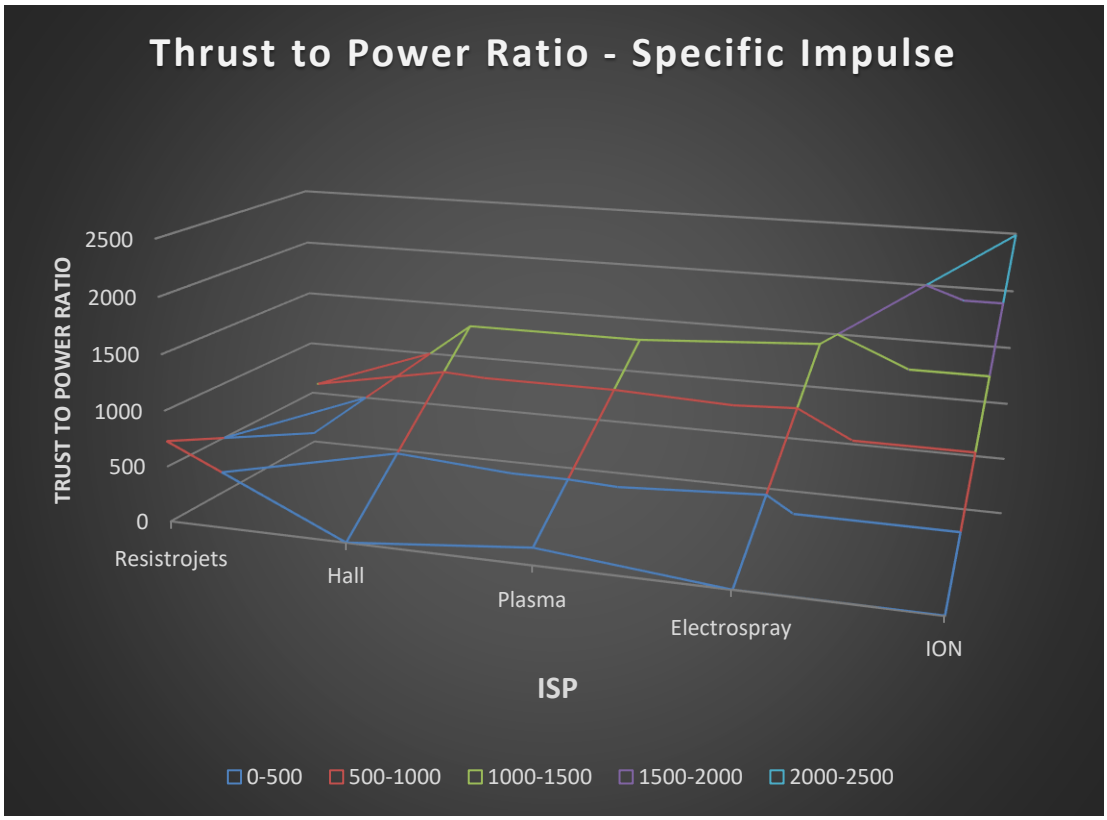

2.4 Microthrusters used in flight

2.4.1 MEMS 1A (Pico 21, PICOSAT-1)

MEMS 1A (Pico 21, PICOSAT-1) was built and launched by Aerospace Corporation, sponsored by DARPA, a US Military organization, on January 27, 2000. It had a mass of 0.275 kg, and was fitted with a Minotaur I Rocket device, and was launched with cold gas propulsion system, with 0.1 N thrust with 5 thrusters. It was placed in an orbit of 750 km SSO with an angle of 97.5º. Its mission was designed within the wider premises of Space Technology and reflected RF Payload and System. The organization had the mission of demonstrating the basic functional elements of a low-power LEO "swarm" or formation of PICOSAT array, and in order to achieve this the device needed to communicate from space using node-type radios and to report the results of MEMS-switched tests. The experiment involved the validation of MEMS radio frequency switches. The two orbiting picosats had to be to be tethered because they had communicated via micropower radios. The tether would keep them within range of each other for crosslink purposes. The device was operational until February 9, 2009 and decayed due to gradual battery power.[20][21]

2.4.2 MEMS 1B (Pico 23, PICOSAT-1)

MEMS 1B (Pico 23, PICOSAT-1) was built and launched by Aerospace Corporation, sponsored by DARPA, a US Military organization, on January 27, 2000. It had a mass of 0.275 kg, and was fitted with a Minotaur I Rocket device, and was launched with cold gas propulsion system, with 0.1 N thrust with 5 thrusters. It was placed in an orbit of 750 km SSO with an angle of 97.5º. Its mission was designed within the wider premises of Space Activity and reflected Science/ Robotic exploration. The organization had the mission of demonstrating the basic functional elements of a low-power LEO "swarm" or formation of PICOSAT array, and in order to achieve this the device needed to communicate from space using node-type radios and to report the

[20] https://directory.eoportal.org/web/eoportal/satellite-missions/o/opal
[21] https://www.nanosats.eu/

results of MEMS-switched tests. The experiment involved the validation of MEMS radio frequency switches. The two orbiting picosats had to be to be tethered because they had communicated via micropower radios. The tether would keep them within range of each other for crosslink purposes. The device was operational until January 31, 2003, when it reentered into the atmosphere. [22][23]

2.4.3 MEPSI 1A (MEMS-based PicoSat Inspector)

MEPSI 1A (MEMS-based PicoSat Inspector) was built and launched by Aerospace Corporation in collaboration with NASA Jet Propulsion Laboratory, sponsored by DARPA, a US Military organization, on November 23, 2002. It was a 1U type of device, was fitted with a shuttle device, and was launched with cold gas propulsion system, with 0.1 N thrust with 5 thrusters. It was placed in an orbit of 287 km with an angle of 51.6º. Its mission was designed within the wider premises of Space Activity and reflected Design & Verification Science. The organization had the mission of demonstrating the capability of deploying an onboard miniature autonomous inspector, tasked to conduct visual inspection of the host satellite. The Pair was connected with 15.2 m tether and Cold gas propulsion system, with 0.1N thrust with 5 thrusters. This propulsion system included MEMS[24] pressure transducers. The device was operational until January 31, 2003, when it reentered into the atmosphere.[20][25]

2.4.4 MEPSI 1B (MEMS-based PicoSat Inspector)

MEPSI 1B (MEMS-based PicoSat Inspector) was built and launched by Aerospace Corporation in collaboration with NASA Jet Propulsion Laboratory, sponsored by DARPA, a US Military organization, on November 23, 2002. It was a 1U type of device, and was fitted with a shuttle device, and was launched with cold gas propulsion system, with 0.1 N thrust with 5 thrusters. It was placed in an orbit of 387

[22] https://www.nanosats.eu/
[23]https://directory.eoportal.org/web/eoportal/satellite-missions/s/stpsat-1
[24] http://www.skyrocket.de/space/doc_sdat/mepsi.htm
[25] https://directory.eoportal.org/web/eoportal/satellite-missions/o/opal

km with an angle of 51.6º. Its mission was designed within the wider premises of Space Technology, and reflected System Design & Verification Science. The organization had the mission of demonstrating the basic functional elements of a low-power LEO "swarm" or formation of PICOSAT array, and in order to achieve this the device needed to communicate from space using node-type radios and to report the results of MEMS-switched tests. The experiment involved the validation of MEMS radio frequency switches. The two orbiting picosats had to be to be tethered because they had communicated via micropower radios. The tether would keep them within range of each other for crosslink purposes. The device was operational until February 9, 2009 and decayed due to gradual battery power decayed.[26] [20]

2.4.5 ION

ION was built and launched by the US University of Illinois, on July 26, 2006. It was a 2U type of device, and was fitted with a dnepr device. The launch failed. Its mission was designed within the wider premises of Space Science, and the study of the upper atmosphere. The organization had the mission of: (1) measuring oxygen airglow emissions from the Earth's mesosphere; (2) testing a new MicroVacuum Arc Thruster (μVAT) with high dynamic range; (3) testing a new SID processor board; (4) testing, a small CMOS camera for earth imaging; and (5) measuring molecular oxygen airglow emissions from the Earth's mesosphere using a 760nm photometer. Oxygen chemistry at this 90km altitude emits a dim glow of light and learning how energy transfers across large spatial regions contribute to knowledge of upper atmospheric dynamics was important. This airglow emission is absorbed by the Earth's lower atmosphere preventing study with Earth-based sensors. The launch of the device failed and the mission was ended.[27]

[20] https://www.nanosats.eu/
[26] https://directory.eoportal.org/web/eoportal/satellite-missions/o/opal
[27] http://cubesat.ece.illinois.edu/

2.4.6 MEPSI 2A

MEPSI 2A was built and launched by Aerospace Corporation in collaboration with NASA Jet Propulsion Laboratory, sponsored by DARPA, a US Military organization, on December 9, 2006. It was a 1U type of device. Its mission was designed within the wider premises of Space Technology, and reflected System Design & Verification Science. The pair was connected with 15.2 m tether and Cold gas propulsion system, with 0.1N thrust with 5 thrusters. This propulsion system included MEMS pressure transducers. The device was operational until it reentered the atmosphere on March 8, 2007, and is considered short-lived.[2820]

2.4.7 MEPSI 2B

MEPSI 2B was built and launched by Aerospace Corporation in collaboration with NASA Jet Propulsion Laboratory, sponsored by DARPA, a US Military organization, on December 9, 2006. It was a 1U type of device. Its mission was designed within the wider premises of Space Technology, and reflected System Design & Verification Science. The Pair was connected with 15.2 m tether and Cold gas propulsion system, with 0.1N thrust with 5 thrusters. This propulsion system included MEMS pressure transducers. The device was operational until it reentered the atmosphere on March 8, 2007, and is considered short-lived.[2920]

2.4.8 CanX-2

CanX-2 was built and launched by the Canadian Institute Space Flight Laboratory, on April 28, 2008. It was a 3U type of device, and was fitted with a PSLV device. It was placed in an orbit of 625 km with an of 97.94^{o}. Its propulsion system

[20] https://www.nanosats.eu/
[28] http://www.skyrocket.de/space/doc_sdat/mepsi.htm
[29]http://www.theoac.ca/Storage/31/2603_Facilities_Infrastructure_Programs_UTIAS_SFL_Big_Performance_Smaller_Satellites_Robert_Zee.pdf

consisted of a liquid-fueled cold-gas thruster system, using sulfur hexafluoride (SF6, high storage density) as a propellant with a total mass of < 0.5 kg. It featured a thrust level of 50-100 mN with a specific impulse of 500-1000 m/s providing a total delta v of > 35 m/s. The nozzle was oriented such that thrusting induced a major-axis spin on CanX-2. NanoPS involves mainly attitude control maneuvers that spin the satellite about one axis. Its mission was designed within the wider premises of Space Technology, and the study of the upper atmosphere. It involved: (1) a GPS radio occultation experiment to characterize the upper atmosphere (University of Calgary); (2) an atmospheric spectrometer to measure greenhouse gases (York University); and, (3) a space materials experiment to evaluate the effects of atomic oxygen on a protective coating (University of Toronto). The technologies that were successfully tested include a novel propulsion system (Nanosatellite Propulsion System, or "NANOPS"), custom UHF and S-band radios, innovative attitude sensors and actuators, and a modified commercial GPS receiver. It is still operational.[30]

2.4.9 CanX-6

CanX-6 was built and launched by the Canadian Institute Space Flight Laboratory, on April 28, 2008. It was a 6.5 kg device, and was fitted with a PSLV device. It was placed in an orbit of 625 km with an angle of 97.94^{o}. The device included a novel SFL-designed cold gas propulsion system and miniature attitude determination and control subsystem sensors and actuators to name a few. Its mission was designed within the wider premises of Space Technology. Its mission was to test an Automatic Identification System (AIS) receiver developed by COM DEV for detection of signals transmitted by maritime vessels. It is still operational.[3120]

[20]https://www.nanosats.eu/
[30]http://www.theoac.ca/Storage/31/2603_Facilities_Infrastructure_Programs_UTIAS_SFL_Big_Performance_Smaller_Satellites_Robert_Zee.pdf
[31]http://www.theoac.ca/Storage/31/2603_Facilities_Infrastructure_Programs_UTIAS_SFL_Big_Performance_Smaller_Satellites_Robert_Zee.pdf

2.4.10 PSSC (PSSCT, Pico Satellite Solar Cell Testbed)

PSSC (PSSCT, Pico Satellite Solar Cell Testbed) was built and launched by the US Military organization The Aerospace Corporation, on November 29, 2008. It was a 6.5 kg device, and was fitted with a shuttle device. It was placed in an orbit of 345 km with an angle of 97.94º. Its mission was designed within the wider premises of Space Technology. Its mission was to monitor accelerated radiation degradation of triple-junction solar cells in a high radiation environment. The device was operational until March 19, 2009 and it reentered the atmosphere on February 12, 2010.[3220]

2.4.11 KKS-1 (Kouku Kosen Satellite-1, KISEKI)

KKS-1 (Kouku Kosen Satellite-1, KISEKI) was built and launched by the Japanese Tokyo Metropolitan College of Industrial Technology, on January 23, 2009. It was a 3.17 kg device, and was fitted with an H-IIA device. It was placed in an orbit of 660 km with an angle of 98º. Its mission was designed within the wider premises of Space Technology and System Design and Verification. KKS-1 was an educational satellite that was developed by the students and teaching staffs of Tokyo Metropolitan College of Industrial Technology as MONOZUKURI education of aerospace engineering. It had a micro propulsion system onboard, and undertook the first space-demonstration experiment of laser ignition thruster. Its attitude controls were facilitated through a Small Reaction Wheel. It provided photographs taken by a CMOS camera（320×240 pixel color). The KKS-1 carried messages from supporters to space. The device is operational.[3320]

[20]https://www.nanosats.eu/
[32]http://webcache.googleusercontent.com/search?q=cache:FxV3-nFGIs8J:https://directory.eoportal.org/web/eoportal/satellite-missions/p/pssct+&cd=1&hl=et&ct=clnk&gl=ee
[33] http://www.metro-cit.ac.jp/~kks-1/kks-gs-top-e.htm

2.4.12 PSSC-2 (Pico Satellite Solar Cell Testbed-2, PSSC Testbed-2, PSSCT-2)

PSSC-2 (Pico Satellite Solar Cell Testbed-2, PSSC Testbed-2, PSSCT-2) was built by the US military organization The Aerospace Corporation, and was launched on July 20, 2011. It was a 3.7 kg device, and was fitted with a shuttle device. It was placed in an orbit of 370 km with an angle of 51.6º. Its mission was designed within the wider premises of Space Technology and System Design and Verification. Its mission was to test a low cost risk reduction for the upcoming SENSE and Compact Total Electron Content Sensor (CTECS) that characterizes the ionosphere by measurement of the occultation of GPS signals - a precursor of an instrument with the same function on SENSE. PSSC2 also carried over the task from PSSC1 of characterizing the performance of advanced solar cells from Spectrolab and Emcore. Finally, PSSC2 hosted an upgraded Miniature Tracking Vehicle payload, similar to that flown on PSSC1 that served as an orbiting reference for ground tracking systems. The device was operational until it reentered the atmosphere on August 12, 2011.[3420]

2.4.13 STRaND-1 (Surrey Training, Research and Nanosatellite Demonstrator)

STRaND-1 (Surrey Training, Research and Nanosatellite Demonstrator) was built by the UK company Surrey Satellite Technology in collaboration with the University of Surrey Space Center, and was launched on February 25, 2013. It was a 3U device, and was fitted with a PSLV device. It was fitted with a BPS (Butane Propulsion Subsystem), and a PPT (Pulsed plasma Thruster). Its mission was designed within the wider premises of Space Technology. It was placed in an orbit of 781 km with an angle of 51.6º. Its mission was to tech technologies for future commercial operations. It had a modern Commercial off the Shelf (COTS) Android smartphone as a payload. The device was operational, went silent in March 30, 2013, but came back on July 23, 2013.[3520]

[20]https://www.nanosats.eu/
[34]https://directory.eoportal.org/web/eoportal/satellite-missions/p/pssct-2
[35]http://www.sstl.co.uk/Missions/STRaND-1--Launched-2013/STRaND-1/STRaND-1--Smartphone-nanosatellite

2.4.14 Delfi-n3Xt

Delfi-n3Xt was built by the Dutch Delft University of Technology, and was launched on November 21, 2013. It was a 3U device, and was fitted with a Dnepr device. It was also fitted with cold gas mircopropulsion and the experimental ISIS Transceiver (ITRX). Its mission was designed within the wider premises of Space Technology and Space Design and Verification. It was placed in an orbit of 670 km with an angle of 97.79º. Its mission was related to education, technology demonstration and nanosatellite bus advancement. The device was operational till February 21, 2014, after which contact was lost.[3620]

2.4.15 Wren

Wren was developed by the German company Stadoko UG, and was launched on November 21, 2013. It was a PocketCube 1p device, and was fitted with a Dnepr device. Its mission was designed within the wider premises of Space Technology and Space Design and Verification. It was fitted with a camera, 4 pulsed plasma thrusters, and a 3 axis reaction wheel and a color camera. It was placed in an orbit of 670 km with an angle of 97.79º. This crowd-funded femto-satellite by start-up company STADOKO was developed to test miniaturized thrusters, 3-axis control and a new image based navigation system. It was equipped with a camera system to take pictures of the Earth, Sun and Deep Space. In addition to the conventional gyro- and magnetic field attitude sensors, those three components constituted an adaptive feedback guidance system. The device failed after a short while and was operational till February 24, 2013, as it failed, after which contact was lost.[3720]

[20]https://www.nanosats.eu/
[36] http://www.delfispace.nl/index.php/general/project-team
[37] http://www.pocketqubeshop.com/blogs/news/10370774-meet-the-pocketqube-team-wren

2.4.16 SNAP

SNAP was developed by the US Military organization Space & Missile Defense Command, and was launched on December 12, 2013. It was a 3U device, and was fitted with an Atlas V device. It was placed in an orbit of 467 x 883 km with an angle of 120.5^{o}. Its mission was designed within the wider premises of Space Technology and Space Design and Verification. Its mission was to related to the SMDC Nanosatellite Program (SNaP) - Joint Capabilities Technology Demonstrations.[3820]

2.4.17 POPSAT-HIP 1

POPSAT-HIP 1 was developed by the Singapore based Microspace Rapid Pte Ltd., and was launched on June 19, 2014. It was a 3U device, and was fitted with a Dnepr device. Its mission was designed within the wider premises of Space Technology and Space Design and Verification. It was placed in an orbit of 610 km with an angle of 97.99^{o}. Its mission was to demonstrate the functionality of a high resolution optical payload and attitude control propulsion system on a Cubesat Class Nano-satellite. The device was operational for almost a year.[3920]

2.4.18 CanX-4

CanX-4 was built and launched by the Canadian Institute Space Flight Laboratory, on June 30, 2014. It was a 7kg type of device, and was fitted with a PSLV device. It was placed in an orbit of 660 km with an angle of 98.2^{o}. Its mission was designed within the wider premises of Space Technology and Space Design and Verification. It primary mission was to demonstrate on-orbit formation flying. In this context, formation flying is defined as two or more satellites controlling their position and orientation with respect to one another to achieve a predefined configuration necessary for coordinated operations. It is still operational.[4020]

[20]https://www.nanosats.eu/
[38] http://www.nasa.gov/directorates/heo/home/CSLI_selections.html#.VFu-wvnCZ8E
[39]http://www.dk3wn.info/sat/afu/sat_popsat.shtml
[40] https://directory.eoportal.org/web/eoportal/satellite-missions/c-missions/canx-4-5

2.4.19 CanX-5

CanX-5 was built and launched by the Canadian Institute Space Flight Laboratory, on June 30, 2014. It was a 7kg type of device, and was fitted with a PSLV device. It was placed in an orbit of 660 km with an angle of 98.2º. Its mission was designed within the wider premises of Space Technology and Space Design and Verification. It primary mission was to demonstrate on-orbit formation flying. In this context, formation flying is defined as two or more satellites controlling their position and orientation with respect to one another to achieve a predefined configuration necessary for coordinated operations. It is still operational.[4120]

2.4.20 AeroCube-8B (IMPACT)

AeroCube-8B (IMPACT) was built by the US military organization The Aerospace Corporation, and was launched on May 20, 2015. It was a 1.5U device, and was fitted with an Atlas V device. It was placed in an orbit of 370 x 700 km with an angle of 55º. Its mission was designed within the wider premises of Space Technology and In-Space propulsion technologies. Its mission was to: (1) demonstrate the functioning of an Scalable ion-Electrospray Propulsion system (SiEPro); (2) measure IV curves for 4-junction IMM solar cells and 5-junction SBT cell; (3) demonstrate CNT harness and use of CNT/PEEK material; and, (4) evaluate CNT radiation-shielding material. The device was is still operational.[4220]

2.4.21 BRICSat-P

BRICSat-P (Ballistic Reinforced Communication Satellite, previously PSat B, ParkinsonSat B) was built by the US university, US Naval Academy, and was launched on May 05, 2015. It was a 1.5U device, and was fitted with an Atlas V device. It was placed in an orbit of 370 x 700 km with an angle of 55º. Its mission was designed

[20]https://www.nanosats.eu/
[41] https://directory.eoportal.org/web/eoportal/satellite-missions/c-missions/canx-4-5
[42]http://www.ulalaunch.com/uploads/docs/Launch/AtlasV_AFSPC-5_ULTRASat_CubeSat_descriptions.pdf

within the wider premises of Space Technology. Its primary objectives were to integrate a miniature size propulsion system into a 1.5U CubeSat and perform three maneuvers in space: de-tumbling, pointing control, and delta-V. Secondary objective was to expand APRS network. APRS constellation transponder with downlink on 437.975MHz and with uplink on 145.825MHz 1k2 and 9k6 AX25 - PSK31 Xponder with 28.120 MHz uplink and UHF FM downlink on 435.350 MHz. The device was operational but subsequently faced power problems and weak signals.[4320]

2.4.22 USS Langley (Unix Space Server)

USS Langley (Unix Space Server) was built by the US university US Naval Academy, and was launched on May 05, 2015. It was a 3U device, and was fitted with an Atlas V device. It was placed in an orbit of 370 x 700 km with an angle of 55º. Its mission was designed within the wider premises of Space Technology and System Design and Verifcation. Its primary mission was to fly the Unix-Space-Server (USS) to experiment with using a server in space of Amateur Experimentation and the secondary mission was to continue the PSK-31 multi-user transponder experiments.[4420]

2.4.23 AeroCube-8A (IMPACT)

AeroCube-8A (IMPACT) was built by the US military organization The Aerospace Corporation, and was launched on May 20, 2015. It was a 1.5 U device, and was fitted with an Atlas V device. It was placed in an orbit of 370 x 700 km with an angle of 55º. Its mission was designed within the wider premises of Space Technology and In-Space propulsion technologies. Its mission was to: (1) demonstrate Scalable ion-Electrospray Propulsion system (SiEPro); (2) measure IV curves for 4-junction IMM solar cells and 5-junction SBT cell; (3) demonstrate CNT harness and use of

[20]https://www.nanosats.eu/
[43] http://space.skyrocket.de/doc_sdat/psat.htm
[44] http://www.eham.net/articles/34674

CNT/PEEK material; and (4) evaluate CNT radiation-shielding material. The device is still operational.[4520]

2.4.24 SERPENS

SERPENS was built by the Brazilian University SERPENS (Sistema Espacial para Realização de Pesquisa e Experimentos com Nanossatélites) programme university consortium, and was launched on August 19, 2015. It was a 3 U device, and was fitted with an H-2B device. Its mission was designed within the wider premises of Space Technology. It was a transponder to test VHF and S-band communications for store and forward messaging, a UHF transponder fully compatible with the HUMSAT store and forward messaging system and pulsed plasma thruster (PPT) built by Mars Space Ltd. and Clyde Space. The device was operational and reentered earth's atmosphere |on March 27, 2016.[4620]

2.4.25 TW-1A (STU-2, Shankeda 2, Tianwang-1A, Sat-A, SECM-1)

TW-1A (STU-2, Shankeda 2, Tianwang-1A, Sat-A, SECM-1) was built by the Chinese Institute Shanghai Engineering Centre for Microsatellites (SECM), and was launched on September 25, 2015. It was a 3 U device, and was fitted with an Chang Zheng 11 (CZ-11) device. It was placed in an orbit of 470 x 485 km with an angle of 97.3^{o}. Its mission was designed within the wider premises of Space Technology. It involved GAMALINK, which is an S-band inter-satellite communication module, a novel dual band GPS/BD receiver, an AIS receiver, and an ADS-B receiver, all being designed based on SDR technologies. It also included a novel cold-gas micro propulsion module based on MEMS technology which was used for orbit and constellation control. TW-1 project consisted of three CubeSats carrying different payloads and instruments with one 3U CubeSat and two 2U CubeSats, forming an along-trace satellite network

[20]https://www.nanosats.eu/
[45]http://www.ulalaunch.com/uploads/docs/Launch/AtlasV_AFSPC-5_ULTRASat_CubeSat_descriptions.pdf
[46] http://www.amsatuk.me.uk/iaru/finished_detail.php?serialnum=418

and/or constellation. CubeSats networking was based on Gamalink. The mission involved: (1) monitoring sea ice and gaining the maritime traffic information in polar regions based on AIS receiver and camera; () demonstration of autonomous formation flying including the along-track orbital (ATO) formation and the projected circular orbital (PCO) formation; (3) in-orbit demonstration and validation of ADS-B receiver/ Gamalink / Micro-propulsion; and, imaging the satellite separating process. The device is still operational.[4720]

2.4.26 TW-1B (STU-2, Shankeda 2, Tianwang-1A, Sat-A, SECM-1)

TW-1B (STU-2, Shankeda 2, Tianwang-1A, Sat-A, SECM-1) was built by the Chinese Institute Shanghai Engineering Centre for Microsatellites (SECM), and was launched on September 25, 2015. It was a 2 U device, and was fitted with an Chang Zheng 11 (CZ-11) device. It was placed in an orbit of 470 x 485 km with an angle of 97.3º. Its mission was designed within the wider premises of Space Technology. It involved GAMALINK, which is an S-band inter-satellite communication module, a novel dual band GPS/BD receiver, an AIS receiver, and an ADS-B receiver, all being designed based on SDR technologies. It also included a novel cold-gas micro propulsion module based on MEMS technology which was used for orbit and constellation control. TW-1 project consisted of three CubeSats carrying different payloads and instruments with one 3U CubeSat and two 2U CubeSats, forming an along-trace satellite network and/or constellation. CubeSats networking was based on Gamalink. The mission involved: (1) monitoring sea ice and gaining the maritime traffic information in polar regions based on AIS receiver and camera; () demonstration of autonomous formation flying including the along-track orbital (ATO) formation and the projected circular orbital (PCO) formation; (3) in-orbit demonstration and validation of ADS-B receiver/ Gamalink / Micro-propulsion; and, imaging the satellite separating process. The device is still operational.[4820]

[20]https://www.nanosats.eu/
[47] http://www.amsatuk.me.uk/iaru/formal_detail.php?serialnum=468
[48] http://www.amsatuk.me.uk/iaru/formal_detail.php?serialnum=468

2.4.27 TW-1C (STU-2, Shankeda 2, Tianwang-1A, Sat-A, SECM-1)

TW-1C (STU-2, Shankeda 2, Tianwang-1A, Sat-A, SECM-1) was built by the Chinese Institute Shanghai Engineering Centre for Microsatellites (SECM), and was launched on September 25, 2015. It was a 2 U device, and was fitted with an Chang Zheng 11 (CZ-11) device. It was placed in an orbit of 470 x 485 km with an angle of 97.3º. Its mission was designed within the wider premises of Space Technology. It involved GAMALINK, which is an S-band inter-satellite communication module, a novel dual band GPS/BD receiver, an AIS receiver, and an ADS-B receiver, all being designed based on SDR technologies. It also included a novel cold-gas micro propulsion module based on MEMS technology which was used for orbit and constellation control. TW-1 project consisted of three CubeSats carrying different payloads and instruments with one 3U CubeSat and two 2U CubeSats, forming an along-trace satellite network and/or constellation. CubeSats networking was based on Gamalink. The mission involved: (1) monitoring sea ice and gaining the maritime traffic information in polar regions based on AIS receiver and camera; () demonstration of autonomous formation flying including the along-track orbital (ATO) formation and the projected circular orbital (PCO) formation; (3) in-orbit demonstration and validation of ADS-B receiver/ Gamalink / Micro-propulsion; and, imaging the satellite separating process. The device is still operational.[4920]

2.4.28 Aerocube-7A

Aerocube-7A (OCSD, Optical Communications and Sensor Demonstration, IOCPS-A, Integrated Optical Communications and Proximity Sensors) was built by the US military organization The Aerospace Corporation, and was launched on August 10, 2015. It was a 1.5 U device, and was fitted with an Atlas V device. It was placed in an orbit of 500 x 600 km with an angle of 63º. Its mission was designed within the wider

[20]https://www.nanosats.eu/
[49] http://www.amsatuk.me.uk/iaru/formal_detail.php?serialnum=468

premises of Space Technology. Its mission was to: (1) demonstrate optical communications from a CubeSat to a 30 cm diameter ground station from LEO at a rate of at least 5 Mbps; and, (2) demonstrate tracking of a nearby spacecraft using a commercial COTS automotive anti-collision radar sensor and an inexpensive optical mouse sensor. It was semi-operational, as a software update anomaly disabled the attitude control main processor and was booted into a partially updated program. The device is still operational.[5020]

2.4.29 Aerocube-8C (IMPACT)

Aerocube-8C (IMPACT)was built by the US military organization The Aerospace Corporation, and was launched on November 11, 2016. It was a 1.5 U device, and was fitted with an Atlas V device. It was placed in an orbit of 617 km with an angle of 98º. Its mission was designed within the wider premises of Space Technology and In-Space Propulsion Technologies. Its mission was to: (1) demonstrate Scalable ion-Electrospray Propulsion system (SiEPro); (2) measure IV curves for 4-junction IMM solar cells and 5-junction SBT cell; (3) demonstrate CNT harness and use of CNT/PEEK material; and, (4) evaluate CNT radiation-shielding material. The device is still operational.[5120]

2.4.30 Aerocube-8D (IMPACT)

Aerocube-8C (IMPACT) was built by the US military organization The Aerospace Corporation, and was launched on November 11, 2016. It was a 1.5 U device, and was fitted with an Atlas V device. It was placed in an orbit of 617 km with an angle of 98º. Its mission was designed within the wider premises of Space Technology and In-Space Propulsion Technologies. Its mission was to: (1) demonstrate

[20]https://www.nanosats.eu/
[50]https://www.nasa.gov/directorates/spacetech/small_spacecraft/feature/Orbital_Testing_Begins_for_Advanced_Small_Spacecraft_Communications
[51]https://www.nasa.gov/directorates/spacetech/small_spacecraft/feature/Orbital_Testing_Begins_for_Advanced_Small_Spacecraft_Communications

Scalable ion-Electrospray Propulsion system (SiEPro); (2) measure IV curves for 4-junction IMM solar cells and 5-junction SBT cell; (3) demonstrate CNT harness and use of CNT/PEEK material; and, (4) evaluate CNT radiation-shielding material The device is still operational.[5220]

2.4.31 Biarri-Point

Biarri-Point was built by the US Air Force, and was launched on April 18, 2017. It was a 3 U device, and was fitted with an Atlas V device. Its mission was designed within the wider premises of Space Technology and In-Space Propulsion Technologies. Biarri is an international defense-science collaborative program, with the US, Canada, the UK, and Australia each contributing a subsystem of the mission. One of the benefits of such collaboration is the capability of building a process that fosters participation of nations, especially as it relates to space related programs. This program involved integrating several payloads from the participating nations into three Colony 2 3U-cubesats that were supplied by the USA, with the system integration of the payloads being carried out by AFRL The device is still operational.[5320]

2.4.32 Ursa Maior

Ursa Maior was built by the University of Rome, Italy, and was launched on June 23, 2017. It was a 3 U device, and was fitted with PSLV and QB50 devices. It was placed in an orbit of 500 km with an angle of 97º. Its mission was designed within the wider premises of Space Technology. The space station will operate to conduct scientific experiments in the framework of the QB50 project. Micropropulsion system which was the main goal is to design and test a new integrated MEMS (Micro Electro Mechanical System) valve-nozzle system. The whole system is designed to fit in a 1/2 U of the CubeSat. The device is still operational.[5420]

[20]https://www.nanosats.eu/
[52]https://www.nasa.gov/directorates/spacetech/small_spacecraft/feature/Orbital_Testing_Begins_for_Advanced_Small_Spacecraft_Communications
[53] http://www.acser.unsw.edu.au/downloads/2015Cubesat/28-Lingard.pdf
[54]http://www.amsatuk.me.uk/iaru/formal_detail.php?serialnum=410

2.4.33 PACSCISAT

PACSCISAT was built by the US based Tyvak/ Terran Orbital company, and was launched on June 23, 2017. It was a 3 U device, and was fitted with PSLV device. It was placed in an orbit of 500 km with an angle of 97º. Its mission was designed within the wider premises of Space Technology. The mission related to technology demonstration for deorbiting. It passed built-in-tests (BIT) on both its primary and redundant Smart Energetics Architecture (SEA) sequencing system and devices and fired Modular Architecture Propulsion System (MAPS) rocket motors. The device was operational till September, 2017.[5520]

2.4.34 D-Sat (Deorbit Satellite)

D-Sat (Deorbit Satellite) was built by the Italian company D-Orbit, and was launched on June 23, 2017. It was a 3 U device, and was fitted with PSLV device. It was placed in an orbit of 500 km with an angle of 97º. Its mission was designed within the wider premises of Space Technology. Its mission was to demonstrate in-orbit the capability of D-Orbit's technology. It was the first satellite ever to be actively de-orbited in a quick, safe, reliable and controlled way. It also provided disaster Alert proof of concept payload and demonstrated de-orbit capabilities. The device was operational till October 10, 2017.[5620]

2.4.35 LituanicaSAT-2

D-Sat (Deorbit Satellite) was built by the Lithuanian company NanoAvionics LLC, and was launched on June 23, 2017. It was a 3 U device, and was fitted with PSLV device. It was placed in an orbit of 500 km with an angle of 97º. Its mission was designed within the wider premises of Space Technology. The primary objective of the

[20]https://www.nanosats.eu/
[55] http://isro.gov.in/pslv-c38-cartosat-2-series-satellite/pslv-c38-cartosat-2-series-satellite-brochure
[56] http://www.amsatuk.me.uk/iaru/finished_detail.php?serialnum=399

experiment was to demonstrate the orbital maneuvering and drag compensation capabilities of a CubeSat using an integral green monopropellant microthruster. The idea behind this experiment as to further advance the technology of nanosatellite micro propulsion that is required to implement future projects of CubeSat constellations. To contribute to the QB50 mission objectives the thruster was designed to implement orbital maintenance/correction of a CubeSat by producing incremental (to minimize the effects of thrust vector misalignment) thrust in the direction of the velocity vector to overcome atmospheric drag and thus considerably prolong satellite's orbital lifetime. It had three 3 main modules: a science unit, a functional unit and an experimental unit. The science unit contained a set of standardized sensors for QB50 scientific mission provided by MSSL and an interface board. The device is still operational.[5720]

2.4.36 NanoACE

NanoACE was built by the US based Tyvak/ Terran Orbital company, and was launched on July 07, 2017. It was a 3 U device, and was fitted with a Sojuz-2-1a device. It was placed in an orbit of 600 km with an angle of 97.6^{o}. Its mission was designed within the wider premises of Space Technology. The primary objective was to validate the endeavor suite technologies that will be used for future missions and is solely for the purpose of internal Tyvak development as an attitude control experiment. It included a VACCO propulsion module, a Validate the Command and Data Handling (CDH) system, Guidance Navigation and Control (GNC) software and actuators, as well as test visible & IR cameras. The device is still operational.[5820]

2.4.37 Aerocube-7B

Aerocube-7B (OCSD-B, Optical Communications and Sensor Demonstration, IOCPS-B, Integrated Optical Communications and Proximity Sensors) was built by the

[20]https://www.nanosats.eu/
[57] https://en.wikipedia.org/wiki/Lituanica_SAT-2
[58] http://isro.gov.in/pslv-c38-cartosat-2-series-satellite/pslv-c38-cartosat-2-series-satellite-brochure

US military organization The Aerospace Corporation, and was launched on November 12, 2016. It was a 1.5 U device, and was fitted with an Antares 230 device. Its mission was to: (1) demonstrate optical communications from a CubeSat to a 30 cm diameter ground station from LEO at a rate of at least 5 Mbps; and, (2) demonstrate tracking of a nearby spacecraft using a commercial COTS automotive anti-collision radar sensor and an inexpensive optical mouse sensor. The device is still operational.[5920]

2.4.38 Aerocube-7C

Aerocube-7C (OCSD-B, Optical Communications and Sensor Demonstration, IOCPS-B, Integrated Optical Communications and Proximity Sensors) was built by the US military organization The Aerospace Corporation, and was launched on November 12, 2016. It was a 1.5 U device, and was fitted with an Antares 230 device. Its mission was to: (1) demonstrate optical communications from a CubeSat to a 30 cm diameter ground station from LEO at a rate of at least 5 Mbps; and, (2) demonstrate tracking of a nearby spacecraft using a commercial COTS automotive anti-collision radar sensor and an inexpensive optical mouse sensor. The device is still operational.[6020]

2.4.39 CANYVAL-X 2U Tom

CANYVAL-X 2U Tom was built by the South-Korean Yonsei University of Rome, Italy, and was launched on January 12, 2018. It was a 2 U device, and was fitted with PSLV-XL device. It was placed in an orbit of 505 km with an angle of 97^{o}. Its mission was designed within the wider premises of Space Science. It is a CubeSat astronomy device using virtual telescope alignment. The two cubesats maintain inertial-hold in about 10 min using vision alignment system. It could pave the way for a new class of instrument that can peer through the sun's glare or at distant alien planets, without requiring a massive single scope. Its mission was to demonstrate key technologies for using free-flying coronagraphs in space, including micro-propulsion

[20]https://www.nanosats.eu/
[59]https://www.nasa.gov/directorates/spacetech/small_spacecraft/feature/Orbital_Testing_Begins_for_Advanced_Small_Spacecraft_Communications
[60]https://www.nasa.gov/directorates/spacetech/small_spacecraft/feature/Orbital_Testing_Begins_for_Advanced_Small_Spacecraft_Communications

using millinewton thrusters, relative position sensing, and communications control between the two spacecrafts. The device is still operational.[6120]

2.4.40 GOMX-48

GOMX-48 was built by the Denmark based GomSpace Company, and was launched on February 02, 2018. It was a 6 U device, and was fitted with Long March 2D device. It was placed in an orbit of 500 km. Its mission was designed within the wider premises of Space Activity. Its mission was to demonstrate inter-satellite linking and station keeping capabilities and key enabling technologies for the future. The device is still operational.[6220]

[20]https://www.nanosats.eu/
[61] http://www.skyandtelescope.com/astronomy-news/the-rise-of-cubesat-astronomy-08032016/
[62] http://www.gomspace.com/documents/investor/GOMX-4B.pdf

CHAPTER 3 – PROPUSLION ANALYSIS FOR CUBESATS: 1.5U, 3U AND 6U

3.1 Cubesat Size 1.5U, 3U and 6U

This chapter consists a research for the microthruster selection of the 40 cubesats missions that are analyzed in 2nd chapter. In the 1st chapter it is noticed that 1U volume is the most ‘‘preferred’’ space for propellants’ installation. So one operational cubesat with propulsion need to be at least 1.5U (for propellants installation).

3.1.1 Cubesat missions with 1.5U dimensions

The summary of 1.5U cubesats is 20. Cold gas thruster ‘’comes first’’ with 60%. With 20% are the electrospray thrusters. Plasma with 20% takes the 3rd place . Finally there 2 missions with one ION thruster (launch failure) and one with solid. So in the next paragraph the main research will take place between cold gas and electrospray thrusters.

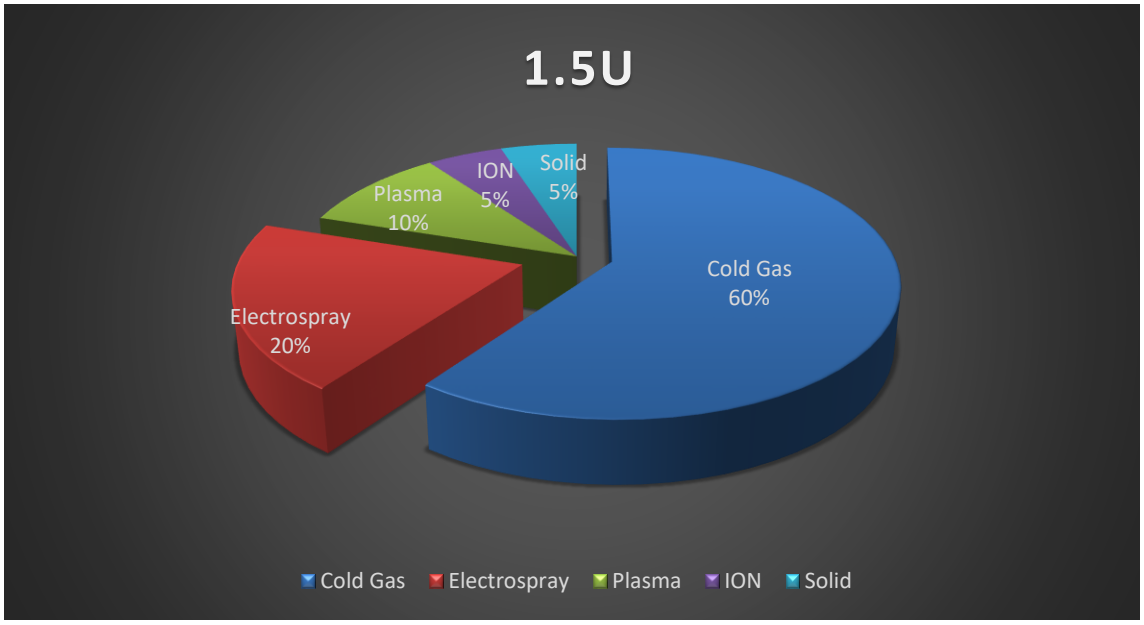

Engine	1.5U Cubesats
Cold Gas	12
Electrospray	4
Plasma	2
ION	1
Solid	1

3.1.2 Cubesat missions with 3U dimensions

The summary of 3U cubesats is 15. Cold gas is again the most preferred thruster taking 40%. However on the 2nd place is the solid propellant with 20%. After solid propellant comes plasma thruster with 13%. At the last place with 1 mission are all the others thrusters (Electrospray, Laser and Liquid). So in the next paragraph the main research will take place between cold gas and solid thrusters.

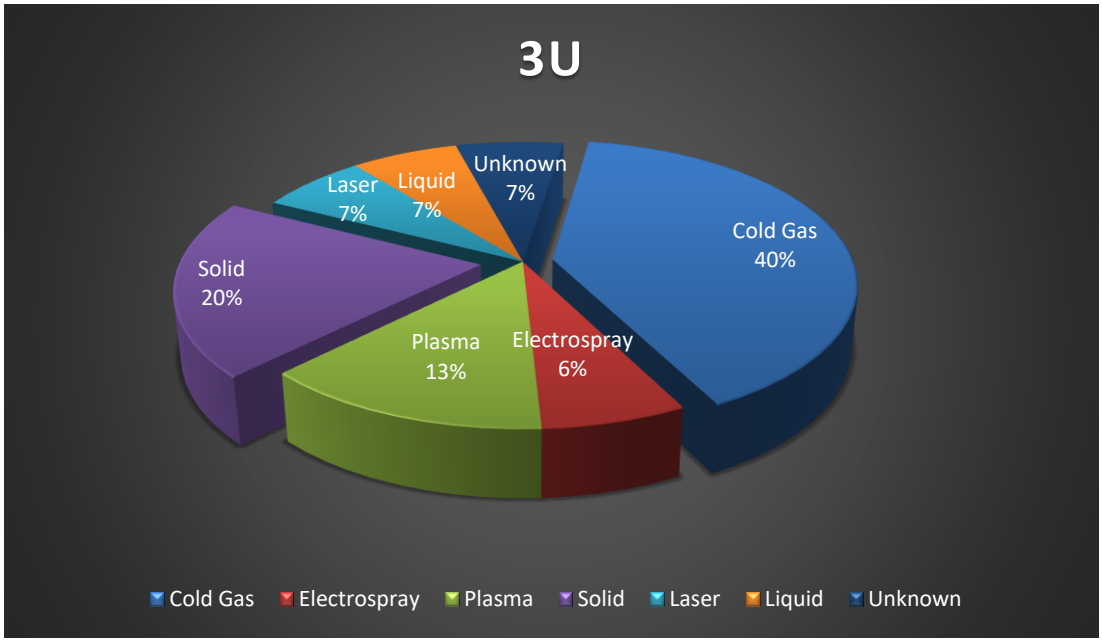

Engine	3U Cubesats
Cold Gas	6
Electrospray	1
Plasma	2
Solid	3
Laser	1
Liquid	1
Unknown	1

3.1.3 Cubesat missions with 6U dimensions

The summary of 6U cubesats is only 5. Cold gas is again the most preferred thruster taking 80%. The different propellant mission the PSSC (PSSCT, Pico Satellite Solar Cell Testbed) cubesat with a solid thruster. So in the next paragraph the research will take place between cold gas and solid thrusters.

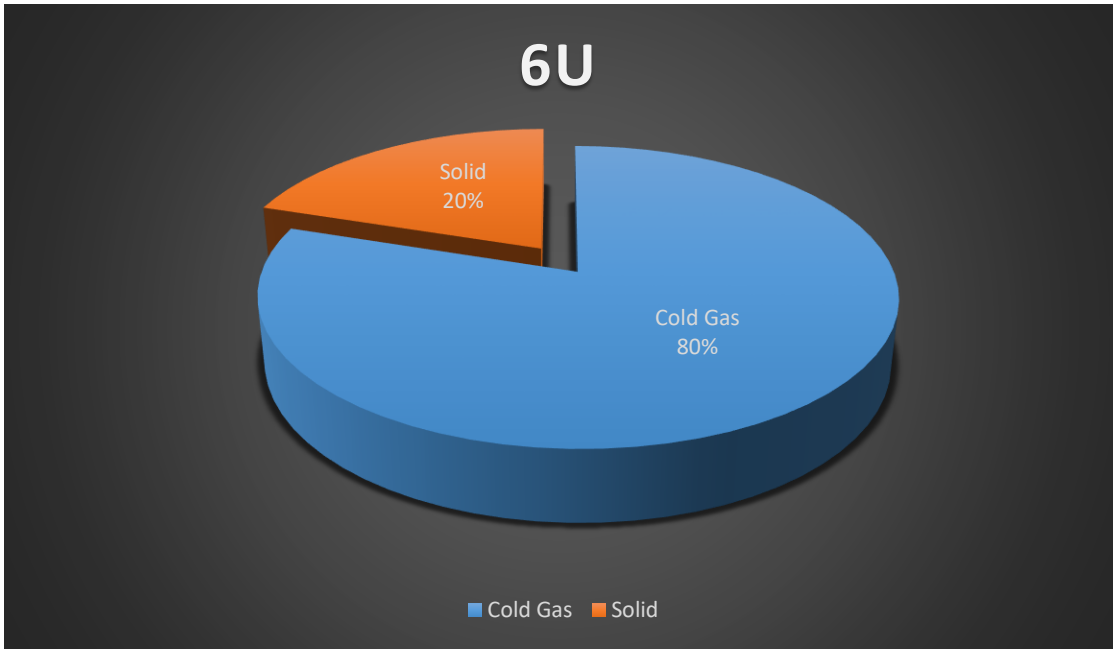

Engine	6U Cubesats
Cold Gas	4
Solid	1

3.2 Microthrusters for 1.5U, 3U and 6U satellites

3.2.1 Microthrusters for 1.5U satellite

From the 1.5U satellites with microthrusters the 12 were cold gas and 4 were electrospray. The missions with electrospray thrusters are AeroCube-8B, AeroCube-8A, AeroCube-8C and AeroCube-8D from the Aerospace Corporation. The thruster of Aerocube-8A, 8B, 8C and 8D is the **S-iEPS** (Scalable ion-Electrospray Propulsion system)

The characteristics of this thruster are:

Engine	Thrust (mN)	Isp (s)	Propellant
S-iEPS	0.1	1200	ionic liquid

So the electrospray propulsion system that is used in a 1.5U cubesat is the **S-iEPS**.

The cold gas cubesat missions are 12. The missions with cold gas are MEMS 1A (Pico 21, PICOSAT-1), MEMS 1B (Pico 23, PICOSAT-1), MEPSI 1A (MEMS-

based PicoSat Inspector), MEPSI 1B (MEMS-based PicoSat Inspector), MEPSI 2A, MEPSI 2B, TW-1B (STU-2, NJUST 2, Tianwang-1B, Sat-B, SECM-1), TW-1C (STU-2, NJFA , Tianwang-1C, Sat-C, SECM-1), Aerocube-7A (OCSD, Optical Communications and Sensor Demonstration, IOCPS-A, Integrated Optical Communications and Proximity Sensors), Aerocube-7B,Aerocube-7C and CANYVAL-X 2U .

The MEMS 1A (Pico 21, PICOSAT-1), MEMS 1B (Pico 23, PICOSAT-1), MEPSI 1A (MEMS-based PicoSat Inspector), MEPSI 1B (MEMS-based PicoSat Inspector), MEPSI 2A, MEPSI 2B from DARPA contain **MEMS Cold Gas** Thruster. But this thruster is for altitude control.

The TW-1B (STU-2, NJUST 2, Tianwang-1B, Sat-B, SECM-1), TW-1C (STU-2, NJFA , Tianwang-1C, Sat-C, SECM-1) contain also **MEMS Cold Gas** thruster.

The Aerocube-7A (OCSD, Optical Communications and Sensor Demonstration, IOCPS-A, Integrated Optical Communications and Proximity Sensors), Aerocube-7B and Aerocube-7C missions contain also **MEMS Cold Gas** thruster.

The CANYVAL-X 2U Tom is a South Korea satellite with **1 DOF mCAT x4** engine. But this thruster is also for altitude control.

Engine	Thrust (mN)	Isp (s)	Propellant
MEMS Cold Gas	1	50–75	Methane

So the mainly cold gas propulsion systems that are used in a 1.5U cubesat is the **MEMS Cold Gas thruster** cubesat which usage is for attitude control. From the other categories of microthrusters (Plasma, ION and Solid) the propulsion system is used mainly for attitude control purpose.

In conclusion the appropriate thruster for 1.5U satellite is the electrospray **S-iEPS** engine.

3.2.2 Microthrusters for 3U satellite

From the 3U satellites with microthrusters the 5 had cold gas and 3 had solid. The missions with solid thrusters are PSSC-2 (Pico Satellite Solar Cell Testbed-2, PSSC Testbed-2, PSSCT-2), PACSCISAT (Tyvak-53b, PacSci EMC, Pacific Scientific) and D-Sat (Deorbit Satellite).

The thruster of PSSC-2 cubesat consists of four ammonium perchlorate solid rocket motors which provide 40 Ns of impulse each and could extend orbital lifetime by

an additional two months or alternatively, actively deorbit the satellite. The solid thruster that used was the **STAR 4G.**

The thruster of PACSCISAT consists of **4-MAPS** solid[63][64][65], clean-burning propellant array of rocket motors, which were fired in pairs to maneuver the satellite. It demands very low power. It has no heaters or valves.

The thruster of D-Sat consists of a solid-propellant rocket motors for de-orbiting missions developed and produced by Bayern-Chemie [66]. So this thruster is not used for lifetime increase.

So the characteristics of our 2 applicable thrusters are:

Engine	Thrust (mN)	Isp (s)	Propellant
STAR 4G	13	269.4	Al and Ammonium perchlorat
MAP		210	

So the solid propulsion systems that is used in a 3U cubesat are the **STAR 4G** and the **MAP**.

The cold gas cubesat missions are 5. The missions with cold gas are CanX-2, SNAP, POPSAT-HIP 1, TW-1A (STU-2, Shankeda 2, Tianwang-1A, Sat-A, SECM-1) and NanoACE.

The first is CanX-2 from Space Flight Laboratory (SFL). This satellite has **CNAPS** thruster.

The Snap satellite has **SNAP-1** engine. The propellant mass for Butane which has the maximum performance is 32.9 grams and its ΔV is 3.47 m/sec.

The Popsat-HIP 1 satellite has **POPSAT-HIP 1** engine. Propellant's mass is approximately 23.9 gram and its ΔV is 3.05 m/sec. This propellant is used for attitude control corrections.

The TW-1A is a China 3U satellite cubesat. This satellite has **MEMS Cold Gas** thruster.

The NanoACE satellite has **VACCO** engine. It contains Butane thrusters which combine low power piezovalve technology and low-pressure compact propellant storage for efficient attitude control and low delta-v in a simple system. So its usage its mainly for attitude control.

[63] https://psemc.com/products/satellite-propulsion-system/#1520706709192-e73c4257-95c1
[64]https://www.businesswire.com/news/home/20170804005525/en/PacSci-EMC-Proves-Propulsion-Technology-Demonstrator-Satellite
[65] https://psemc.com/products/satellite-propulsion-system/
[66] https://bayern-chemie.com/projects/

Engine	Thrust (mN)	Isp (s)	Propellant
CNAPS	10–40	<35	SF6
SNAP-1	50	69	Liq. Butane
POPSAT-HIP1	1	43	Argon
MEMS Cold Gas	1	50–75	Methane
Vacco	10-25	70	Butane Micro Thruster

So the mainly cold gas propulsion systems that are used in a 3U cubesat is the **CNAPS** and the **SNAP-1** thruster cubesat.

3.2.3 Microthrusters for 6U satellite

From the 6U satellites with microthrusters 4 were cold gas and one was solid. The solid one was placed at the PSSC (PSSCT, Pico Satellite Solar Cell Testbed) cubesat[67]. This thruster consists of four ammonium perchlorate solid rocket motors which provide 40 Ns of impulse each and could extend orbital lifetime by an additional two months or alternatively, actively deorbit the satellite. This **solid thruster** is the **STAR 4G** . Its characteristics are:

Thrust (mN)	Isp (s)	Propellant
13	269.4	Al and Ammonium perchlorat

So the only solid propulsion system that is used in a 6U cubesat is the **STAR 4G** cubesat.

The cold gas cubesat missions are 4. The first 3 missions are CanX-6, CanX-4 and CanX-5 from Space Flight Laboratory (SFL). Both 3 satellites had **CNAPS** thruster. Its characteristics are:

Thrust (mN)	Isp (s)	Propellant
10–40	<35	SF6

The last cubesat is the GOMX-4B[6869]. The GomX-4B satellite is a cooperation between ESA (European Space Agency) and GomSpace ApS of Aalborg, Denmark.

[67] https://space.skyrocket.de/doc_sdat/pssct-2.htm
[68] https://directory.eoportal.org/web/eoportal/satellite-missions/g/gomx-4
[69]http://www.esa.int/Our_Activities/Space_Engineering_Technology/ESA_s_GomX-4B_CubeSat_relaying_data_across_space_from_Danish_twin

The thruster is approximately 120 grams of butane. This propulsion system is used so as to recompense the orbit altitude from the launch , to achieve station keeping and to avoid potential risk collision. So this propulsion system is used for station keeping and not for deorbiting.

So the only cold gas propulsion system that is used in a 6U cubesat is the **CNAPS** thruster cubesat.

3.3 Performance of 1.5U, 3U and 6U microthrusters

It the paragraph 3.2 are listed all the operational microthrusters from previous successful missions which can provide the necessary ΔV so as to increase satellite's operational time. This paragraph constitutes a comparison among all thrusters that can be located in 1.5U, 3U and 6U cubesats.

3.3.1 Performance of 1.5U microthruster

From all thrusters that have been located in a 1.5U cubesat, the only one which can provide sufficient performance is the **S-iEPS** (Scalable ion-Electrospray Propulsion system) engine[7071].

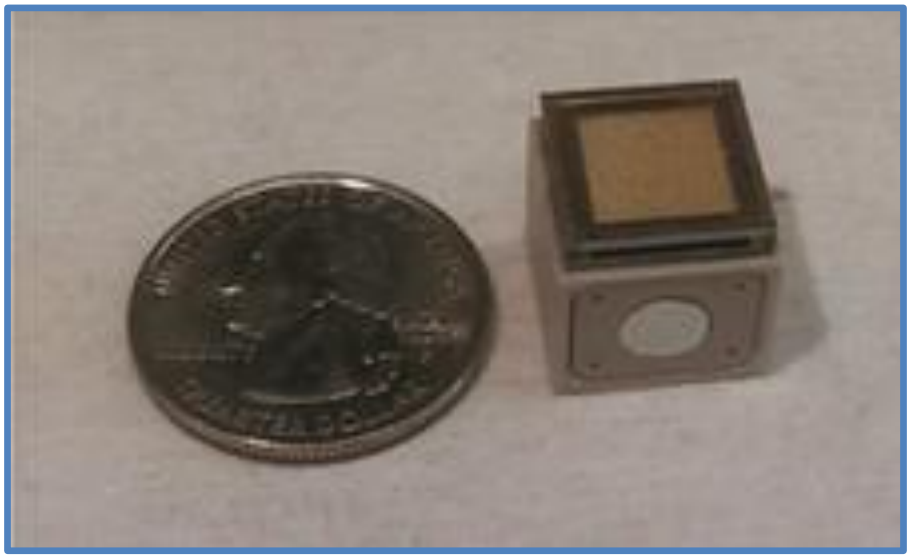

Figure 1 S-iEPS[68]

[70]https://www.nasa.gov/sites/default/files/atoms/files/small_spacecraft_technology_state_of_the_art_2015_tagged.pdf
[71] http://erps.spacegrant.org/uploads/images/2015Presentations/IEPC-2015-149_ISTS-2015-b-149.pdf

This thruster is constructed at MIT and constitutes a development of MEMS electrospray thruster. This propulsion system have 8 thrusters which are able to provide 74μN thrust at a specific impulse > 1150s.The power demand is < 1.5W.

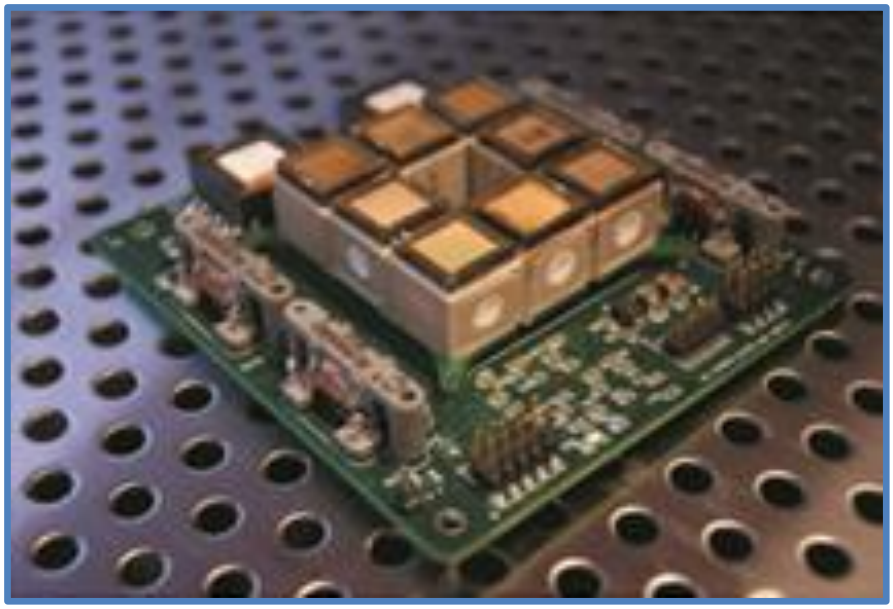

Figure 2 Scalable ion-Electrospray Propulsion system[69][72]

Engine	Thrust (mN)	Isp (s)	Propellant
S-iEPS	74±3.7μN	1167.5±60.7s	ionic liquid

[72] http://erps.spacegrant.org/uploads/images/2015Presentations/IEPC-2015-149_ISTS-2015-b-149.pdf

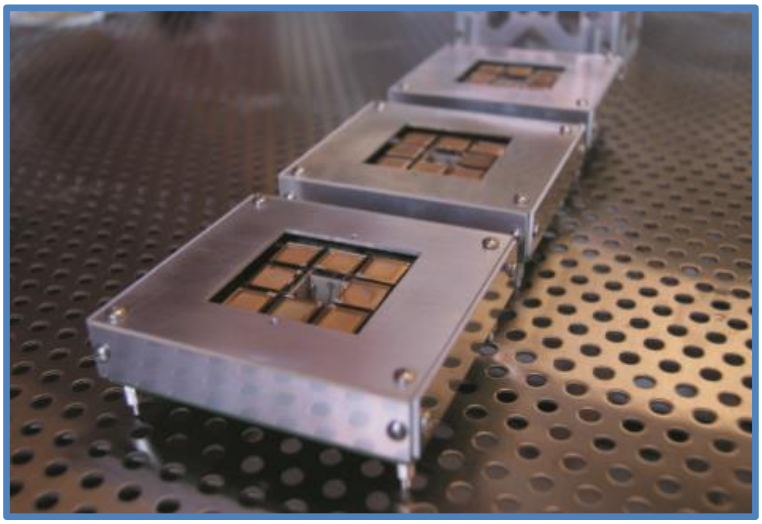

Figure 3 Scalable ion-Electrospray Propulsion system[69][70]

This thruster was tested by Aerospace Corporation and have been used in 3 of its space missions (Aerocube-8A, 8B, 8C and 8D).

3.3.2 Performance of 3U microthrusters

The engines that have been used in a 3U cubesat are the cold gases CNAPS, SNAP-1 and the solids STAR 4G and MAP. The CNAPS and STAR-4G are analyzed in the 3.3.3 paragraph. From their comparison STAR-4G achieves better performance characteristics.

The cold gas **SNAP-1**[73][74][75][76][77] engine was used in SNAP-1 satellite mission to bring this satellite in formation Tsinghua1 micro-satellite. The deorbit altitude the thruster achieved was approximately on the first phase was 3.4 km and on the second 540m.

[74] https://digitalcommons.usu.edu/cgi/viewcontent.cgi?article=2030&context=smallsat
[75] https://royalsocietypublishing.org/doi/pdf/10.1098/rsta.2002.1123
[76] http://ysc.sm.bmstu.ru/microsat/e-library/SSTL/SNAP-1%20Propulsion.pdf
[77] https://digitalcommons.usu.edu/cgi/viewcontent.cgi?article=2040&context=smallsat

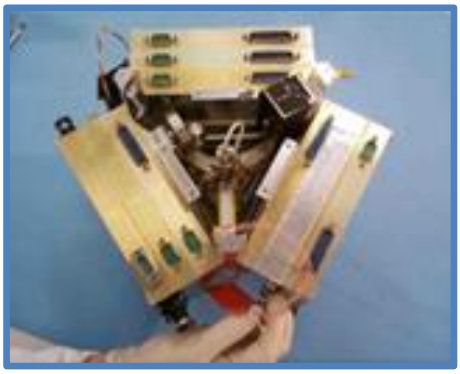

Figure 4 SNAP-1[75]

The total effective ΔV was approximately 1.9 - 2.1 m/s and the Isp approximately 43 s which is much lower than the theoretical Isp = 70s.

Figure 5 SNAP-1 engine[75]

So **SNAP-1** engine's capabilities are very significant in formation's satellite control. However in comparison with **STAR-4G** (on the next paragraph 3.3.3) , SNAP-1's deorbiting performance is much lower.

The **MAP**[78] solid engine that is a clean burning solid propellant-based array of rocket motors and thrusters. The usage of this technology doesn't demand large propellant tank and a high electric current draw. It can be used for 3U cubesats, 6U cubesats and bigger satellites.

[78] https://psemc.com/products/satellite-propulsion-system/

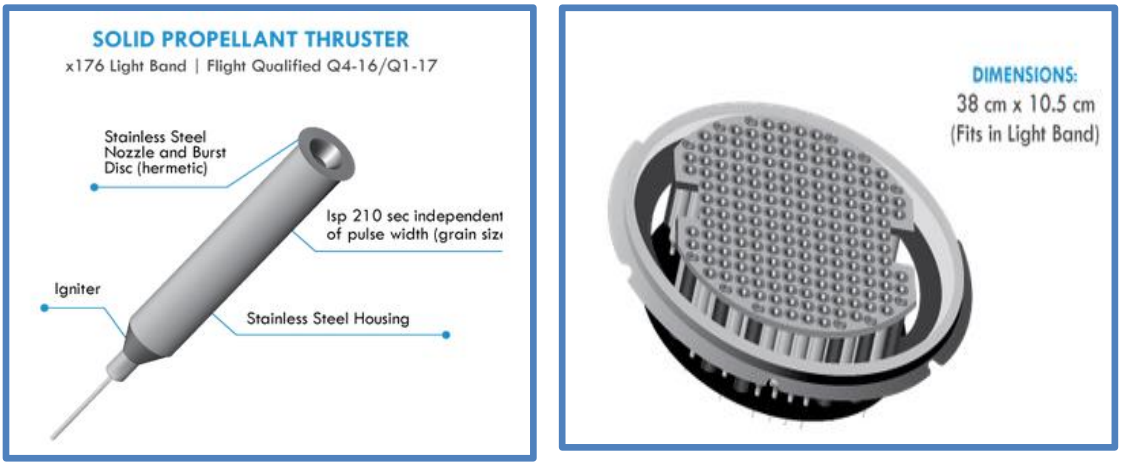

Figure 6 MAP solid engine[76]

The start-up of this system demands only 300 milliseconds. This engine can be offered in a variety of configurations.

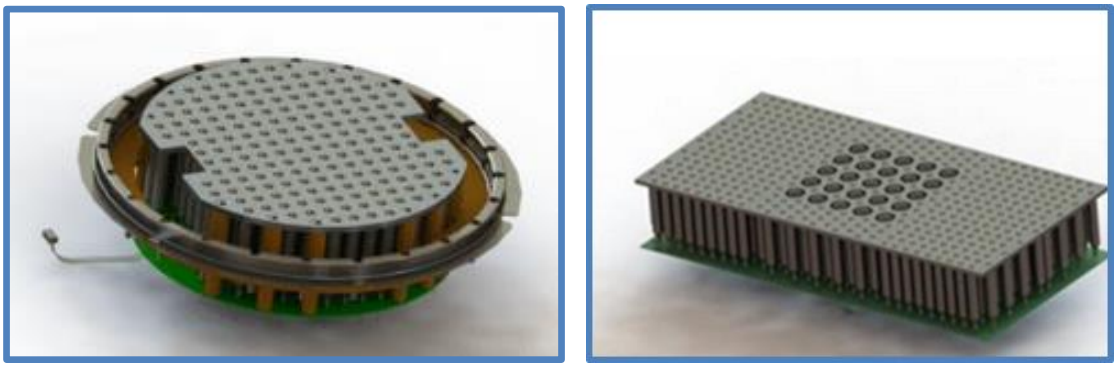

Figure 7 MAP solid engine configurations[76]

MAP has lower Isp in comparison with STAG -4G engine. However it is a more advance technology and offers a lot of capabilities not only increasing the orbital decay but maneuvering the satellite.

3.3.3 Performance of 6U microthrusters

The engines that have been used in a 6U cubesat are the cold gas **CNAPS** and the solid **STAR 4G.**

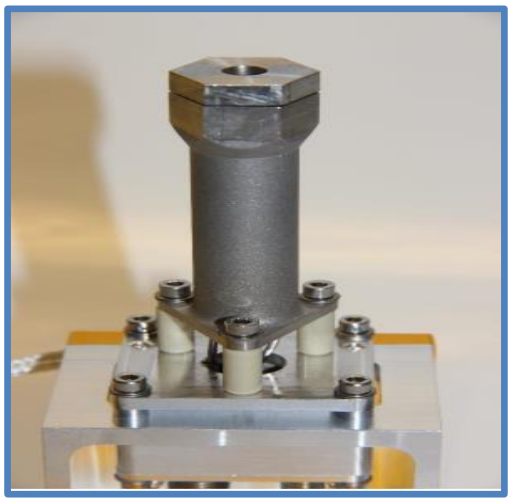

Figure 8 CNAPS engine[7778]

The cold gas **CNAPS[7980]** engine constitutes a development of a nitrous oxide monopropellant thruster and have been used at CanX-4,-5, -6 missions. Its characteristics are:

Engine	Manufacturer	Thrust	Specific Impulse	Propellant
CNAPS	UTIAS/SFL	12.5-40mN	40s	Sulfur Hexafluoride

The solid **STAR 4G engine[8182]** is constructed for the New Millennium ST-5 mission. The space mission PSSC (PSSCT, Pico Satellite Solar Cell Testbed) was from Aerospace Corporation. It's characteristics are:

[79] http://mstl.atl.calpoly.edu/~bklofas/Presentations/SummerWorkshop2016/1_StephenMauthe.pdf
[80]https://www.nasa.gov/sites/default/files/atoms/files/small_spacecraft_technology_state_of_the_art_2015_tagged.pdf
[81]https://www.nasa.gov/sites/default/files/atoms/files/small_spacecraft_technology_state_of_the_art_2015_tagged.pdf
[82] http://richard.hofer.com/pdf/jannaf_mueller_2010.pdf

Engine	Manufacturer	Thrust	Specific Impulse	Total Impulse
STAR 4G	ATK	13mN	269.4s	595s

Figure 9 STAR 4G engine[7980]

The STAR 4G engine's dimensions are 1.4U and its mass is 1.5kg. The operational usage requires at least 2 motor burns.

Figure 10 STAR 4G engine in operation[7980]

Payload Mass	ΔV	Altitude
1kg	1170 m/s	2700km
3 kg	620 m/s	1250km
10kg	235 m/s	435 km

So the lowest the payload mass the the highest ΔV achievable.

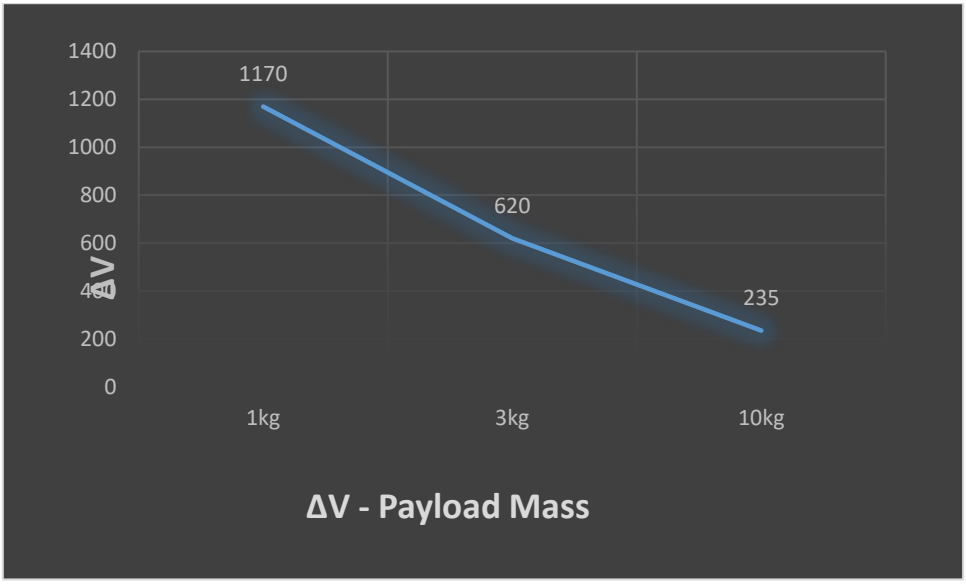

Relative with Isp the lowest the payload mass the highest Isp achievable.

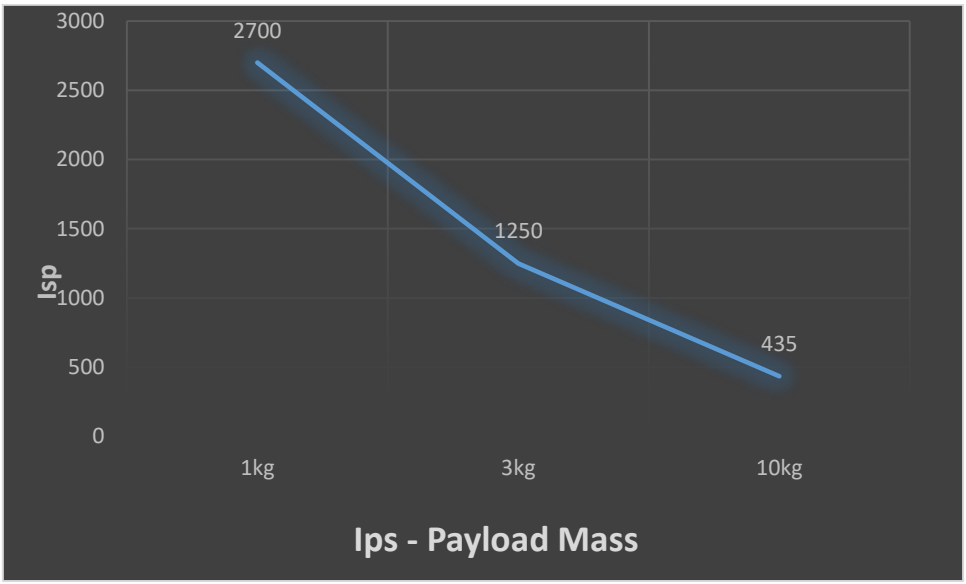

From the CNAPS and STAR 4G engine the solid propellant is more efficient producing more Isp which leads to higher ΔV. Higher ΔV provides more lifetime for our satellite.

3.3.4 IFM Nano Thruster

This engine is included in this research because it constites ESA's Next Generation of satellite Gravity Missions propulsion system. It belongs to FOTEC group and demands 0.6U dimensions. Its technology is FEEP (Field Emission Electric Propulsion) and it is based on ION category engines and can be used in 3U and 6U cubesats.

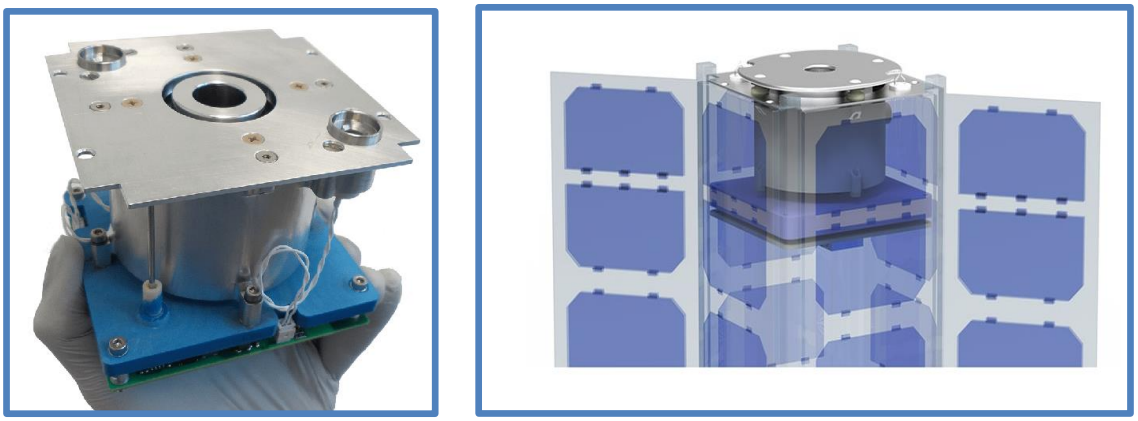

Figure 11 IFM Nano Thruster[8182]

IFM Nano Thruster 's[8384] characteristics are:

[83] https://www.cubesatshop.com/product/ifm-nano-thruster/
[84]https://www.cubesatshop.com/wp-content/uploads/2017/04/ENP-IFM-Nano-Thruster-Product-Overview.pdf

Engine	IFM Nano Thruster
Dynamic thrust range	10 μN to 0.5 mN
Nominal thrust	350 μN
Specific impulse	2,000 to 5000 s
Propellant mass	250 g
Total impulse	more than 5,000 Ns
Power at nominal thrust	35 W incl. neutralizer

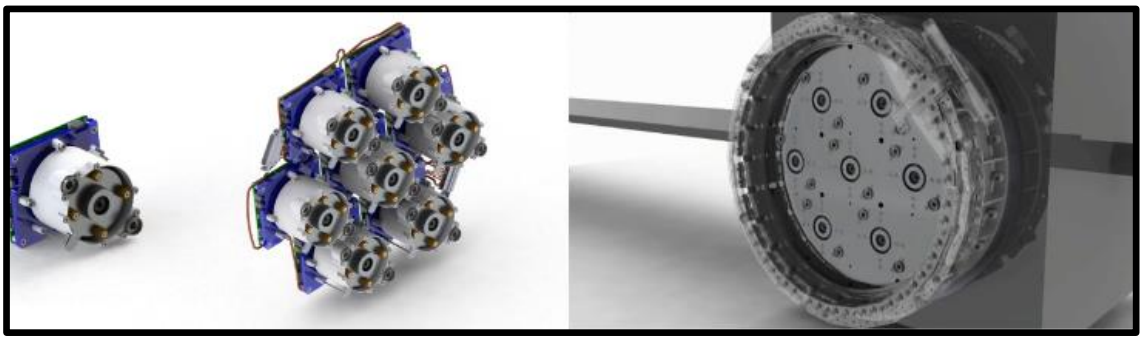

Figure 12 Cluster of IFM Nano Thruster[8182]

The total ΔV that achieved relative with spacecraft mass is:

Mass	ΔV
2	2879
3	2141
5	1415
10	766

CHAPTER 4 – CONCLUSIONS AND FUTURE PLANS

4.1 Conclusions

According the research among 925 satellites below 10kg,it is shown that only 40 of them had propulsion system. Most of these engine systems were equipped with cold gas, electrospray and solid types. The most preferred orbit altitudes are approximately the 400km, due to ISS orbit position (via the NANORACKS ISS Microsatellite Deployment System) and the 600km, where lifetime of Nano-satellite is expanding dramatically (approximately 6100 days).

Concerning dimensions of cubesats equipped with propulsion system, most of them are 3U, taking into account that any propulsion system requires at least 0.5U space. One significant finding is the fact that the ‘’smallest’’ cubesats with propellant, capable of ΔV maneuvers, are the 1.5U and not the 1U. This is important because at the beginning, one of the research goals was the the analysis of 1U cubesat propellant.

It is essential that space cubesat missions with propellants have been increased significantly after 2014 (60% of them were launched from 2014 till April 2018). So the ‘’trend’’ is the installation of microthrusters which can increase significantly the lifetime of the satellite.

The nation with the most cubesat missions with propellants is the United States, where most of microthrusters have been manufactured and tested. The S-iEPS (Scalable ion-Electrospray Propulsion system) is constructed at MIT and constitutes a improvement of MEMS electrospray thruster. This thruster was tested by Aerospace Corporation and has been used in 3 of its space missions (Aerocube-8A, 8B, 8C and 8D).

The comparison between the SATELLITE ORBITAL DECAY CALCULATIONS program (translated to Matlab language) and the MATLAB TOOL FOR ORBITAL DECAY program showed that, increasing satellite’s mass leads to lifetime increasing, whereas satellite’s Effective Area (m^2) increasing , leads to lifetime reduction. Having used the ORBITAL MECHANICS for Engineering Students (Curtis, H.D. Orbital Mechanics for Engineering Students. 3rd Edition) MATLAB

LIFETIME CALCULATION program ,which is the most reliable orbital decay calculation program from the 3 ‘’free’’ lifetime calculations programs, showed why the 600km orbit height has been used in multiple missions. The duration of the mission is estimated approximately at 6100 days. Moreover in this work provides another tool in orbital decay calculation for every cubesat without height restrictions, taking under consideration a lot of parameters.

Analyzing the engine’s performance characteristics, the propulsion system with the highest produced thrust is the Solid, proving its wide use. The propulsion system that generate the highest thrust to specific impulse is solid rocket. The electric propellants are more efficient in comparison with the non-electric engines relative with the produced Isp. Plasma and Electrospray engines demands the least power. Their high Isp combined with their small dimensions and low demands of power explain their wide usage among 1.5U cubesats.

The electric thrusters provide approximately similar performance relative with Power - Specific Impulse. The electric thrusters provide approximately similar Thrust to Power ratio with Isp. Among all the electric thrusters the electrospray engine produces the highest performance characteristics.

Most of 1.5U propellants are cold gas but the most recommended engine is the S-iEPS (Scalable ion-Electrospray Propulsion system) because of its high Isp and the evolved technology. The most of 3U propellants are cold gas again but the most recommended engines are the solids STAR 4G and MAP. STAR 4G engine is a very reliable thruster in comparison to MAP engine whereas the MAP engine is a more evolved engine in comparison with STAR 4G.

The most of 6U propellants are cold gas again, but the most recommended engine is the solid STAR 4G. Another significant propellant is the IFM Nano Thruster which is compatible with both 3U and 6U .It is the most evolved engine and has the most beneficial characteristics among all the thrusters.

4.2 Future Research Goals

The next step in this kind of technology is the development of the characteristics of the already existing microthrusters in a way to be easier to operate and more efficient relative with their lifetime. In addition, more elaborate study of the atmosphere at altitudes between 400-800 Km, which is one of the most important drag factors to any satellite, could enlighten the quality of altitude loss in terms of ΔV characteristics in relation to the shape of satellites. Furthermore, research is required to identify the most effective altitude, where a different type of propulsion system can be installed in order to achieve the optimum solution for fuel and lifetime.

Finally, another important step is the development of an algorithm that will be capable of selecting the proper propellant system for every cubesat mission.

BIBLIOGRAPHY

Kyriakos Gouskos-Katsaros, Petros Doukas, Filippos Parisis, Professor I. Koukos, Dr Georgios Mantzouris (2018) . Modeling the Orbital Parameters of a Low Orbit Satellite in Order to Determine the Degradation of Orbit

Academy, A. S. (1985). Terrestrial Atmospheric Modelling. Retrieved from https://www.spaceacademy.net.au/watch/debris/atmosmod.htm

Curtis, H. D. (2005). Orbital Mechanics for Engineering Students. Oxford: Elsevier Butterworth.

Elert, G. (2018). The Physics Hypertextbook. Retrieved from Equations of Motion: https://physics.info/motion-equations/

Gaposchkin, E., & Coster, A. (1998). Analysis of Satellite Drag. In The Lincoln Laboratory Journal, Volume I, Number 2 (pp. 203-224).

Keesee, J. (2003). The environment of space. Masachusetts Institute of Technology, MIT Open Courseware. Sunnyvale: Lockheed Missiles & Space Company.

Montenbruck, O., & Gill, E. (2000). Satellite Orbits Models, Methods and Applications. Springer.

NANONRACKS. (2018). NANORACKS The Operating System of Space. Retrieved from ISS MicroSat Deployment: http://nanoracks.com/products/iss-microsat-deployment/

NANORACKS. (2013). NanoRacks CubeSat Deployer (NRCSD). Houston: NanoRacks, LLC. Retrieved from http://nanoracks.com/wp-content/uploads/NanoRacks-CubeSat-Interface-Control-Document-CubeSat-Guide.pdf

Panwar, R. (n.d.). Satellite Orbital Decay Calculations. Sydney: The Australian Space Weather Agency.

Priesto, D. M., Graziano, P. B., & Roberts, P. C. (2016). Spacecraft Drag Modelling. Cranfield University.

Veris, A. d. (2016). Practical Astrodynamics. Rome: Springer Aerospace Technology.

Vinti, J. P., Der, G. J., & Bonavito, N. L. (1998). Orbital and Celestial Mechanics. American Institute of Aeronautics and Astronautics, Inc.

Ahmed, Z.; Gimelshein, S.F.; Ketsdever, A.D. Numerical analysis of free-molecule microresistojet performance. J. Propuls. Power 2006, 22, 749–756.

Alexander, M.S.; Smith, K.L.; Paine, M.D.; Stark, J.P. Voltage-modulated flow rate for precise thrust control in colloid electrospray propulsion. J. Propuls. Power 2007, 23, 1042–1048.

Alexander, M.S.; Stark, J.; Smith, K.L.; Stevens, B.; Kent, B. Electrospray performance of Microfabricated colloid thruster arrays. J. Propuls. Power 2006, 22, 620–627.

Anis, A. Cold gas propulsion system-an ideal choice for remote sensing small satellites. In Remote Sensing-Advanced Techniques And Platforms; InTech: Rijeka, Croatia, 2012.

Bauer, H. Stability boundaries of liquid-propelled space vehicles with sloshing. AIAA J. 1963, 1, 1583–1589.

Biagioni, L.; Saverdi, M.; Andrenucci, M. Scaling and performance prediction of Hall effect thrusters. In Proceedings of the 39th AIAA/ASME/SAE/ASEE Joint Propulsion Conference and Exhibit, Huntsville, AL, USA, 20–23 July 2003.

Botter, T.; Coverstone, V.L.; Burton, R.L. Structural Dynamics of Spin-Stabilized Solar Sails with Applications to UltraSail. J. Guid. Control Dyn. 2008, 31, 402.

Brinza, D.; Wang, J.; Polk, J.; Henry, M. Deep space 1 measurements of ion propulsion contamination. J. Spacecr. Rocket 2001, 38, 426–432.

Brito, C.M.; Elaskar, S.A.; Brito, H.H.; Paoletti, N.R. Zero-dimensional model for preliminary design of ablative pulsed plasma Teflon R thrusters. J. Propuls. Power 2004, 20, 970–977.

Burton, R.L.; Turchi, P. Pulsed plasma thruster. J. Propuls. Power 1998, 14, 716–735.

Cheng, S.Y.; Martinez-Sanchez, M. Hybrid particle-in-cell erosion modeling of two Hall thrusters. J. Propuls. Power 2008, 24, 987–998.

Chianese, S.G.; Micci, M.M. Microwave electrothermal thruster chamber temperature measurements and performance calculations. J. Propuls. Power 2006, 22, 31.

Courtney, D.G.; Dandavino, S.; Shea, H. Comparing Direct and Indirect Thrust Measurements from Passively Fed Ionic Electrospray Thrusters. J. Propuls. Power 2015, 32, 392–407.

Curtis, H.D. Orbital Mechanics for Engineering Students. 3rd Edition. Oxford: Butterworth-Heinemann.

Dankanich, J.W. Direct drive for low power Hall thrusters. In Proceedings of the 41st AIAA/ASME/SAE/ASEE Joint Propulsion Conference and Exhibit, Tucson, AZ, USA, 10–13 July 2005; Volume 4118, pp. 10–13.

Dannenmayer, K.; Mazouffre, S. Elementary scaling relations for Hall effect thrusters. J. Propuls. Power 2011,27, 236.

David, A.O.; Knoll, A.K. Experimental Demonstration of an Aluminum-Fueled Propulsion System for CubeSat Applications. J. Propuls. Power 2017, 33, 1320–1324.

Dubey, N.; Ravi, V.; Kushari, A. Discharge frequency modulation of pulsed plasma thruster. J. Spacecr. Rocket 2005, 42, 761.

Eldad, O.; Lightsey, E.G.; Claudel, C. Minimum-Time Attitude Control of Deformable Solar Sails with Model Uncertainty. J. Spacecr. Rocket 2017, 54, 863–870.

Fearn, D.G.; Solutions, E.; Crookham, C. The Future Development of Gridded Ion Engines. In Proceedings of the 39th AIAA/ASME/SAE/ASEE Joint Propulsion Conference and Exhibit, Huntsville, AL, USA, 20–23 July 2003; p. 4714.

Frisbee, R.H. Advanced space propulsion for the 21st century. J. Propuls. Power 2003, 19, 1129–1154.

Gamero-Castano, M.; Hruby, V. Electrospray as a source of nanoparticles for efficient colloid thrusters. J. Propuls. Power 2001, 17, 977–987.

Gibbon, D. A Review of the use of butane as a low cost propellant. In Proceedings of the 2010 Space Propulsion, San Sebastian, Spain, 3–6 May, 2010; p. 11.

Gibbs, S.C.; Dowell, E.H. Membrane paradox for solar sails. AIAA J. 2014, 52, 2904–2907.

Goebel, D.M.; Katz, I. Fundamentals of Electric Propulsion: Ion and Hall Thrusters; Jet Propulsion Laboratory (JPL): Pasadena, CA, USA, 2008; Volume 1, pp. 6–7, 22, 26, 148, 189, 192, 243–244, 325, 327.

Goebel, D.M.; Polk, J.E.; Mikellides, I.G. Ion thruster performance impacts due to cathode wear. J. Propuls. Power 2011, 27, 768.

Grustan-Gutierrez, E.; Gamero-Castaño, M. Microfabricated Electrospray Thruster Array with HighHydraulic Resistance Channels. J. Propuls. Power 2017, 33, 984–991.

Hall, E.H. On a New Action of the Magnet on Electric Currents. Am. J. Math. 1879, 2, 287–292.

Hillier, A.; Branam, R.; Huffman, R.; Szabo, J.; Paintal, S. High thrust density propellants in Hall thrusters. In Proceedings of the 49th AIAA Aerospace Sciences Meeting Including the New Horizons Forum and Aerospace Exposition, Orlando, FL, USA, 4–7 January 2011; p. 524.

Ito, T.; Gascon, N.; Crawford,W.S.; Cappelli, M.A. Experimental characterization of a micro-Hall thruster. J. Propuls. Power 2007, 23, 1068–1074.

Keidar, M. Micro-Cathode Arc Thruster for small satellite propulsion. In Proceedings of the 53rd AIAA Aerospace Sciences Meeting, Kissimmee, FL, USA, 5–9 January 2015; p. 0938

Keidar, M.; Boyd, I.D.; Antonsen, E.L.; Gulczinski, F.S.; Spanjers, G.G. Propellant charring in pulsed plasma thrusters. J. Propuls. Power 2004, 20, 978–984.

Keidar, M.; Boyd, I.D.; Beilis, I.I. Model of Particulate Interaction with Plasma in a Te on Pulsed Plasma Thruster. J. Propuls. Power 2001, 17, 125–131.

Ketsdever, A.D.; Wadsworth, D.C.; Muntz, E. Gas-surface Interaction Model Influence on Predicted Performance of Microelectromechanical System Resistojet. J. Thermo Phys. Heat Transf. 2001, 15, 302–307.

Kieckhafer, A.; King, L.B. Energetics of propellant options for high-power Hall thrusters. J. Propuls. Power 2007, 23, 21–26.

Kim, D.Y.; Micci, M.M. Molecular Dynamics Simulations of a Liquid Gallium Electrospray Thruster. J. Propuls. Power 2013, 29, 899–905.

Krejci, D.; Mier-Hicks, F.; Fucetola, C.; Lozano, P.; Schouten, A.H.; Martel, F. Design and Characterizationof a Scalable ion Electrospray Propulsion System. In Proceedings of the 30th International Symposium onSpace Technology and Science, 34th International Electric Propulsion Conference and 6th Nano-satelliteSymposium, Hyogo-Kobe, Japan, 4–10 July 2015.

Krejci, D.; Mier-Hicks, F.; Thomas, R.; Haag, T.; Lozano, P. Emission Characteristics of Passively Fed Electrospray Microthrusters with Propellant Reservoirs. J. Spacecr. Rocket 2017, 54, 447–458.

Lary, E.; Meyerand, R.; Salz, F. Ion acceleration in a gyro-dominated neutral plasma-theory. Bull. Am. Phys. Soc. Ser. II 1962, 7, 441.

Lee, I.W.; Richard, D.; Branam, R.E.H. Nano-Satellite Gatling-Gun Pulsed Plasma Thruster. In Proceedings of the 49th AIAA Aerospace Sciences Meeting including the New Horizons Forum and Aerospace Exposition, Orlando, FL, USA, 4–7 January 2011; p. 22.

Lee, R.H.; Bauer, A.; Killingsworth, M.D.; Lilly, T.; Duncan, J.; Ketsdever, A. Free-molecule-microresistojet performance using water propellant for nanosatellite applications. J. Spacecr. Rocket 2008, 45, 264–269.

Legge, R.S.; Lozano, P.C. Electrospray propulsion based on emitters microfabricated in porous metals.J. Propuls. Power 2011, 27, 485–495.

Ley,W.;Wittmann, K.; Hallmann,W. Handbook of Space Technology; JohnWiley & Sons: Hoboken, NJ, USA, 2009; Volume 22, p. 154.

Martinez-Sanchez, M.; Pollard, J.E. Spacecraft electric propulsion—An overview. J. Propuls. Power 1998, 14, 688–699.

Matticari, G.; Noci, G.; Siciliano, P.; Colangelo, G.; Schmidt, R. Cold gas micro propulsion prototype for very fine spacecraft attitude/position control. In Proceedings of the AIAA/ASME/SAE/ASEE 42nd joint propulsion conference, Sacramento, CA, USA, 9–12 July 2006; pp. 5378–5390.

Michael, D.; Souder, M.W. Solar Sail Technology for Nanosatellites. In Proceedings of the 5th AIAA/AAS Astrodynamics Specialist Conference and Exhibit, Honolulu, HI, USA, 18–21 August 2008; p. 11.

Mier-Hicks, F.; Lozano, P.C. Spacecraft-Charging Characteristics Induced by the Operation of Electrospray Thrusters. J. Propuls. Power 2016, 33, 456–467.

Mikellides, I.G.; Katz, I.; Hofer, R.R.; Goebel, D.M. Magnetic shielding of a laboratory Hall thruster. I. Theory and validation. J. Appl. Phys. 2014, 115, 043303.

Mikellindes, P.G.; Turchi, P.J. Modeling of Late-Time Ablation in Teflon Pulsed Plasma Thruster. In Proceedings of the AIAA Joint Propulsion Conference, Lake Buena Vista, FL, USA, 1–3 July 1996.

Miller, S.W.; Prince, B.D.; Bemish, R.J.; Rovey, J.L. Electrospray of 1-Butyl-3-Methylimidazolium Dicyanamide Under Variable Flow Rate Operations. J. Propuls. Power 2014, 30, 1701–1710.

Murphy, D.; Murphey, T.; Gierow, P. Scalable solar sail subsystem design considerations. In Proceedings of the 43rd AIAA/ASME/ASCE/AHS/ASC Structures, Structural Dynamics, and Materials Conference, Denver, CO, USA, 22–25 April 2002; p. 1703.

Pigeon, C.E.; Nathan, G.; Orr, B.P.L. A Low Power Cylindrical Hall Thruster for Next Generation Microsatellites. In Proceedings of the 29th Annual AIAA/USU Conference on Small Satellites, Logan, UT, USA, 8–13 August 2015; p. 9.

Polzin, K.A. Comprehensive review of planar pulsed inductive plasma thruster research and technology. J. Propuls. Power 2011, 27, 513–531.

Rayburn, C.D.; Campbell, M.E.; Mattick, A.T. Pulsed Plasma Thruster System for Microsatellites. J. Spacecr. Rocket 2005, 42, 161–170.

Reid, M.R.; Scharfe, D.B.; Saleem, F.A.; Webb, R.N. Preheating Cold Gas Thruster Flow through a Thermal Energy Storage Conversion System. J. Propuls. Power 2013, 29, 1488–1492.

Rizvi, F. Solar Sail Coning Control to Induce Orbital Effects in Spinning Versus Non-Spinning Sails. In Advances in Solar Sailing; Springe: New York, NY, USA, 2014; pp. 737–753.

Robin, M.; Brogan, T.; Cardiff, E. An Ammonia Microresistojet (MRJ) for micro Satellites. In Proceedings of the 44th AIAA/ASME/SAE/ASEE Joint Propulsion Conference & Exhibit, Hartford, CT, USA, 21–23 July 2008.

Rossi, C.; Larangot, B.; Pham, P.Q.; Briand, D.; de Rooij, N.F.; Puig-Vidal, M.; Samitier, J. Solid propellant microthrusters on silicon: Design, modeling, fabrication, and testing. J.Microelectron. Syst. 2006, 15, 1805–1815.

Sackheim, R.L.; Masse, R.K. Green propulsion advancement: Challenging the maturity of monopropellant hydrazine. J. Propuls. Power 2014, 30, 265–276.

Sathiyanathan, K.; Lee, R.; Chesser, H.; Dubois, C.; Stowe, R.; Farinaccio, R.; Ringuette, S. Solid propellant microthruster design for nanosatellite applications. J. Propuls. Power 2011, 27, 1288–1294.

Seikel, G.; Reshotko, E. Hall current ion accelerator. Bull. Am. Phys. Soc. Ser. II 1962, 7, 414.

Skuhersky, M.; Balestrero Machado, L.;Wilde, M.; Brett, C. CERBERUS: Prototype for an Agile Inspection and Servicing Satellite Using Thrust-Vectoring Cold-Gas Propulsion. In Proceedings of the AIAA SPACE and Astronautics Forum and Exposition, Orlando, FL, USA, 12–14 September 2017; p. 5116.

Slough, J.; Andreason, S.; Ziemba, T.; Ewing, J. Micro-discharge micro-thruster. In Proceedings of the 41st AIAA/ASME/SAE/ASEE Joint Propulsion Conference and Exhibit, Tucson, AZ, USA, 10–13 July 2005; Volume 4047.

Song, W.; Shumlak, U. Ultrasonically aided electrospray source for charged particles approaching monodisperse distributions. J. Propuls. Power 2010, 26, 353–363.

Stratton, J. The use of the AEROJET MR-103H thruster on the New Horizons mission to Pluto. In Proceedings of the 55th International Astronautical Congress 2004, Vancouver, BC, Canada, 4–8 October 2004; Vulume 30, p. 30.

Sutton, G.P.; Biblarz, O. Rocket Propulsion Elements, 7th ed.; John Wiley & Sons, Inc.: Hoboken, NJ, USA, pp. 31–32, 34, 52, 133, 253, 260–261, 315, 417, 428, 608; 2001

Tamida, T.; Osuga, H.; Yamamoto, N.; Takegahara, H.; Aoyagi, J.; Kuriki, K. Performance Improvement of Hall Thrusters Using a Pulse-Synchronous Driver System. J. Propuls. Power 2015, 31, 956–961.

Thrasher, J.; Williams, S.; Takahashi, P.; Sousa, J. Pulsed Plasma Thruster Development Using a Novel HAN-Based Green Electric Monopropellant. In Proceedings of the 52nd AIAA/SAE/ASEE Joint Propulsion Conference, Salt Lake City, UT, USA, 25–27 July 2016; p. 4846.

Tummala, A.R.; Dutta, A. An Overview of Cube-Satellite Propulsion Technologies and Trends. Aerospace 2017, 4, 58.

Yamamoto, N.; Komurasaki, K.; Arakawa, Y. Discharge current oscillation in Hall thrusters. J. Propuls. Power 2005, 21, 870–876.

Zhang, K.; Chou, S.; Ang, S.S. Development of a solid propellant microthruster with chamber and nozzle etched on a wafer surface. J. Micromech. Microeng. 2004, 14, 785.

Zhurin, V.; Kaufman, H.; Robinson, R. Physics of closed drift thrusters. Plasma Sources Sci. Technol. 1999, 8, R1.

Zondervan, K.; Fuller, J.; Rowen, E. CubeSat Solid Rocket Motor Propulsion Systems providing Delta-Vs greater than 500 m/s. In Proceedings of the 28th Annual AIAA/USA Conference on Small Satellites, Logan, UT, USA, 4–7 August 2014.

APPENDIX

A1. SATELLITE ORBITAL DECAY CALCULATIONS

This program is a translation in Matlab from QBASIC language. The Australian Government Bureau of Meteorology has published the Satellite Orbital Decay Calculations article which is a simple simulation to calculate orbital lifetimes of satellites for low earth orbits (below 500km). The result is the total lifetime from the initial altitude until 200 km which is practical the atmosphere. The program is written below:

```
M = * * *;          % satellite mass (kg)

A = * * *;          % satellite area (m^2)
H = * * *;          % starting height (km)
F10 = 68.88889;     % solar radio flux
Ap = 7.822;         % geomagnetic index
Re = 6378000;          % earth radius (m)
Me = 5.98e24;          % earth mass (kg)
G = 6.67e-11;          % constant of gravitation
Pi = 3.1416;
T = 0;                 % Time (days)
dT = 0.1;              % Time increment (days)
D9 = dT*3600*24;       % Time increment in seconds
H1 = 10;               % Height increment of satellite(km)
H2 = H;                % Current height(km)
R = Re+H*1000          % orbit height radius (m)
P = 2*pi*sqrt(R^3/(Me*G)); % Period (sec)
                    % % % % % % % %
  while H>180
SH = (900 + 2.5 * (F10 - 70) + 1.5 * Ap) / (27 - .012 * (H -
200));
DN = 6E-10 * exp(-(H - 175) / SH); % atmosphere density
dP = 3 * pi * A / M * R * DN * D9; % Period reduction
P = P - dP;
T = T + dT;                        % compute new values
R = (G * Me * P * P / 4 / pi / pi)^ .33333 % new orbital radius
H = (R - Re) / 1000            % new altitude (semi major axis)
```

A2. MATLAB TOOL FOR ORBITAL DECAY

The Matlab Tool for Orbital Decay : **computeOrbitalDecay (a,e,A,Cd,m0,F107,Ap)** uses more variables such us the eccentricity and coefficient drag. As eccentricity it is chosen the value of ISS (e = 0.0003390) and for coefficient drag Cd=2.2. The program prints a diagram with the cubesat starts at a variety of altitudes , below 500 km.

```
function [P,t] = computeOrbitalDecay(a,e,A,Cd,m0,F107,Ap)
                                % % Purpose:
% Given a satellite starting semi-major axis and its corresponding
eccentricity,
% this routine will compute the orbital trajectory of this satellite
until
% it reaches 180 km in height at which point it will most
% likely re-enter the atmosphere within a fraction of a day.
                            % % Source References:
% Pamrar, R. Satellite Orbital Decay Calclulations. The Australian
Space Weather Agency.
% http://www.sws.bom.gov.au/Category/Educational/Space%20Weather/ ...
% Space%20Weather%20Effects/SatelliteOrbitalDecayCalculations.pdf
% % Revision History:
%  Darin C. Koblick          (c) 02-12-2016
%% ------------------------------------------------------
if exist('getConst','file')
    const = getConst();
    Re = const.Earth.Rad;       % Earth Radius (km)
    Mu = const.Earth.Mu;        % Earth's Gravitational Constant
else
    Re = 6378.137;
    Mu = 398600.4418;
end
%% Demonstration of Decay in absense of any user inputs:
if nargin == 0
       a  =  Re+(375:25:450);                % Semi-Major Axis (km)
       m0 = ***;                             % Satellite Mass (kg)
       A  =  ***;                            %
       e  =  0.0003390;                      % Eccentricity
       Cd = 2.2;                             % Coefficient of Drag
```

```
    F107 = 68.8889;                          % F10.7 Solar Radio Flux
      Ap = 7.822222222;                      % Geomagnetic Index

[P,t] = computeOrbitalDecay(a,e,A,Cd,m0,F107,Ap);
figure('color',[1 1 1]);
plot(t./86400,((P./(2.*pi)).^2.*Mu).^(1/3)-Re,'k','linewidth',2);
grid on;
xlabel('Time (Days)');
ylabel('Altitude (km)');
title(['Vectorized Orbital Decay vs. Time ','A*C_D =,num2str(A*Cd)]);
ylim([180 max(a-Re)]);
[P,t] = deal([]);
    return;
end
P = 2*pi.*sqrt(a.^3./Mu);  % Orbital Period (sec)
Ae = A.*Cd;                % Effective Cross Sectional Area
dt = min(0.5*P);           % Time step in seconds
t = 0;                     % Elapsed Propagation Time (sec)
% % Defined inline Orbital Routines:
h = @(P)((P./(2.*pi)).^2.*Mu).^(1/3)-Re; % Compute the circular height
(km)
rP = @(a,e)a.*(1-e); % Compute the Perigee Radius calculation
he = @(a,e)(rP(a,e)-Re)+900.*e.^(0.6); % Compute the effective height
(km)
 % % Very Basic Atmospheric Model:
m = @(h)27-0.012.*(h-200);                    % 180 < h [km] < 500
H = @(h)(900 + 2.5.*(F107-70) + 1.5.*Ap)./m(h);   % Equivalent height
in km
 rho = @(h)6e-10.*exp(-(h-175)./H(h));             % Density (kg m^-3)
         % % Find the period corresponding to a height of 180 km:
 P_min = 2*pi.*sqrt((Re+180).^3./Mu);
  % Iterate satellite orbit with time:
 while any(P(end,:) > P_min,2)
     hh = he(h(P(end,:))+Re,e);
     idx = hh >= 180;
     % Compute the change in orbital period:
     dP = bsxfun(@rdivide,-3.*pi.*(hh+Re).*1000.*rho(hh).*Ae.*dt,m0);
     P(end+1,idx) = P(end,idx)+dP(idx); % # ok < AGROW >
```

```
        t(end+1,1) = t(end,1)+dt;    % # ok < AGROW >
 end
 % Clean-up the results such that the period does not fall below
P_min:
P(P<P_min) = NaN;
End
```

A3. ORBITAL MECHANICS for Engineering Students MATLAB LIFETIME CALCULATION

This is a program written in MATLAB from the book Orbital Mechanics for Engineering Students, Third Edition, Howard D. Curtis. It calculates the lifetime of satellite taking under consideration a number of parameters. The program is functioning simultaneously with other programs so as to provide the total orbital decay.

A3.1 Atmospheric drag calculation

```
function Example_12_01
% wwwwwwwwwwwwwwwwwwwwwwwwwwwww
%
% This function solves Example 12.1 by using MATLAB's ode45 to
numerically
% integrate Equation 12.2 for atmospheric drag.
%
% User M-functions required: sv_from_coe, atmosphere
% User subfunctions required: rates, terminate
%  -------------------------------------------------------------------
----
%...Preliminaries:
close all, clear all, clc
%...Conversion factors:
hours = 3600; %Hours to seconds
days = 24*hours; %Days to seconds
deg = pi/180; %Degrees to radians%...Constants;
mu = 398600; %Gravitational parameter (km^3/s^2)
RE = 6378; %Earth's radius (km)
```

```
wE = [ 0 0 7.2921159e-5]'; %Earth's angular velocity (rad/s)
%...Satellite data:
CD = 2.2; %Drag coefficient
m = 1; %Mass (kg)
A = pi/4*(1^2) ; %Frontal area (m^2)
%...Initial orbital parameters (given):
rp = RE + 215; %perigee radius (km)
ra = RE + 420; %apogee radius (km)
RA = 339.94*deg; %Right ascension of the node (radians)
i = 65.1*deg; %Inclination (radians)
w = 58*deg; %Argument of perigee (radians)
TA = 332*deg; %True anomaly (radians)
%...Initial orbital parameters (inferred):
e = (ra-rp)/(ra+rp); %eccentricity
a = (rp + ra)/2; %Semimajor axis (km)
h = sqrt(mu*a*(1-e^2)); %angular momentum (km^2/s)
T = 2*pi/sqrt(mu)*a^1.5; %Period (s)
%...Store initial orbital elements (from above) in the vector coe0:
coe0 = [h e RA i w TA];
%...Obtain the initial state vector from Algorithm 4.5 (sv_from_coe):
[R0 V0] = sv_from_coe(coe0, mu); %R0 is the initial position vector
%V0 is the initial velocity vector
r0 = norm(R0); v0 = norm(V0); %Magnitudes of R0 and V0
%...Use ODE45 to integrate the equations of motion d/dt(R,V) = f(R,V)
% from t0 to tf:
t0 = 0; tf = 120*days; %Initial and final times (s)
y0 = [R0 V0]'; %Initial state vector
nout = 40000; %Number of solution points to output
tspan = linspace(t0, tf, nout); %Integration time interval
% Set error tolerances, initial step size, and termination event:
options = odeset('reltol', 1.e-8, ...
'abstol', 1.e-8, ...
'initialstep', T/10000, ...
'events', @terminate);
global alt %Altitude
[t,y] = ode45(@rates, tspan, y0,options); %t is the solution times
```

```
%y is the state vector history%...Extract the locally extreme
altitudes:
altitude = sqrt(sum(y(:,1:3).^2,2)) - RE; %Altitude at each time
[max_altitude,imax,min_altitude,imin] = extrema(altitude);
maxima = [t(imax) max_altitude]; %Maximum altitudes and times
minima = [t(imin) min_altitude]; %Minimum altitudes and times
apogee = sortrows(maxima,1); %Maxima sorted with time
perigee = sortrows(minima,1); %Minima sorted with time
figure(1)
apogee(1,2) = NaN;
%...Plot perigee and apogee history on the same figure:
plot(apogee(:,1)/days, apogee(:,2),'b','linewidth',2)
hold on
plot(perigee(:,1)/days, perigee(:,2),'r','linewidth',2)
grid on
grid minor
xlabel('Time (days)')
ylabel('Altitude (km)')
ylim([0 1000]);
%...Subfunctions:
% wwwwwwwwwwwwwwwwwwwwwwwwwwwwwwwwwwwwwwwwwwwwwwwwwwwwwwwww
function dfdt = rates(t,f)
% wwwwwwwwwwwwwwwwwwwwwwwwwww
%
% This function calculates the spacecraft acceleration from its
% position and velocity at time t.
%  ------------------------------------------------------------------
----
R = f(1:3)'; %Position vector (km/s)
r = norm(R); %Distance from earth's center (km)
alt = r - RE; %Altitude (km)
rho = atmosphere(alt); %Air density from US Standard Model (kf/m^3)
V = f(4:6)'; %Velocity vector (km/s)
Vrel = V - cross(wE,R); %Velocity relative to the atmosphere (km/s)
vrel = norm(Vrel); %Speed relative to the atmosphere (km/s)
uv = Vrel/vrel; %Relative velocity unit vector
ap = -CD*A/m*rho*... %Acceleration due to drag (m/s^2)
```

```
(1000*vrel)^2/2*uv; %(converting units of vrel from km/s to m/s)
a0 = -mu*R/r^3; %Gravitational acceleration (km/s^2)
a = a0 + ap/1000; %Total acceleration (km/s^2)
dfdt = [V a]'; %Velocity and the acceleraion returned to ode45
end %rates
% wwwwwwwwwwwwwwwwwwwwwwwwwwwwwwwwwwwwwwwwwwwwwwwwwwww
% wwwwwwwwwwwwwwwwwwwwwwwwwwwwwwwwwwwwwwwwwwwwwwwwwwww
function [lookfor stop direction] = terminate(t,y)
% wwwwwwwwwwwwwwwwwwwwwwwwwwwwwwwwwwwwwwwwwwwwwwwwwwww
%% This function specifies the event at which ode45 terminates.
%  ------------------------------------------------------------------
----
lookfor = alt - 100; % = 0 when altitude = 100 km
stop = 1; % 1 means terminate at lookfor = 0; Otherwise 0
direction = -1; % -1 means zero crossing is from above
end %terminate
% wwwwwwwwwwwwwwwwwwwwwwwwwwwwwwwwwwwwwwwwwwwwwwwwwwww
end %Example_12_01
% wwwwwwwwwwwwwwwwwwwwwwwwwwwwwwwwwwwwwwwwwwwwwwwwwwww
```

A3.2 Classical orbital elements calculation

```
% wwwwwwwwwwwwwwwwwwwwwwwwwwwwwwwwwwwwwwwwwwwwwwwwwwww
function coe = coe_from_sv(R,V,mu)
% wwwwwwwwwwwwwwwwwwwwwwwwwwwwwwwww
%{
% This function computes the classical orbital elements (coe)
% from the state vector (R,V) using Algorithm 4.1.
%
mu - gravitational parameter (km^3/s^2)
R - position vector in the geocentric equatorial frame (km)
V - velocity vector in the geocentric equatorial frame (km)
r, v - the magnitudes of R and V
vr - radial velocity component (km/s)
H - the angular momentum vector (km^2/s)
h - the magnitude of H (km^2/s)
incl - inclination of the orbit (rad)
```

```
N - the node line vector (km^2/s)
n - the magnitude of N
cp - cross product of N and R
RA - right ascension of the ascending node (rad)
E - eccentricity vector
e - eccentricity (magnitude of E)
eps - a small number below which the eccentricity is considered
to be zero
w - argument of perigee (rad)
TA - true anomaly (rad)
a - semimajor axis (km)
pi - 3.1415926...
coe - vector of orbital elements [h e RA incl w TA a]
User M-functions required: None
%}
% ------------------------------------------
eps = 1.e-10;
r = norm(R);
v = norm(V);
vr = dot(R,V)/r;
H = cross(R,V);
h = norm(H);
%...Equation 4.7:
incl = acos(H(3)/h);
%...Equation 4.8:
N = cross([0 0 1],H);
n = norm(N);
%...Equation 4.9:
if n ~= 0
RA = acos(N(1)/n);
if N(2) < 0
RA = 2*pi - RA;
end
else
RA = 0;
end
%...Equation 4.10:
```

```
E = 1/mu*((v^2 - mu/r)*R - r*vr*V);
e = norm(E);
%...Equation 4.12 (incorporating the case e = 0):
if n ~= 0
if e > eps
w = acos(dot(N,E)/n/e);
if E(3) < 0
w = 2*pi - w;
end
else
w = 0;
end
else
w = 0;
end
%...Equation 4.13a (incorporating the case e = 0):
if e > eps
TA = acos(dot(E,R)/e/r);
if vr < 0
TA = 2*pi - TA;
end
else
cp = cross(N,R);
if cp(3) >= 0
TA = acos(dot(N,R)/n/r);
else
TA = 2*pi - acos(dot(N,R)/n/r);
end
end
%...Equation 4.62 (a < 0 for a hyperbola):
a = h^2/mu/(1 - e^2);
coe = [h e RA incl w TA a];
end %coe_from_sv
```

A3.3 Density for altitudes from sea level calculation

```
function density = atmosphere(z)
%
% ATMOSPHERE calculates density for altitudes from sea level
% through 1000 km using exponential interpolation.
%wwwwwwwwwwwwwwwwwwwwwwwwwwwwwwwwwwwwwwwwwwwwwwwwwwwwwwww
%...Geometric altitudes (km):
h = ...
[ 0 25 30 40 50 60 70 ...
80 90 100 110 120 130 140 ...
150 180 200 250 300 350 400 ...
450 500 600 700 800 900 1000];
%...Corresponding densities (kg/m^3) from USSA76:
r = ...
[1.225 4.008e-2 1.841e-2 3.996e-3 1.027e-3 3.097e-4 8.283e-5 ...
1.846e-5 3.416e-6 5.606e-7 9.708e-8 2.222e-8 8.152e-9 3.831e-9 ...
2.076e-9  5.194e-10  2.541e-10  6.073e-11  1.916e-11  7.014e-12  2.803e-12
...
1.184e-12  5.215e-13  1.137e-13  3.070e-14  1.136e-14  5.759e-15  3.561e-
15];
%...Scale heights (km):
H = ...
[ 7.310 6.427 6.546 7.360 8.342 7.583 6.661 ...
5.927 5.533 5.703 6.782 9.973 13.243 16.322 ...
21.652 27.974 34.934 43.342 49.755 54.513 58.019 ...
60.980 65.654 76.377 100.587 147.203 208.020];
%...Handle altitudes outside of the range:
if z > 1000
z = 1000;
elseif z < 0
z = 0;
end
%...Determine the interpolation interval:
for j = 1:27
if z >= h(j) && z < h(j+1)
i = j;
end
```

```
end
if z == 1000
i = 27;
end
%...Exponential interpolation:
density = r(i)*exp(-(z - h(i))/H(i));
end %atmopshere
```

A3.4 Universal Kepler's equation calculation

```
% wwwwwwwwwwwwwwwwwwwwwwwwwwwwwwwwwwwwwwwwwwwwwwwwwwwwww
% Example_3_06
% wwwwwwwwwwww
%{
This program uses Algorithm 3.3 and the data of Example 3.6
to solve the universal Kepler's equation.
mu - gravitational parameter (km^3/s^2)
x - the universal anomaly (km^0.5)
dt - time since x = 0 (s)
ro - radial position when x = 0 (km)
vro - radial velocity when x = 0 (km/s)
a - semimajor axis (km)
User M-function required: kepler_U
%}
% ------------------------------------------------

global mu
mu = 398600;
%...Data declaration for Example 3.6:
ro = 10000;
vro = 3.0752;
dt = 3600;
a = -19655;
```

```
%...
%...Pass the input data to the function kepler_U, which returns x
%...(Universal Kepler's requires the reciprocal of semimajor axis):
x = kepler_U(dt, ro, vro, 1/a);
%...Echo the input data and output the results to the command window:
fprintf('-----------------------------------------------------')
fprintf('\n Example 3.6\n')
fprintf('\n Initial radial coordinate (km) = %g',ro)
fprintf('\n Initial radial velocity (km/s) = %g',vro)
fprintf('\n Elapsed time (seconds) = %g',dt)
fprintf('\n Semimajor axis (km) = %g\n',a)
fprintf('\n Universal anomaly (km^0.5) = %g',x)
fprintf('\n-----------------------------------------------------\n')
% wwwwwwwwwwwwwwwwwwwwwwwwwwwwwwwwwwwwwwwwwwwwwww
```

A3.5 State vector (R,V) calculation

```
% wwwwwwwwwwwwwwwwwwwwwwwwwwwwwwwwwwwwwwwwwwwwwww
% Example_3_07
% wwwwwwwwwwww
%
% This program computes the state vector (R,V) from the initial
% state vector (R0,V0) and the elapsed time using the data in
% Example 3.7.
%
% mu - gravitational parameter (km^3/s^2)
% R0 - the initial position vector (km)
% V0 - the initial velocity vector (km/s)
% R - the final position vector (km)
% V - the final velocity vector (km/s)
% t - elapsed time (s)
%
% User m-functions required: rv_from_r0v0
% -----------------------------------------------
clear all; clc
```

```
global mu
mu = 398600;
%...Data declaration for Example 3.7:
R0 = [ 7000 -12124 0];
V0 = [2.6679 4.6210 0];
t = 3600;
%...
%...Algorithm 3.4:
[R V] = rv_from_r0v0(R0, V0, t);
%...Echo the input data and output the results to the command window:
fprintf('-------------------------------------------------------')
fprintf('\n Example 3.7\n')
fprintf('\n Initial position vector (km):')
fprintf('\n r0 = (%g, %g, %g)\n', R0(1), R0(2), R0(3))
fprintf('\n Initial velocity vector (km/s):')
fprintf('\n v0 = (%g, %g, %g)', V0(1), V0(2), V0(3))
fprintf('\n\n Elapsed time = %g s\n',t)
fprintf('\n Final position vector (km):')
fprintf('\n r = (%g, %g, %g)\n', R(1), R(2), R(3))
fprintf('\n Final velocity vector (km/s):')
fprintf('\n v = (%g, %g, %g)', V(1), V(2), V(3))
fprintf('\n-------------------------------------------------------\n')
% wwwwwwwwwwwwwwwwwwwwwwwwwwwwwwwwwwwwwwwwwwwwwwwwwwwwwwwwwww
```

A3.6 Orbital elements calculation

```
% Example_4_03
% ~~~~~~~~~~~~
%{
This program uses Algorithm 4.2 to obtain the orbital
elements from the state vector provided in Example 4.3.
pi - 3.1415926...
deg - factor for converting bet~een degrees and radians
mu - gravitational parameter (km^3/s^2)
r - position vector (km) in the geocentric equatorial frame
```

```
v - velocity vector (km/s) in the geocentric equatorial frame
coe - orbital elements [h e RA incl ~ TA a]
~here h = angular momentum (km^2/s)
e = eccentricity
RA = right ascension of the ascending node (rad)
incl = orbit inclination (rad)
~ = argument of perigee (rad)
TA = true anomaly (rad)
a = semimajor axis (km)
T - Period of an elliptic orbit (s)
User M-function required: coe_from_sv
%}
% ------------------------------------------------
clear all; clc
deg = pi/180;
mu = 398600;
%...Data declaration for Example 4.3:
r = [ -6045 -3490 2500];
v = [-3.457 6.618 2.533];
%...
%...Algorithm 4.2:
coe = coe_from_sv(r,v,mu);
%...Echo the input data and output results to the command ~indo~:
fprintf('-----------------------------------------------------')
fprintf('\n Example 4.3\n')
fprintf('\n Gravitational parameter (km^3/s^2) = %g\n', mu)
fprintf('\n State vector:\n')
fprintf('\n r (km) = [%g %g %g]', ...
r(1), r(2), r(3))
fprintf('\n v (km/s) = [%g %g %g]', ...
v(1), v(2), v(3))
disp(' ')
fprintf('\n Angular momentum (km^2/s) = %g', coe(1))
fprintf('\n Eccentricity = %g', coe(2))
fprintf('\n Right ascension (deg) = %g', coe(3)/deg)
fprintf('\n Inclination (deg) = %g', coe(4)/deg)
fprintf('\n Argument of perigee (deg) = %g', coe(5)/deg)
```

```
fprintf('\n True anomaly (deg) = %g', coe(6)/deg)
fprintf('\n Semimajor axis (km): = %g', coe(7))
%...if the orbit is an ellipse, output its period (Equation 2.73):
if coe(2)<1
T = 2*pi/sqrt(mu)*coe(7)^1.5;
fprintf('\n Period:')
fprintf('\n Seconds = %g', T)
fprintf('\n Minutes = %g', T/60)
fprintf('\n Hours = %g', T/3600)
fprintf('\n Days = %g', T/24/3600)
end
fprintf('\n------------------------------------------------------\n')
% ~~~~~~~~~~~~~~~~~~~~~~~~~~~~~~~~~~~~~~~~~~~~~~~~
```

A3.7 State vector calculation

```
% wwwwwwwwwwwwwwwwwwwwwwwwwwwwwwwwwwwwwwwwwwwwwwww
% Example_4_07
% wwwwwwwwwwww
%{
This program uses Algorithm 4.5 to obtain the state vector from
the orbital elements provided in Example 4.7.
pi - 3.1415926...
deg - factor for converting between degrees and radians
mu - gravitational parameter (km^3/s^2)
coe - orbital elements [h e RA incl w TA a]
where h = angular momentum (km^2/s)
e = eccentricity
RA = right ascension of the ascending node (rad)
incl = orbit inclination (rad)
w = argument of perigee (rad)
TA = true anomaly (rad)
a = semimajor axis (km)
```

```
r - position vector (km) in geocentric equatorial frame
v - velocity vector (km) in geocentric equatorial frame
User M-function required: sv_from_coe
%}
% ------------------------------------------------
clear all; clc
deg = pi/180;
mu = 398600;
%...Data declaration for Example 4.5 (angles in degrees):
h = 80000;
e = 1.4;
RA = 40;
incl = 30;
w = 60;
TA = 30;
%...
coe = [h, e, RA*deg, incl*deg, w*deg, TA*deg];
%...Algorithm 4.5 (requires angular elements be in radians):
[r, v] = sv_from_coe(coe, mu);
%...Echo the input data and output the results to the command window:
fprintf('-----------------------------------------------------')
fprintf('\n Example 4.7\n')
fprintf('\n Gravitational parameter (km^3/s^2) = %g\n', mu)
fprintf('\n Angular momentum (km^2/s) = %g', h)
fprintf('\n Eccentricity = %g', e)
fprintf('\n Right ascension (deg) = %g', RA)
fprintf('\n Argument of perigee (deg) = %g', w)
fprintf('\n True anomaly (deg) = %g', TA)
fprintf('\n\n State vector:')
fprintf('\n r (km) = [%g %g %g]', r(1), r(2), r(3))
fprintf('\n v (km/s) = [%g %g %g]', v(1), v(2), v(3))
fprintf('\n-----------------------------------------------------\n')
% wwwwwwwwwwwwwwwwwwwwwwwwwwwwwwwwwwwwwwwwwwwwwwwwwwwwwwwwww
```

A3.8 Global extrema points from a time series calculation

```
function [xmax,imax,xmin,imin] = extrema(x)
%EXTREMA   Gets the global extrema points from a time series.
%    [XMAX,IMAX,XMIN,IMIN] = EXTREMA(X) returns the global minima and
maxima
%   points of the vector X ignoring NaN's, where
%    XMAX - maxima points in descending order
%    IMAX - indexes of the XMAX
%    XMIN - minima points in descending order
%    IMIN - indexes of the XMIN
%
%   DEFINITION (from http://en.wikipedia.org/wiki/Maxima_and_minima):
%    In mathematics, maxima and minima, also known as extrema, are
points in
%    the domain of a function at which the function takes a largest
value
%   (maximum) or smallest value (minimum), either within a given
%    neighbourhood (local extrema) or on the function domain in its
entirety
%   (global extrema).
%
%   Example:
%      x = 2*pi*linspace(-1,1);
%          y = cos(x) - 0.5 + 0.5*rand(size(x)); y(40:45) = 1.85;
y(50:53)=NaN;
%      [ymax,imax,ymin,imin] = extrema(y);
%      plot(x,y,x(imax),ymax,'g.',x(imin),ymin,'r.')
%
%   See also EXTREMA2, MAX, MIN
%   Written by
%   Lic. on Physics Carlos Adri?n Vargas Aguilera
%   Physical Oceanography MS candidate
%   UNIVERSIDAD DE GUADALAJARA
%   Mexico, 2004
%
%   nubeobscura@hotmail.com
% From       : http://www.mathworks.com/matlabcentral/fileexchange
% File ID    : 12275
```

```
% Submited at: 2006-09-14
% 2006-11-11 : English translation from spanish.
% 2006-11-17 : Accept NaN's.
% 2007-04-09 : Change name to MAXIMA, and definition added.
xmax = [];
imax = [];
xmin = [];
imin = [];
% Vector input?
Nt = numel(x);
if Nt ~= length(x)
 error('Entry must be a vector.')
end
% NaN's:
inan = find(isnan(x));
indx = 1:Nt;
if ~isempty(inan)
 indx(inan) = [];
 x(inan) = [];
 Nt = length(x);
end
% Difference between subsequent elements:
dx = diff(x);
% Is an horizontal line?
if ~any(dx)
 return
end
% Flat peaks? Put the middle element:
a = find(dx~=0);              % Indexes where x changes
lm = find(diff(a)~=1) + 1;    % Indexes where a do not changes
d = a(lm) - a(lm-1);          % Number of elements in the flat peak
a(lm) = a(lm) - floor(d/2);   % Save middle elements
a(end+1) = Nt;
% Peaks?
xa  = x(a);             % Serie without flat peaks
b = (diff(xa) > 0);     % 1  =>  positive slopes (minima begin)
                        % 0  =>  negative slopes (maxima begin)
```

```
xb  = diff(b);          % -1 =>  maxima indexes (but one)
                        % +1 =>  minima indexes (but one)
imax = find(xb == -1) + 1; % maxima indexes
imin = find(xb == +1) + 1; % minima indexes
imax = a(imax);
imin = a(imin);
nmaxi = length(imax);
nmini = length(imin);
% Maximum or minumim on a flat peak at the ends?
if (nmaxi==0) && (nmini==0)
 if x(1) > x(Nt)
  xmax = x(1);
  imax = indx(1);
  xmin = x(Nt);
  imin = indx(Nt);
 elseif x(1) < x(Nt)
  xmax = x(Nt);
  imax = indx(Nt);
  xmin = x(1);
  imin = indx(1);
 end
 return
end
% Maximum or minumim at the ends?
if (nmaxi==0)
 imax(1:2) = [1 Nt];
elseif (nmini==0)
 imin(1:2) = [1 Nt];
else
 if imax(1) < imin(1)
  imin(2:nmini+1) = imin;
  imin(1) = 1;
 else
  imax(2:nmaxi+1) = imax;
  imax(1) = 1;
 end
 if imax(end) > imin(end)
```

```
  imin(end+1) = Nt;
 else
  imax(end+1) = Nt;
```

A3.9 Global extrema points 2 from a time series calculation

```
function [xymax,smax,xymin,smin] = extrema2(xy,varargin)
%EXTREMA2   Gets the extrema points from a surface.
%   [XMAX,IMAX,XMIN,IMIN] = EXTREMA2(X) returns the maxima and minima
%   elements of the matriz X ignoring NaN's, where
%    XMAX - maxima points in descending order (the bigger first and so
on)
%    IMAX - linear indexes of the XMAX
%    XMIN - minima points in descending order
%    IMIN - linear indexes of the XMIN.
%   The program uses EXTREMA.
%
%    The extrema points are searched only through the column, the row
and
%   the diagonals crossing each matrix element, so it is not a perfect
%    mathematical program and for this reason it has an optional
argument.
%   The user should be aware of these limitations.
%
%   [XMAX,IMAX,XMIN,IMIN] = EXTREMA2(X,1) does the same but without
%    searching through the diagonals (less strict and perhaps the user
gets
%   more output points).
%
%   DEFINITION (from http://en.wikipedia.org/wiki/Maxima_and_minima):
%    In mathematics, maxima and minima, also known as extrema, are
points in
%    the domain of a function at which the function takes a largest
value
%   (maximum) or smallest value (minimum), either within a given
%    neighbourhood (local extrema) or on the function domain in its
entirety
%   (global extrema).
%
```

```
%   Note: To change the linear index to (i,j) use IND2SUB.
%
%   Example:
%      [x,y] = meshgrid(-2:.2:2,3:-.2:-2);
%      z = x.*exp(-x.^2-y.^2); z(10,7)= NaN; z(16:19,13:17) = NaN;
%      surf(x,y,z), shading interp
%      [zmax,imax,zmin,imin] = extrema2(z);
%      hold on
%       plot3(x(imax),y(imax),zmax,'bo',x(imin),y(imin),zmin,'ro')
%       for i = 1:length(zmax)
%        text(x(imax(i)),y(imax(i)),zmax(i),['   ' num2str(zmax(i))])
%       end
%       for i = 1:length(zmin)
%        text(x(imin(i)),y(imin(i)),zmin(i),['   ' num2str(zmin(i))])
%       end
%      hold off
%
%   See also EXTREMA, MAX, MIN
%   Written by
%   Lic. on Physics Carlos Adri?n Vargas Aguilera
%   Physical Oceanography MS candidate
%   UNIVERSIDAD DE GUADALAJARA
%   Mexico, 2005
%
%   nubeobscura@hotmail.com
% From        : http://www.mathworks.com/matlabcentral/fileexchange
% File ID     : 12275
% Submited at: 2006-09-14
% 2006-11-11 : English translation from spanish.
% 2006-11-17 : Accept NaN's.
% 2006-11-22 : Fixed bug in INDX (by JaeKyu Suhr)
% 2007-04-09 : Change name to MAXIMA2, and definition added.
M = size(xy);
if length(M) ~= 2
 error('Entry must be a matrix.')
end
N = M(2);
```

```
M = M(1);
% Search peaks through columns:
[smaxcol,smincol] = extremos(xy);
% Search peaks through rows, on columns with extrema points:
im = unique([smaxcol(:,1);smincol(:,1)]); % Rows with column extrema
[smaxfil,sminfil] = extremos(xy(im,:).');
% Convertion from 2 to 1 index:
smaxcol = sub2ind([M,N],smaxcol(:,1),smaxcol(:,2));
smincol = sub2ind([M,N],smincol(:,1),smincol(:,2));
smaxfil = sub2ind([M,N],im(smaxfil(:,2)),smaxfil(:,1));
sminfil = sub2ind([M,N],im(sminfil(:,2)),sminfil(:,1));
% Peaks in rows and in columns:
smax = intersect(smaxcol,smaxfil);
smin = intersect(smincol,sminfil);
% Search peaks through diagonals?
if nargin==1
 % Check peaks on down-up diagonal:
 [iext,jext] = ind2sub([M,N],unique([smax;smin]));
 [sextmax,sextmin] = extremos_diag(iext,jext,xy,1);
 % Check peaks on up-down diagonal:
 smax = intersect(smax,[M; (N*M-M); sextmax]);
 smin = intersect(smin,[M; (N*M-M); sextmin]);
 % Peaks on up-down diagonals:
 [iext,jext] = ind2sub([M,N],unique([smax;smin]));
 [sextmax,sextmin] = extremos_diag(iext,jext,xy,-1);
 % Peaks on columns, rows and diagonals:
 smax = intersect(smax,[1; N*M; sextmax]);
 smin = intersect(smin,[1; N*M; sextmin]);
end
% Extrema points:
xymax = xy(smax);
xymin = xy(smin);
% Descending order:
[temp,inmax] = sort(-xymax); clear temp
xymax = xymax(inmax);
smax = smax(inmax);
[xymin,inmin] = sort(xymin);
```

```
smin = smin(inmin);
%%%%%%%%%%%%%%%%%%%%%%%%%%%%%%%%%%%%%%%%%%%%%%%%%%%%%%%%%%%%
function [smax,smin] = extremos(matriz)
% Peaks through columns or rows.
smax = [];
smin = [];
for n = 1:length(matriz(1,:))
 [temp,imaxfil,temp,iminfil] = extrema(matriz(:,n)); clear temp
 if ~isempty(imaxfil)     % Maxima indexes
  imaxcol = repmat(n,length(imaxfil),1);
  smax = [smax; imaxfil imaxcol];
 end
 if ~isempty(iminfil)     % Minima indexes
  imincol = repmat(n,length(iminfil),1);
  smin = [smin; iminfil imincol];
 end
end
function [sextmax,sextmin] = extremos_diag(iext,jext,xy,A)
% Peaks through diagonals (down-up A=-1)
[M,N] = size(xy);
if A==-1
 iext = M-iext+1;
end
[iini,jini] = cruce(iext,jext,1,1);
[iini,jini] = ind2sub([M,N],unique(sub2ind([M,N],iini,jini)));
[ifin,jfin] = cruce(iini,jini,M,N);
sextmax = [];
sextmin = [];
for n = 1:length(iini)
 ises = iini(n):ifin(n);
 jses = jini(n):jfin(n);
 if A==-1
  ises = M-ises+1;
 end
 s = sub2ind([M,N],ises,jses);
 [temp,imax,temp,imin] = extrema(xy(s)); clear temp
 sextmax = [sextmax; s(imax)'];
```

```
 sextmin = [sextmin; s(imin)'];
end
function [i,j] = cruce(i0,j0,I,J)
% Indexes where the diagonal of the element io,jo crosses the
left/superior
% (I=1,J=1) or right/inferior (I=M,J=N) side of an MxN matrix.
arriba = 2*(I*J==1)-1;
si = (arriba*(j0-J) > arriba*(i0-I));
i = (I - (J+i0-j0)).*si + J+i0-j0;
j = (I+j0-i0-(J)).*si + J;
% Carlos Adri?n Vargas Aguilera. nubeobscura@hotmail.com
```

A3.10 Lagrange f and g coefficients calculation

```
% wwwwwwwwwwwwwwwwwwwwwwwwwwwwwwwwwwwwwwwwwwwwwwwwwwwwww
function [f, g] = f_and_g(x, t, ro, a)
% wwwwwwwwwwwwwwwwwwwwwwwwwwwwwwwwwwwwwwwwwwwwwwwwwwwwww
%{
This function calculates the Lagrange f and g coefficients.
mu - the gravitational parameter (km^3/s^2)
a - reciprocal of the semimajor axis (1/km)
ro - the radial position at time to (km)
t - the time elapsed since ro (s)
x - the universal anomaly after time t (km^0.5)
f - the Lagrange f coefficient (dimensionless)
g - the Lagrange g coefficient (s)
User M-functions required: stumpC, stumpS
%}
% ------------------------------------------------
global mu
z = a*x^2;
%...Equation 3.69a:
f = 1 - x^2/ro*stumpC(z);
%...Equation 3.69b:
g = t - 1/sqrt(mu)*x^3*stumpS(z);
end
% wwwwwwwwwwwwwwwwwwwwwwwwwwwwwwwwwwwwwwwwwwwwwwwwwwwwww
```

A3.11Time derivatives of the Lagrange f and g coefficients

```
function [fdot, gdot] = fDot_and_gDot(x, r, ro, a)
% wwwwwwwwwwwwwwwwwwwwwwwwwwwwwwwwwwwwwwwwwwwwwwwwwwwwwww
%{
This function calculates the time derivatives of the
Lagrange f and g coefficients.
mu - the gravitational parameter (km^3/s^2)
a - reciprocal of the semimajor axis (1/km)
ro - the radial position at time to (km)
t - the time elapsed since initial state vector (s)
r - the radial position after time t (km)
x - the universal anomaly after time t (km^0.5)
fdot - time derivative of the Lagrange f coefficient (1/s)
gdot - time derivative of the Lagrange g coefficient (dimensionless)
User M-functions required: stumpC, stumpS
%}
% ------------------------------------------------
global mu
z = a*x^2;
%...Equation 3.69c:
fdot = sqrt(mu)/r/ro*(z*stumpS(z) - 1)*x;
%...Equation 3.69d:
gdot = 1 - x^2/r*stumpC(z);
% wwwwwwwwwwwwwwwwwwwwwwwwwwwwwwwwwwwwwwwwwwwwwwwwwwwwwww
```

B1. SOLAR RADIATION FLUX (F10.7cm)[85]

DATE	F10.7CM
5 /11/2018	68
6 /11/2018	68
7 /11/2018	68
8 /11/2018	68
9 /11/2018	68
10 /11/2018	68
11 /11/2018	68
12 /11/2018	70
13 /11/2018	70
14 /11/2018	70
15 /11/2018	70
16 /11/2018	70
17 /11/2018	70
18 /11/2018	69
19 /11/2018	69
22 /11/2018	68
21 /11/2018	68
22 /11/2018	68
23 /11/2018	68
24 /11/2018	68
25 /11/2018	68
26 /11/2018	68
27 /11/2018	68
28 /11/2018	68
29 /11/2018	68
30 /11/2018	68
1 /12/2018	68
2 /12/2018	68
3 /12/2018	70
4 /12/2018	70
5 /12/2018	70
6 /12/2018	70
7 /12/2018	70
8 /12/2018	70
9 /12/2018	70
10 /12/2018	70
11 /12/2018	70
12 /12/2018	70
13 /12/2018	70
14 /12/2018	70
15 /12/2018	69
16 /12/2018	69
17 /12/2018	68
18 /12/2018	68
19 /12/2018	68

The average is 68,88889

[85] https://www.swpc.noaa.gov/products/usaf-45-day-ap-and-f107cm-flux-forecast

B2. GEOMAGNETIC INDEX *AP[86]

DATE	*Ap
5 /11/2018	20
6 /11/2018	12
7 /11/2018	8
8 /11/2018	5
9 /11/2018	5
10 /11/2018	15
11 /11/2018	12
12 /11/2018	5
13 /11/2018	5
14 /11/2018	12
15 /11/2018	5
16 /11/2018	5
17 /11/2018	5
18 /11/2018	5
19 /11/2018	5
22 /11/2018	5
21 /11/2018	5
22 /11/2018	5
23 /11/2018	5
24 /11/2018	5
25 /11/2018	8
26 /11/2018	12
27 /11/2018	10
28 /11/2018	5
29 /11/2018	5
30 /11/2018	20
1 /12/2018	15
2 /12/2018	15
3 /12/2018	15
4 /12/2018	8
5 /12/2018	5
6 /12/2018	12
7 /12/2018	8
8 /12/2018	10
9 /12/2018	5
10 /12/2018	5
11 /12/2018	5
12 /12/2018	5
13 /12/2018	5
14 /12/2018	5
15 /12/2018	5
16 /12/2018	5
17 /12/2018	5
18 /12/2018	5
19 /12/2018	5

The average is 7,822222

[86] https://www.swpc.noaa.gov/products/usaf-magnetometer-analysis